Carrier Synchronization in OFDM without Use of Pilots

by

Per Kristian Remvik

A DISSERTATION SUBMITTED IN PARTIAL FULFILMENT OF THE
REQUIREMENTS FOR THE DEGREE OF

DOKTOR INGENIØR

Department of Telecommunications
The Norwegian University os Science and Technology
N-7034 Trondheim
Norway

2000

"Would you tell me please, which way I ought to go from here?"
"That depends a good deal on where you want to go," said the cat.
"I don't much care where," said Alice.
"Then it doesn't matter which way you go," said the cat.

Lewis Carroll

Summary

Among new emerging digital communication systems, there is a clear trend of an increasing number of services using high capacity broad band connections, e.g. transfer of images, video and high quality sound. This makes it necessary to find bandwidth efficient modulation formats and efficient channel equalization solutions at the receiver. A modulation format, with possibilities for both relatively simple equalizer structures and bandwidth efficient solutions is Orthogonal Frequency Division Multiplexing (OFDM). The symbol stream is divided into N parallel symbol streams, which are modulated on to separate subchannels. The frequency spectra of the subchannels overlap, but the orthogonality of the subchannels are maintained in the time domain at the sampling instant.

To obtain orthogonality between subchannels in OFDM system, one of the assumptions which are made, is exact knowledge of the carrier frequency at the receiver. In the case of a carrier frequency offset (CFO) between transmitter and receiver, the orthogonality between subchannels are lost. With a CFO some of the signal power will be transferred into interference power, i.e. noise, reducing the system performance. All digital transmission systems suffers from performance degradation in the case of a CFO and it is thus important to minimize the CFO, i.e. perform carrier frequency synchronization. The CFO generated interference is special for the OFDM systems and makes them more vulnerable to CFO than single carrier (SC) systems. In addition, the symbol length is increased in OFDM systems compared to SC systems, reducing the amount of CFO tolerated before phase slipping occurs (i.e. erroneous decisions due to CFO generated phase errors). Extra care should be taken in the case of OFDM systems to synchronize the carrier frequency at the receiver with the carrier of the transmitter.

The main topics of this work have been:

- Carrier synchronization in bandwidth efficient OFDM systems on stationary channels. To obtain maximum bandwidth efficiency, neither pilots, guard intervals, repeated sequences or other redundant signalling is used in the proposed methods.

Four new OFDM carrier frequency acquisition algorithms are proposed, with performance investigated by simulations.

The frequency estimator of Kay is investigated for use in Decision Directed (DD) carrier frequency tracking, with OFDM and non-constant amplitude modulation.

- Consequences of non perfect carrier frequency tracking and time varying transmission channels in OFDM systems. Both OFDM systems using QAM with rectangular pulses and OFDM systems using O-QAM with finite length pulses have been investigated.

Degradation due to non-perfect tracking on stationary channels has been calculated and performance requirements for the developed tracking algorithms are found.

For flat Rayleigh fading channels, degradation due to non-perfect tracking and doppler spread are calculated.

Acquisition

The few bandwidth efficient carrier frequency acquisition algorithms proposed for OFDM in earlier works have assumed oversampled receiver structures and/or more than one filterbank in the receiver, increasing receiver complexity.

In this work, four critically sampled LMS carrier frequency acquisition algorithms have been developed for OFDM systems, using a single filterbank in the receiver to maintain minimum receiver complexity. Error functions for the LMS carrier frequency acquisition algorithm have been developed by identifying similarities between OFDM carrier acquisition, SC timing and SC blind equalization. Neither pilots, guard intervals nor repeated sequences are used in the proposed algorithms.

The performance, i.e. acquisition time for a given steady state variance, of the four developed algorithms have been simulated and compared to each other and to the performance of the ML carrier frequency acquisition algorithm of (Daffra and Chouly 93). Compared with the best of the developed algorithms, the Daffara algorithm performs better for moderate SNR and low number of subchannels. For high number of channels and low SNR the developed algorithms are best. Introducing time dispersive transmission channels or carrier frequency offsets of several sub channel bandwidths, the developed algorithms have significantly shorter acquisition time than the Daffara algorithm.

Compared to the Daffara algorithm, the best of the algorithms developed in this work give lower receiver complexity and larger robustness against noise, large carrier frequency offsets and time dispersive transmission channels.

Tracking

In the literature there exist several methods for carrier frequency tracking in OFDM. Most of these methods assume constant amplitude modulation and use of pilots, guard intervals, repeated sequences or other redundant signalling decreasing bandwidth efficiency.

In this work methods for decision directed (DD) carrier phase tracking and DD carrier frequency tracking in OFDM have been presented for use with higher order modulation. These methods operate without redundant signalling, maintaining bandwidth efficiency. Their performances have been investigated by comparing calculated and simulated variance with Cramer Rao Bound (CRB). The best of the proposed algorithms perform close to or equal to CRB. The proposed DD tracking algorithms perform better than DA tracking with a factor close (or equal) to the pilot spacing in the DA systems.

The proposed phase error estimator performs equal to CRB independent of constellation size and number of symbols used for averaging. For the eight frequency error estimators proposed in this work, the performance equals CRB for constant amplitude modulation. Using higher order modulation, the performance ranges from CRB to a loss relative to CRB proportional to the second power of the number of frames used for averaging. For the example systems of Chapter 6, averaging over only a few frames were necessary to obtain adequate carrier estimation accuracy.

Compared to pilot based methods, several of the presented DD carrier tracking methods give better tracking performance and a system with higher bandwidth efficiency.

Performance loss due to imperfect carrier tracking and fading channels

The performance requirements for carrier frequency tracking algorithms, are decided by the system degradation as function of CFO. Earlier works on system degradation due to CFO, have concentrated on OFDM systems using QAM and rectangular pulses on stationary transmission channels.

In this work OFDM systems using QAM with rectangular pulses and OFDM systems using O-QAM with finite length pulses are investigated and compared with respect to CFO generated degradation. This is done both for stationary channels and flat Rayleigh fading channels. In addition, the degradation due to fading (time variations on the transmission channel) is investigated. The focus is degradation due to inter bin interference (IBI) generated by CFO/fading.

The IBI generated by CFO at stationary channels and IBI generated by doppler spread at fading channels are calculated and simulated, they are found to behave similar to the channel noise. This IBI can be viewed as an increase of the AWGN on the channel. On the other hand, if the IBI is generated by CFO on a fading channel, calculations and simulations show that the instant signal power (as decided by the "fade level") and the instant IBI power are highly correlated. The IBI is ignored for low CFO where channel noise is dominating, and the system performs like a standard flat fading system with SNR equal to signal to channel noise power ratio. For high CFO where the IBI is dominating the channel noise is ignored, and the system can be viewed as a stationary channel with SNR equal to the signal to IBI power ratio.

Systems operating at high SNR are found to be more sensitive to CFO and Doppler spread generated IBI than systems operating at low SNR. In the same manner, sensitivity to CFO and doppler spread is proportional to the number of subchannels in the system.

If the number of subchannels in the OFDM system is dictated by spectral requirements, choice of pulseshaping filters decides the number of subchannels and thus the CFO and doppler robustness. If the number of subchannels is dictated by delay spread in the channel, choice of pulseshaping filters have little influence on CFO and doppler robustness.

Using 4-QAM on flat Rayleigh fading channels, CFO generated phase slipping occurs at a lower CFO than CFO generated IBI domination. This results in CFO robustness to be decided by the symbol length and not by IBI generation in OFDM systems with 4-QAM operating on flat Rayleigh fading channels.

Preface

This thesis is submitted in partial fulfilment of the requirements for the doctoral degree of *Doktor ingeniør* at the Norwegian University of Science and Technology (NTNU).

Acknowledgements

I would like to thank Professor Nils Holte for advice and support during the process of writing this thesis. Professor Holte was also helpful in the process of raising funds before the start of the work and at the point when it became clear that some extra time was necessary. I also would like to thank professor Holte for the relaxing discussions during the coffee breaks, about the mysteries of the Norwegian sweet water trout.

I also would like to thank my colleagues and friends at Department of Telecommunications, NTNU and at SINTEF Informatics. The time spent together with them was a pleasure. Due to my urge for discussions most of them have contributed to this work in some manner. Especially, I want to mention Vidar Ringset and Knut Grythe for several interesting discussions about OFDM. Anders Vahlin supported me with the Pulse shaping filters for O-QAM. Special thanks goes to my room mate Trym Holter. Sitting in the same office as me, he was the victim of a never ending stream of questions and discussion topics. Due to his patience and will to answer questions and participate in discussions, his contribution to my work can not be over estimated.

Thanks to my family and friends for encouragement and moments of recreation during all these years. Thanks to my brother Frode for reading parts of this thesis, commenting on my english writing.

Most especially, I would like to thank Aslaug for her patience during a to long period of time, where I managed to participate in much of our common joy but too little of our common duties.

Contents

Chapter 5 Algorithms for carrier tracking in OFDM 79

Chapter 6 System degradation due to non ideal carrier tracking and channel time variations 115

Nomenclature

α_{ro}	Roll-off factor
α	Attenuation of second ray in two ray channel
α_a	Instant channel attenuation on flat Rayleigh fading channel, Chapter 7
α_n	Weight in used for preprocessing before the extra FFT in the receiver of Daffara
$\Gamma_{l, m-n}$	Interference from one quadrature of channel n, into the other quadrature of channel m which is transmitted $(l - 1/2)T$ earlier.
ΔF	A specific Carrier frequency offset
$\Delta F_{tolerated}$	Tolerated Carrier frequency offset (design criterion)
Δf	Carrier frequency offset
$\hat{\Delta f_k}$	Estimated carrier frequency offset at frame k
$\hat{\Delta f_k^K}$	Estimated frequency offset at frame k, based on K frames
δf	Frequency separation
$\delta(t)$	Dirac function
ΔN	Number of samples in the cyclic extension, creating guard interval
Δt	Time separation
$\varepsilon_{D, k}$	Estimated gradient according to Daffara of the likelihood function of frame k, termed the Daffara error function of frame k
$\varepsilon_{G1, k}$	First order Godard based error function, frame k, averaged across the channels

$\varepsilon_{G2,k}$	Second order Godard based error function, frame k, averaged across the channels
$\varepsilon_{G1,k,m}$	First order Godard based error function, channel m, frame k
$\varepsilon_{G2,k,m}$	Second order Godard based error function, channel m, frame k
$\varepsilon_{M,k}$	Mueller and Müller based error function, frame k, averaged across the channels
$\varepsilon_{M,k,m}$	Mueller and Müller based error function, channel m, frame k
$\zeta(t)$	Delay spread in the transmission channel
θ	Phase error
$\hat{\theta}$	Estimated phase error
$\hat{\theta}_{k,m}$	Estimated phase error, frame k, channel m
$\Lambda_{0,0}$	Damping factor of the wanted signal.
$\Lambda_{l,m-n}$	Interference from real part of channel n, symbol l into real part of channel m, symbol 0, and from imaginary part to imaginary part.
μ_D	Step size weight for the LMS update using the Daffara algorithm
μ_M	Step size with Mueller and Müller based acquisition
$\rho(\delta f, \Delta t)$	Envelope correlation coefficient
σ^2, σ_N^2	Transmission channel noise power
ς	The set of subchannels used for pilots
τ	Time variable for time dispersion in time varying channels
τ_D	Delay of second ray in two ray channel
Υ	Performance loss of the chosen tracking algorithm relative to CRB
a_k	Transmitted complex datasymbol number k
$a_{k,n}$	Transmitted complex datasymbol in channel n, frame k
$\hat{a}_k$	Decision / estimate of complex datasymbol number k
$\hat{a}_{k,n}$	Decision / estimate of complex datasymbol transmitted in channel n, frame k
A/D	Analog to digital

AWGN	Additive white Gaussian noise
$b(t)$	Transmission channel impulse response
B_D	Doppler bandwidth of the fading channel
p_{eq}	Probability of error in one quadrature channel
BW	Total OFDM system bandwidth
BW_{Guard}	Total OFDM system bandwidth for systems with guard interval
$BW_{NoGuard}$	Total OFDM system bandwidth for systems without guard interval
c	Speed of light
$c(a^4)$	Fourth order cumulant of a
$c(t)$	Time varying attenuation of flat Rayleigh fading channel
CFO	Carrier Frequency Offset, carrier frequency error
CRB	Cramer Rao bound
$CRB_{\hat{\Delta f}}$	Cramer Rao bound of the carrier frequency offset estimate
$CRB_{\hat{\Delta \theta}}$	Cramer Rao bound of the carrier phase estimate
D	Time delay of length one symbol interval
D	SNR degradation
d	Distance between points in the signal constellation
$D_{\Delta F}$	SNR degradation D for a given CFO, $\Delta f = \Delta F$, measured as the relation between $\mathrm{SNR}_{\Delta f=0}$ and $\mathrm{SNR}_{\Delta f=\Delta F}$
$D(\Delta f)$	SNR degradation D as function of CFO
$D_{tolerated}$	Maximum tolerated SNR degradation due to CFO (design criterion)
D/A	Digital to analog
DA	Data aided
DD	Decision directed
E_0	Power of the received signal component
f_{cT}	Transmitter carrier frequency
f_{cR}	Receiver carrier frequency
f_D	Channel doppler bandwidth
f_s	High sampling rate, i.e. after parallel/serial converter

f_{sG}	High sampling rate in system with Guard channels
FFT	Fast Fourier transform
FLL	Frequency locked loop
$g(t)$	Impulse response of receiver filter
$h(t)$	Impulse response of transmitter-, or pulseshaping- filter
$h(k')$	Time discrete version of $h(t)$
I	Subchannel offset, i.e. difference between input channel of signal at the transmitter and output channel for the same signal at the receiver
I_0	Damping factor of the desired signal.
I_{m-n}	Weight of interference from channel n into channel m.
IBI	Inter Bin Interference
IBI_{CFO}	CFO generated IBI
$IBI_{Doppler}$	Fading generated IBI
ICI	Inter Channel Interference
$Im\{\ \}$	Extraction of imaginary part of signal
ISI	Inter Symbol Interference
J_0	Zero order Bessel function
K	Number of symbols (Single carrier) or frames (OFDM) used for carrier frequency estimation
$K(a, b)$	Covariance between a and b
k	Index of symbol (Single carrier) or frame (OFDM) in the transmitter
k'	Index of samples at the high sampling rate in front of the serial to parallel converter in the OFDM receiver
L	Number of channels used for pilots in OFDM systems
l	Index of symbol (Single carrier) or frame (OFDM) in the receiver
LMS	Least mean square
$LP, LP(t)$	Butterwort low pass filter
M	Symbol constellation size
m	Index of receiver filterbank channel number
ML	Maximum likelihood

N	Number of channels in the OFDM filterbank
N_{Rm}, N_{Im}, N_m	Channel noise in real part, imaginary part and the total complex noise of channel m
NDA	Non data aided
n	Index of transmitter filterbank channel number
$n(t)$	Additive channel noise
Ne	Noise enhancement due to zero forcing equalization
$o_{k,m}$	$(z^*_{k,m}\hat{a}_{k,m})$
OFDM	Orthogonal frequency division multiplexing
O-QAM	Offset QAM
p	Order of Godard error function
$p(\ )$	Convolution of transmitter and receiver filter
$p_{\Delta f > \Delta F}$	Probability for the CFO to exceed ΔF
$p_{k,m}$	$(z_{k+1,m}z^*_{k,m}\hat{a}^*_{k+1,m}\hat{a}_{k,m})$
Phase slipping	When a phase error of $2\pi\Delta fT$ generates decision errors
PLL	Phase locked loop
$Q[\ ]$	Q-function, integral of the Gaussian density
QAM	Quadrature amplitude modulation
R_{tot}	Total symbol rate in the OFDM system
$Re\{\ \}$	Extraction of real part of signal
$s(t)$	Continuous time and amplitude received baseband signal
SC	Single carrier
S-curve	Expectation of the error function, $E[\varepsilon]$, also known as characteristic curve
SER	Symbol error rate
$SER(\Delta f)$	Symbol error rate as function of CFO
SNR	Signal to noise ratio
$SNR_{\Delta f = \Delta F}$	Signal to noise (including IBI) ratio for a CFO of ΔF
SNR_{Guard}	SNR at the data detector for systems with guard interval
$SNR_{NoGuard}$	SNR at the data detector for systems without guard interval

SSB	Single sideband
t	Continuous time
T	Symbol interval
T'	SC symbol interval
T_0	Symbol interval minus guard time for systems using guard interval
$u(m)$	Weighting function
V_0	Power of the signal generated interference, or IBI
v	Velocity of mobile transceiver
$w(k)$	Windowing function
$w_m(k)$	Windowing function subchannel m
Weighting	Use weights during channel averaging
WGN	White Gaussian noise
Windowing	Use weights during time averaging
$x(t)$	Continuous time and amplitude transmitted baseband signal
z_k	Sampled received signal at time $t = kT$
$z_{k,n}$	Sampled received signal in channel n, at time $t = kT$
$\dot{z}$	Output of FFT with preprocessing in the OFDM receiver of (Daffra and Chouly 93)

Chapter 1
Introduction

A block diagram of a typical digital communications system is shown in Figure 1.1. The source signal is processed by the source encoder to generate a digital signal compatible with the digital communications system. The channel encoder adds redundancy and organizes the digital signal to protect against errors during transmission. The task of the modulator is to transform the time discrete symbol sequence from the channel encoder into a time continuous signal suitable for the transmission channel. Using passband transmission channels, one of the operations performed by the modulator is adding a carrier to the time continuous signal to be transmitted, i.e. moving the frequency spectra of the signal to an area around the carrier frequency, compatible with the transmission channel and other systems using the same transmission channel. The transmission channel may distort the signals and introduce noise and interference. The demodulator transforms the received time continuous signal, to a time discrete symbol sequence, which may differ from the transmitted sequence due to the effects of the transmission channel. Removal of the carrier and sampling of the time continuous signal at the symbol rate is included in the operation of converting the time continuous signal to a time discrete symbol stream. Neither exact carrier frequency, carrier phase nor symbol timing is known at the receiver. It is the task of the synchronizer unit in the demodulator to reconstruct these parame-
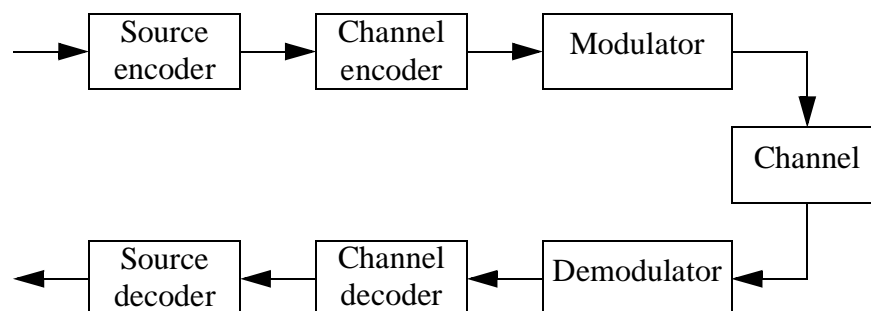
Figure 1.1. *Block diagram of digital communications system*

ters from the signal. The channel decoder corrects transmission errors and removes the redundancy introduced by the channel encoder. The purpose of the source decoder is to reconstruct the original source signal as accurately as possible. Source or channel coding is not treated any further in this work. It will be assumed that the modulator receives a stream of random symbols.

Examining the new emerging digital communications systems, there is a clear trend of an increasing number of services using high capacity, broadband connections, e.g. transfer of still images and video. Several transmission channels suffers from bandwidth limitations and time dispersion. Broadband systems using such transmission channels need bandwidth efficient modulation and channel equalization at the receiver. A modulation format, which exhibits good qualities both for bandwidth efficiency and time dispersion robustness is Orthogonal Frequency Division Multiplexing. (OFDM). Instead of modulating the high rate symbol stream on to a single carrier (SC), the symbol stream is divided in N parallel symbol streams, each modulated by a unique sub carrier on to separate subchannels. The frequency spectra of the subchannels overlap, but the orthogonality of the subchannels are maintained in the time domain at the sampling instant.

OFDM is proposed used for a wide range of applications and channels:

- In mobile cellular radio communication, the system must cope with large time dispersions. Due to the splitting of the symbol stream into N channels in OFDM, the duration of each symbol increase with a factor N, increasing the time dispersion robustness. Independent of the size of N, time dispersion will give a certain level of Inter Symbol Interference (ISI). For some OFDM systems the ISI can be totally avoided by including guard intervals, (Doelz et.al 57), (Clasen and Meyr 94). In this case the channel equalization reduces to a power scaling problem.

- OFDM has been incorporated in standards for both digital audio broadcasting (DAB), (Zimmermann 96) and digital video broadcasting (DVB), (Reimers 97). Use of OFDM with guard intervals in digital broadcasting networks, makes single frequency networks possible, increasing the bandwidth efficiency. OFDM systems are also well suited for co existence with analogue systems, by adjusting the content of each subchannel according to the spectra of the analogue system, (Vahlin 96).

- The twisted pair subscriber lines in the telephony network is a slowly changing channel, with signal to noise ratio (SNR) dependant on the frequency. Using OFDM on such a transmission channel, the system capacity can be maximized by adjusting the transmitted power and signal constella-

tions according to the SNR in each OFDM subchannel. The transmitter is informed about the transmission channel through a return link from the receiver. This is utilized in asymmetric and high bit rate digital subscriber lines (ADSL), (Chow et. al. 91) and VDSL.

- In stationary line of sight radio links there are high bandwidth efficiency requirements, with frequency masks allowing little excess bandwidth. With the use of OFDM this is achievable without the use of sharp and expensive analogue filters, (Vahlin 96).

The orthogonality between subchannels in an OFDM system is lost if the carrier frequency of the demodulator, i.e. of the receiver, differs from the carrier frequency of the modulator, i.e. of the transmitter, (Pollet et. al 95). Loss of orthogonality will transform some of the signal power into noise power, reducing the system performance. The transformation of signal power to noise power makes the OFDM system more vulnerable to carrier frequency offset (CFO) than SC systems. It is thus the task of the synchronizer unit in the demodulator to keep the frequency error at such a low level that these effects are minimized.

The main issue of this work is carrier frequency synchronization in OFDM systems.

Existing synchronization algorithms for OFDM usually depend on pilots or other redundant signalling, increasing system bandwidth. In this work carrier frequency acquisition algorithms and tracking algorithms are developed without the use of redundant signalling. This gives bandwidth efficient solutions. The algorithms developed in this work are intended for stationary channels.

System degradation as function of CFO, decides the carrier frequency tracking performance requirements. Earlier, the consequences of a CFO have been investigated for OFDM systems using QAM on stationary transmission channels. In this work the consequences of CFO are analysed for both stationary transmission channels and flat Rayleigh fading transmission channels, together with the consequences of the fading generated Doppler spread. OFDM systems using QAM and OFDM systems using O-QAM are compared with respect to CFO and Doppler spread robustness.

Carrier phase tracking is also addressed, while timing is only addressed by references to other work.

1.1 Outline of thesis

- Chapter 2: The principles of OFDM are introduced and some characteristic properties are described. Different classes of OFDM systems are reviewed. A short overview of the literature of OFDM systems is presented.

- Chapter 3: A short introduction to the synchronization problem and possible solution strategies in general, with comments on what is special for OFDM. An introduction to the consequences of a carrier frequency offset for different OFDM systems are given, together with an introduction to the consequences of a flat Rayleigh fading channel on the same OFDM systems. An overview of work on timing in OFDM is also included. In the end there is an overview of earlier work in the area of carrier frequency and phase synchronization for OFDM, together with an overview of work concerning consequences of CFO and phase noise in OFDM.

- Chapter 4: Algorithms are developed for carrier frequency acquisition on high capacity stationary channels without the use of pilots. The algorithms assume critically sampling and one single filterbank in the receiver to minimize receiver complexity. The algorithms are developed for use with square pulses without assuming the use of guard interval. The performance of the algorithms are compared to the performance of an existing algorithm requiring double set of filterbanks in the receiver, (Daffra and Chouly 93).

- Chapter 5: Decision directed tracking algorithms for carrier phase and carrier frequency are developed. The algorithms are presented for use with square pulses without assuming the use of guard intervals. The similarity with pilot based algorithms is shown, and the performance of the different algorithms are compared.

- Chapter 6: The consequences of a residual CFO during tracking is analysed for different OFDM systems on stationary and flat Rayleigh fading channels. The CFO robustness for the different systems are compared. The results for the square pulse OFDM system on stationary channels are also used to find quality demands on the CFO tracking algorithms in Chapter 5. The consequences of loss of orthogonality due to a flat Rayleigh fading channel is also discussed for the different OFDM systems.

- Chapter 7: The conclusions of the work are presented.

Chapter 2
OFDM Principles and system model description

This chapter contains a general introduction to Orthogonal Frequency Division Multiplexing (OFDM) which is a class of multi carrier transmission systems with overlapping spectra, and data modulated on to each carrier or subchannel. Different OFDM systems and models are presented, including the models used for calculations and simulation in subsequent chapters. Notation is also established. At the end of the chapter there is an introduction to flat fading channels, describing the physical mechanism of the fading and the channel model used in this work.

The chapter is organised as follows: Chapter 2.1 contains references to earlier work in the area of OFDM systems, Chapter 2.2 describes the basic principles of OFDM, Chapter 2.3 gives an introduction to different OFDM classes, in Chapter 2.4 time discrete implementation of OFDM systems is discussed, Chapter 2.5 contains design criteria for number of subchannels in OFDM systems and Chapter 2.6 describes the transmission channel models used in this work.

2.1 Earlier work in the area of OFDM systems

Transmission with overlapping spectra has become popular during the last decade as increased calculation power has become available in digital transmission systems. On the other hand the first contributions to the literature on the subject date 40 years back, (Doelz et.al 57), (Harmuth 60). These early systems used square pulses, the use of guard interval was included by (Doelz et.al 57). Later the use of FFT for implementation of rectangular pulse systems was proposed by (Weinstein and Ebert 71). Rectangular pulses is an example of pulse shapes of length one symbol. Other pulse shapes of length one symbol exists as well, (Mallory 92), (Li and Stette 95).

Bandlimited pulses for use with Single Sideband (SSB) was first mentioned by (Chang 66) and later the same pulses where used with offset QAM (O-QAM) system, (Saltzberg 67).

2.2 System model

Each subchannel in an OFDM system can be viewed as a Single Carrier (SC) system, the total OFDM system will be a composition of SC systems. In this model each subchannel SC system must fulfill all the criteria of an ordinary SC system, in addition there will be some extra requirements to fulfil, making the different SC systems work together as one OFDM system. OFDM has been proposed used together with several modulation schemes, QAM, O-QAM, single side band and combinations with spread spectrum. In this work the focus is on O-QAM and QAM. First there is a general introduction to OFDM, then the difference between OFDM systems using O-QAM and QAM is described.

OFDM

In an OFDM system there will be several subchannels with a carrier spacing equal to $1/T$, where T is the symbol interval. If the system contains N channels, N symbols will be transmitted simultaneously in one frame. A model of an OFDM system is shown in Figure 2.1

$a_{k,n}$: Data symbol transmitted in channel n, frame k

$\hat{a}_{k,n}$: Estimation of data symbol transmitted in channel n, frame k

T : Symbol interval

N : Number of channels in the OFDM system

$n(t)$: Additive channel noise

$x(t)$: Continuous time and amplitude transmitted baseband signal

$s(t)$: Continuous time and amplitude received baseband signal

$b(t)$: Channel impulse response

f_{cT} : Transmitter carrier frequency

f_{cR} : Receiver carrier frequency

In the rest of Chapter 2 receiver and transmitter carrier frequency is assumed to be equal.
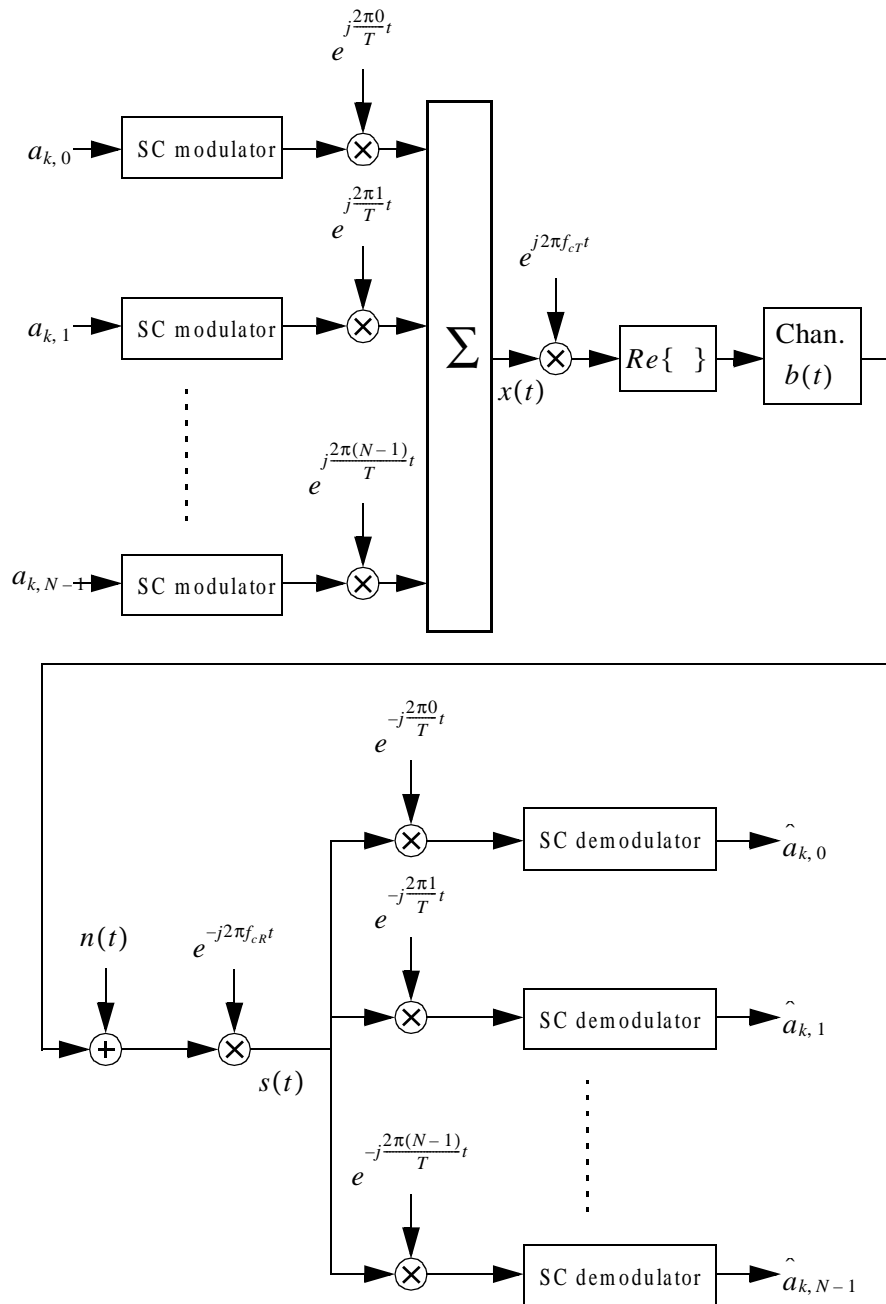
Figure 2.1. *OFDM system model*

Modulator and demodulator

A block diagram of a QAM modulator and demodulator with time continuous transmitter and receiver filters is shown in Figure 2.2
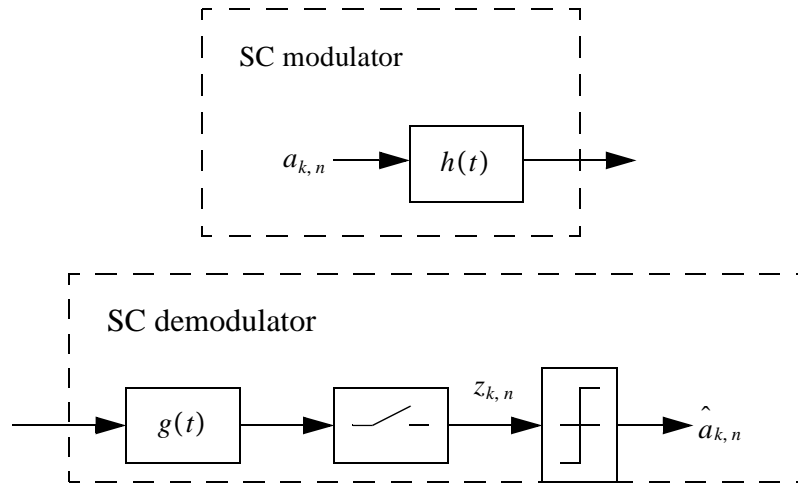
Figure 2.2. *Block diagram of the analytic model of a Single Carrier QAM system*

$h(t)$: Pulse shaping filter

$g(t)$: Receiver filter

$z_{k,n}$: Received, sampled signal, frame k, channel n

In the case of QAM modulation the real and imaginary part of each symbol are transmitted simultaneously and sampled in the receiver simultaneously. An alternative solution is to use O-QAM modulation where the transmission of the imaginary part of the symbol is moved half a symbol interval compared to the real part of the symbol. A block diagram is shown in Figure 2.3

$Re\{\ \}$: Extraction of real part of signal

$Im\{\ \}$: Extraction of imaginary part of signal

Filter requirements

In a SC system, $N = 1$, the design criterion for the receiver and transmitter filters will be no interference between different symbols at the sampling instant, denoted as no Inter Symbol Interference (ISI). For this to be the case the filters must fulfill the
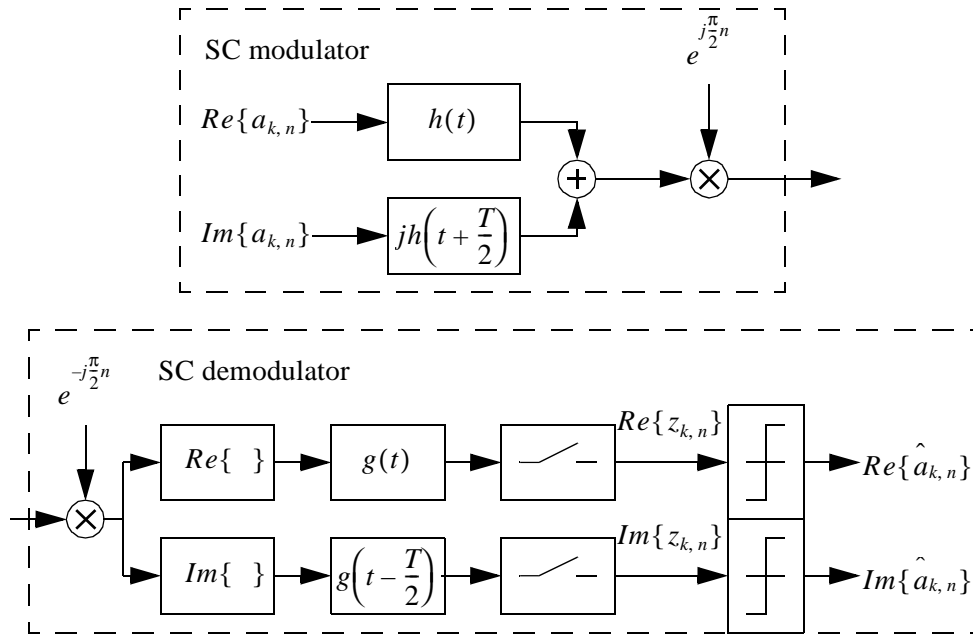
Figure 2.3. *Block diagram of the equivalent complex analytic model of a Single Carrier O-QAM system*

Nyquist Criterion (Lee and Messerschmitt 94). In an OFDM system with pulse shaping filters with non zero excess bandwidth, a carrier spacing of $1/T$ will give overlapping spectra as shown in Figure 2.4
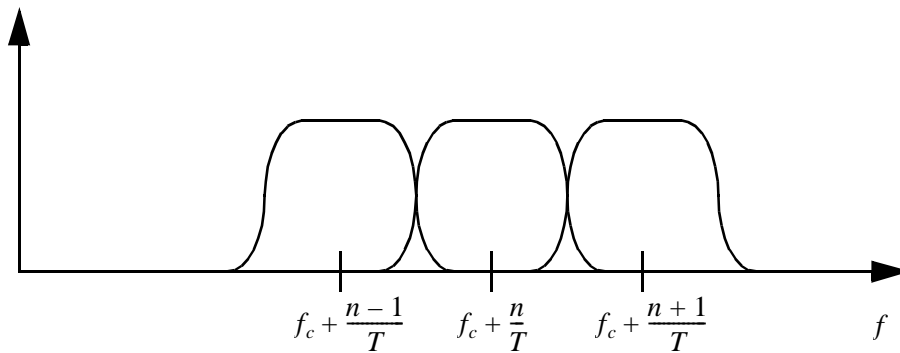
Figure 2.4. *OFDM spectrum*

In this case, transmitter and receiver filters must be designed to avoid both Inter Channel Interference (ICI) and ISI at the sampling instant, i.e. fulfill the generalized Nyquist criterion (Lee and Messerschmitt 94). In this work Inter Bin Interference, (IBI), will refer to both ICI and ISI. With filters fulfilling the criterion, impairment free channel $b(t) = \delta(t)$ and no noise, the received sampled signal equals the transmitted signal $z_{k,m} = a_{k,m}$.

The collection of the N pulseshaping filters in the transmitter is in this work termed the transmitter filterbank, and the collection of the N receiver filters as the receiver filterbank.

2.3 Different OFDM systems

All calculations througout the thesis are based on the OFDM system models with time continious pulseshaping filters presented below in Chapter 2.3.1 and 2.3.2.

2.3.1 QAM and rectangular pulses

One set of transmitter and receiver filters which fulfill the generalized Nyquist criterion are the rectangular shaped filters, with both transmitter and receiver filter of length one symbol interval, T. The amplitude is adjusted to unity pulse power.

$$h(t) = \begin{cases} \dfrac{1}{\sqrt{T}} & 0 < t \leq T \\[2mm] 0 & \text{else where} \end{cases} \tag{2.1}$$

$$g(t) = h(-t) \tag{2.2}$$

According to Equation 2.2 this is a matched filter solution. The transmitted baseband signal $x(t)$ is a sum of N QAM signals at different frequencies.

$$x(t) = \sum_{n=0}^{N-1} \sum_{l=0}^{\infty} a_{l,n} h(t - lT) e^{j\frac{2\pi}{T} nt} \tag{2.3}$$

This gives a system where consecutive symbols do not overlap and ISI is avoided. Assuming transmission over an impairment free channel and no noise, the received sampled signal in channel m, frame k equals:

$$z_{k,m} = \sum_{n=0}^{N-1} a_{k,n} \int_0^T \frac{1}{T} e^{j\frac{2\pi}{T}(n-m)\tau} d\tau = a_{k,m} \tag{2.4}$$

QAM and rectangular pulses with guard interval

Another set of square transmitter and receiver filters which fulfill the generalized Nyquist criterion is the guard interval solution. Transmitter and receiver filters are given by Equation 2.5 and 2.6, and the carrier spacing equals $1/T_0$.

$$h(t) = \begin{cases} \dfrac{1}{\sqrt{T_0 + \Delta}} & 0 < t \le T_0 + \Delta \\ 0 & \text{else where} \end{cases} \tag{2.5}$$

$$g(t) = \begin{cases} \dfrac{\sqrt{T_0 + \Delta}}{T_0} & -(T_0 + \Delta) \le t < -\Delta \\ 0 & \text{else where} \end{cases} \tag{2.6}$$

Extending the length of the transmitter pulse shape with Δ will make the system tolerate time dispersive channels with time dispersion less than Δ, in the sense that no ISI and no ICI are generated.

There are two disadvantages with the guard interval solution (Vahlin 96).

a   The guard interval solution is not a matched filter solution, resulting in a Signal to Noise Ratio (SNR) loss.

b   A guard interval will cause increased use of bandwidth.

$$\frac{BW_{Guard}}{BW_{NoGuard}} = \frac{SNR_{NoGuard}}{SNR_{Guard}} = 1 + \frac{\Delta}{T_0} \tag{2.7}$$

2.3.2 Offset QAM

Square pulses of length T have high spectral sidelobes. To reduce the sidelobe level, pulses of length more than one symbol may be used. Applying O-QAM instead of QAM will increase the freedom in choosing pulse shaping- and receiver- filters, which meet the generalized Nyquist criterion. The filters discussed here for use with OFDM and O-QAM will be limited to pulses which fulfill the following requirements:

i   Real, symmetric transmitter filter, i.e. $h(t) = h(-t)$

ii Matched filter in the receiver, i.e. $g(t) = h(-t)$

iii The cascade of transmitter filter and receiver filter gives no intersymbol interference.

iv There is no inter channel interference in the system

According to iii and iv the pulses must fulfill the generalized Nyquist criterion.

The transmitted signal in an O-QAM OFDM system equals:

$$x(t) = \sum_{n=0}^{N-1} \sum_{l=0}^{\infty} \left(Re\{a_{l,n}\}h(t-lT) + jIm\{a_{l,n}\}h\left(t-lT+\frac{T}{2}\right)\right)e^{j\left(\frac{2\pi}{T}t+\frac{\pi}{2}\right)n} \qquad \textbf{(2.8)}$$

With impairment free channel and no noise, the received sampled real part in channel m at time k equals:

$$Re\{z_{k,m}\} = \sum_{n=0}^{N-1} \sum_{l=0}^{\infty} \int_{-\infty}^{\infty} Re\{a_{l,n}\}h(t-lT)h(t-kT) \qquad \textbf{(2.9)}$$

$$\cdot \cos\left(\left(\frac{2\pi}{T}t+\frac{\pi}{2}\right)(n-m)\right)dt$$

$$-\sum_{n=0}^{N-1} \sum_{l=0}^{\infty} \int_{-\infty}^{\infty} Im\{a_{l,n}\}h\left(t-lT+\frac{T}{2}\right)h(t-kT)$$

$$\cdot \sin\left(\left(\frac{2\pi}{T}t+\frac{\pi}{2}\right)(n-m)\right)dt$$

Similarly the sampled imaginary part will be equal to:

$$Im\{z_{k,m}\} = \sum_{n=0}^{N-1}\sum_{l=0}^{\infty}\int_{-\infty}^{\infty} Im\{a_{l,n}\}h(t-lT+\frac{T}{2})h(t-kT+\frac{T}{2}) \qquad (2.10)$$

$$\cdot \cos\left(\left(\frac{2\pi}{T}t+\frac{\pi}{2}\right)(n-m)\right)dt$$

$$+ \sum_{n=0}^{N-1}\sum_{l=0}^{\infty}\int_{-\infty}^{\infty} Re\{a_{l,n}\}h(t-lT)h(t-kT+\frac{T}{2})$$

$$\cdot \sin\left(\left(\frac{2\pi}{T}t+\frac{\pi}{2}\right)(n-m)\right)dt$$

To avoid ISI and ICI, the second integral of both Equation 2.9 and 2.10 must equal zero for every combination of m, n, k and l. Similarly the first integral must equal one for $n = m \wedge l = k$ and zero for every other combination of m, n, k and l.

Pulses with less than 100% excess bandwidth

Pulses with double sided bandwidth less than $2/T$ that obey point i, ii and iii on page 12, (symmetry and no ISI), will also obey point iv, (no ICI), (Vahlin 96). One class of pulses which fulfill i, ii and iii is the raised cosine pulses, (Lee and Messerschmitt 94). With roll-off factor, α_{ro}, in the region $0 \leq \alpha_{ro} \leq 1$, point iv will thus also be fulfilled.

A short description of the proof of (Vahlin 96) is given. Due to limited bandwidth, the only channels which give contributions to the received symbol in Equation 2.9 and Equation 2.10, are $n = m, m\pm1$. Inserting $n = m$ equals a single carrier system, and with pulses fulfilling the Nyquist criterion, (no ISI), there will only be a contribution for $l = k$. Inserting $n = m\pm1$ and substituting integration variables, all integrands will turn into odd functions of time, integrating from $-\infty$ to ∞ the resulting integrals equals zero. Assuming normalized pulse shapes, impairment free channel and no noise, the received symbols will equal the transmitted symbols

$$Re\{z_{k,m}\} = Re\{a_{k,m}\} \qquad (2.11)$$

$$Im\{z_{k,m}\} = Im\{a_{k,m}\} \qquad (2.12)$$

O-QAM with time limited pulses

Rectangular pulses have a high spectral sidelobe level while bandlimited pulses have long duration in the time domain. Practical approximations to the bandlimited pulses will need long filters which give a high complexity in transmitter and receiver. Alternatively pulses with low spectral sidelobe level and finite length larger than T can be designed. This is possible as long as ii, iii and iv on page 12 are used as conditions during the pulse design. One example is (Vahlin and Holte 96) where the pulse length is given and the out of band power is minimized under the condition of no ISI and no ICI. This gives pulses of finite, relatively short length and low sidelobe level of the spectra.

2.4 Time discrete implementation

The OFDM systems discussed in Chapter 2.3 were based on time continuous filters in each branch or subchannel in the OFDM systems. This is not the case for most normal implementations. Usually the pulse shaping and receiver filtering is done in a time discrete manner. With time discrete pulse shaping the Digital to Analog (D/A) conversion is done after the summation of the channels, while in the receiver the Analog to Digital (A/D) conversion, including the sampling, is done after removal of the carrier. A principal model for QAM OFDM with time discrete pulseshaping filters and normalized bandwidth is shown below in Figure 2.5. The conversion from time continuous to time discrete filtering for the O-QAM OFDM system will be similar.

D/A: Digital to analog converter, including low pass filtering

A/D: Analog to digital converter including lowpass filtering and sampling

k' : Time index at the high sampling rate

$h(k')$: Sampled version of $h(t)$

Simulations of O-QAM systems in later chapters use a structure similar to Figure 2.5. Simulations of QAM systems with rectangular pulses use the structure of Figure 2.6 with the operation of the FFT and the IFFT given by Equation 2.14. During carrier acquisition simulations, Chapter 4, guard channels are included, Chapter 2.4.3.

2.4.1 Time discrete QAM rectangular pulse systems

The discrete time filterbanks in Figure 2.5 operates at the high samplingrate, N/T which gives high computational complexity. The filterbanks for OFDM with QAM and square pulses can be implemented in a more efficient manner by using IFFT and
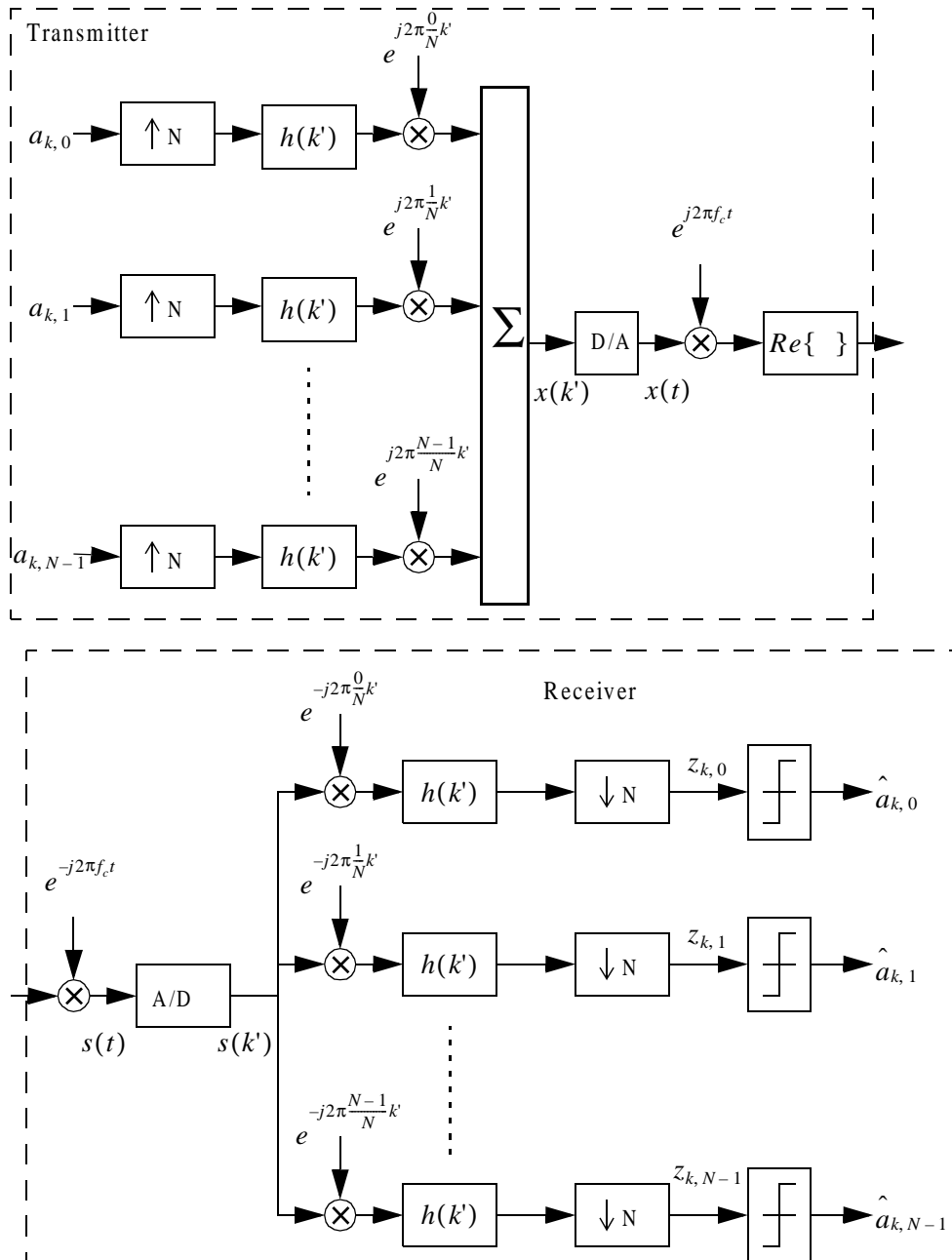
Figure 2.5. *Principle model of OFDM QAM transmitter and receiver with time discrete pulseshaping filters*

FFT. The transmitter consists of an IFFT and a parallel to a serial converter, while the receiver uses a serial to parallel converter in front of a FFT, as shown in Figure 2.6. Both IFFT and FFT operates at the low samplingrate $1/T$.
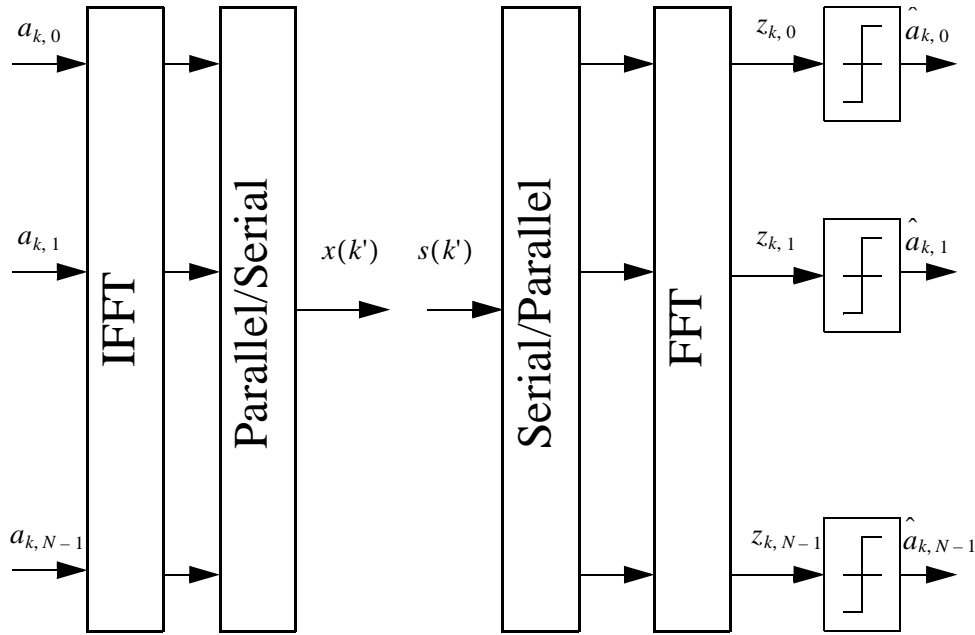
Figure 2.6. *FFT realisation of OFDM QAM system*

The IFFT/FFT realization makes it easy to implement the guard interval discussed in Chapter 2.3.1. This is done by a cyclic extension of the output signal, i.e. for each block of N samples generated by the IFFT, the last ΔN samples are copied and inserted in front of the N length block in the transmitter. Total length of each block is $N + \Delta N$ where the size of ΔN is decided by the length of the guard interval. At the receiver, the first ΔN samples are removed before processing by the FFT.

The inverse discrete Fourier transform (IDFT) and the discrete Fourier transform (DFT), performed by the IFFT and FFT, is shown in Equation 2.13 for a N channel OFDM system with normalized bandwidth in each subchannel, i.e. $T = 1$.

$$x(k') = \frac{1}{N} \sum_{n=0}^{N-1} a(n) e^{j2\pi\frac{n}{N}k'} \quad IDFT$$

$$z(m) = \sum_{k'=0}^{N-1} s(k') e^{-j2\pi\frac{k'}{N}m} \quad DFT$$

(2.13)

Comparing these expressions with the continuous time filters Equation 2.1 and Equation 2.2, reveals that the IDFT/DFT solution is a non symmetric sampling of the continuous pulse shapes. The first sample is at 0 and the last sample at $1-(1/N)$ of a pulse in the interval $[0, 1\rangle$. This non symmetric sampling does not conflict with the requirement of no ISI and no ICI in a impairment free system, but in some occasions the unsymmetrical sampling will give a difference in the behaviour of the time discrete implementation and the time continuous implementation, Chapter 4. An odd IDFT/DFT with symmetrical sampling is shown in Equation 2.14.

$$x(k') = \frac{1}{N} \sum_{n=0}^{N-1} a(n) e^{j2\pi\frac{n}{N}(k'+1/2)} \quad Odd\ IDFT$$

$$z(m) = \sum_{k'=0}^{N-1} s(k') e^{-j2\pi\frac{(k'+1/2)}{N}m} \quad Odd\ DFT$$

(2.14)

2.4.2 Time discrete O-QAM pulse systems

The system in Figure 2.5 can be modified to work with O-QAM including time discrete filterbanks with sampled versions of the time continuous filter $h(k')$ working at the high sampling rate N/T. In the case of timelimited pulse shapes the whole pulse can be used, while in the case of the bandlimited pulses, which are of infinite length, they must be truncated to be implementable. The truncation will lead to both ISI and ICI where the level of interference must be traded against pulse length and system complexity. Similar to OFDM with QAM and square pulses, solutions with reduced computational complexity exists for OFDM with O-QAM, (Hirosaki 81) and (Cariolaro and Vagliani 95). The solutions differ at several points, but all of them include the use of IFFT and FFT. A basic block diagram of the transmitters is shown below in Figure 2.7, the receivers will have a corresponding structure.
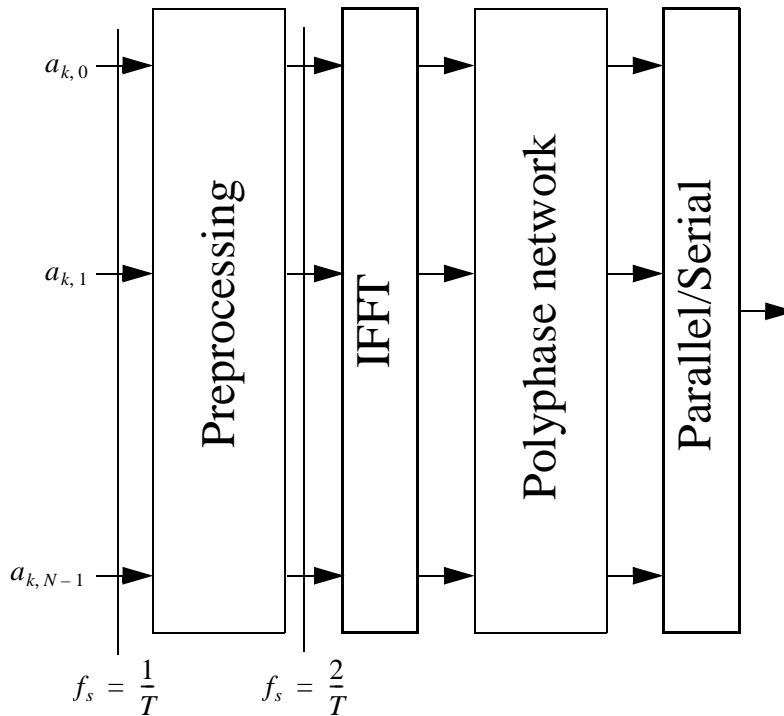
Figure 2.7. *Computational efficient OFDM O-QAM transmitter*

The preprocessing doubles the sampling rate by separating the real and imaginary part in time. In addition the symbols are rearranged and multiplied with different factors for the different solutions. The filterbank is implemented with a N-branch polyphase network, using the original high samplingrate filter $h(k')$ as reference filter. The samplingrate at the IFFT and in the polyphase network equals $2/T$, reducing the computational complexity compared to the solution with a filterbank operating at a sampling rate of N/T. Both N point and $N/2$ point IFFT solutions exists, (Cariolaro and Vagliani 95) and (Hirosaki 81).

2.4.3 Guard channels

If every channel in the OFDM filterbank is used for transmission of data, the frequency spectra in front of the D/A converter will be a repeated spectra with non zero values around half the sampling frequency, $\pm f_s/2$. Where f_s equals the filterbank bandwidth and the high sampling rate in the OFDM system. To achieve good spectral efficiency a steep analog filter is needed in the D/A conversion. This is difficult

to implement. A common approach to avoid this problem, is to extend both transmitter and receiver filterbank with guard channels. The guard channels are divided between the upper and lower end of the filterbanks, Figure 2.8. This will increase the filterbank bandwidth and the high sampling rate in the system to f_{sG}. By not transmitting data in the guard channels, there will not be large signal contributions outside $\pm f_s/2$, creating gaps around $\pm f_{sG}/2$. So despite that the filterbank bandwidth is increased to f_{sG}, the system bandwidth is kept close to f_s. At the same time, the gaps in the frequency spectra allow less steep filters to be used in the D/A conversion. A schematic illustration is shown in Figure 2.8.
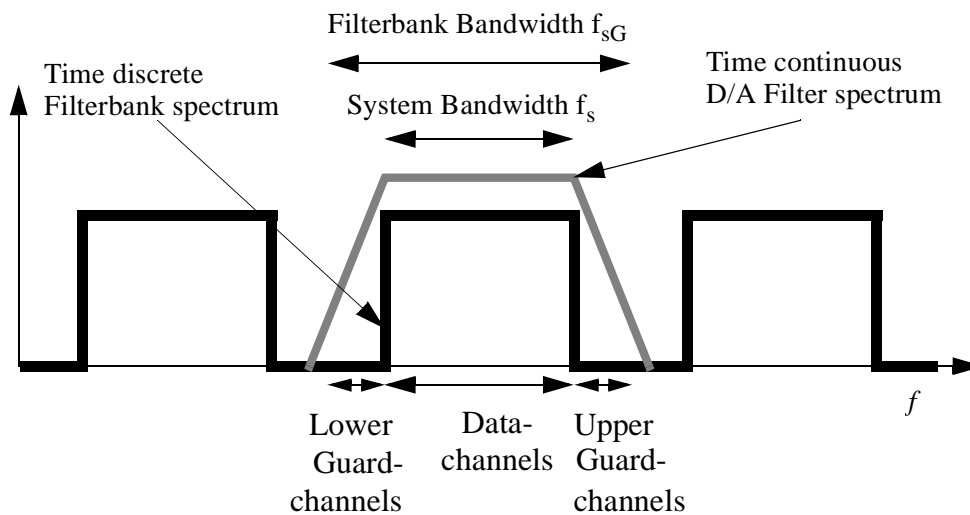
Figure 2.8. *Spectrum for OFDM system with Discrete pulseshaping filters, guard channels and time continuous D/A filter*

2.5 Number of channels in OFDM systems

In Chapter 6 it is concluded that CFO and Doppler spread robustness depend on the number of channels in the OFDM system. The number of channels will be dictated by system requirements. In the case of strong spectral requirements, the frequency mask can dictate the number of channels used in the system, while in the case of multipath channels the number of channels can be dictated by a wish of time dispersion $\ll 1/T$ to make each subchannel behave close to a non time dispersive system.

2.5.1 Number of channels determined by spectral requirements

Usually there are strong spectral requirements for fixed radio links operating on stationary channels, resulting in strict frequency masks which requires a strong out of band attenuation and have small excess bandwidth. In the case of an OFDM system one can focus on the edge channels (channel 0 and $N-1$). The spectral side lobe level of these edge channels must fall off quickly enough, i.e. the transition band must be narrow enough, to fulfil the frequency mask of the total system and thereby avoid cochannel interference (at this point cochannel interference refers to interference between two OFDM systems). The transition band is defined as the area between the subchannel passband (width of $2/T$) and stopband (where the attenuation is above a given limit). The width of the transition band compared to the symbol rate in each subchannel is given by the pulse shaping in the system, but the width compared to the total rate of the system is also decided by the number of subchannels in the system. Multiplying the number of channels N with some factor, multiplies the width of the transition band with the same factor. Use of pulse shapes with slowly decaying sidelobes, i.e. a wide transition band, must be compensated with an increased number of subchannels in the system.

Square pulses have sinc shaped frequency spectra with large side lobes, which fall off as $1/f$ (Lee and Messerschmitt 94). Hence a large number of channels N is necessary to obtain good spectral efficiency. O-QAM OFDM systems can use pulse shapes with, in this context, better spectral behaviour. Bandlimited raised cosine pulses will make it possible to fulfil the frequency mask with a low number of channels, but the long pulse lengths gives high complexity. A O-QAM low complexity solution with good spectral efficiency has been found by (Vahlin and Holte 96). In this work, pulses of finite duration which were optimized for minimum out of band energy under constraint of zero intersymbol and interchannel interference in an OFDM system, were created. The pulses are given as a sum of prolate spheroidal wave functions. The pulses of length $2T$ and $4T$ are shown bellow in Figure 2.9 together with the square pulse.

With finite length, the there will be infinite bandwidth, but the minimisation of the out of band power ensures that the sidelobes will be fast decaying. The spectrum of the pulses in Figure 2.9 is shown in Figure 2.10.

The low side lobe level compared to square pulses will be advantageous if a small number of channels are wanted in a system where spectral efficiency requirements are strong. In order to achieve 5% excess bandwidth of the total system, with a given sidelobe level, (Vahlin 96) has shown how many channels N an OFDM realisation of the systems must use to meet these requirements. The results are presented in
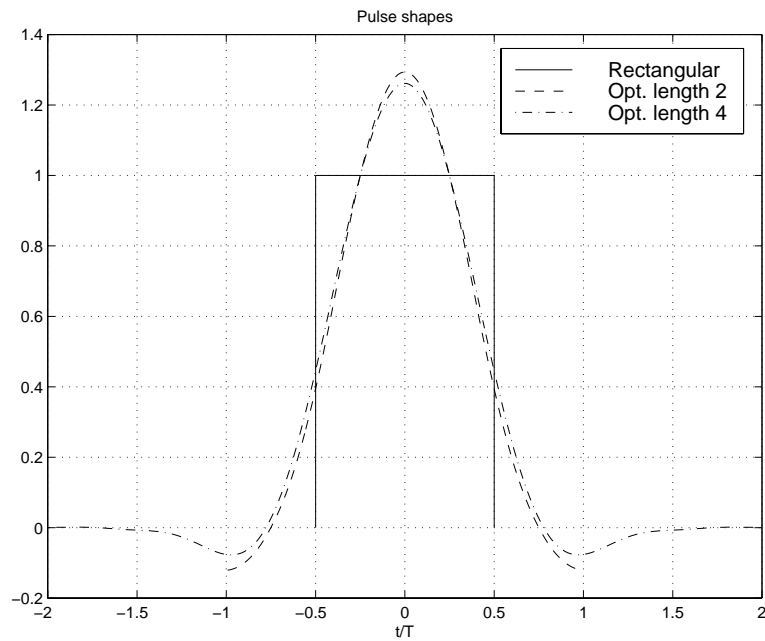
Figure 2.9. *Square and optimized pulse shapes.*
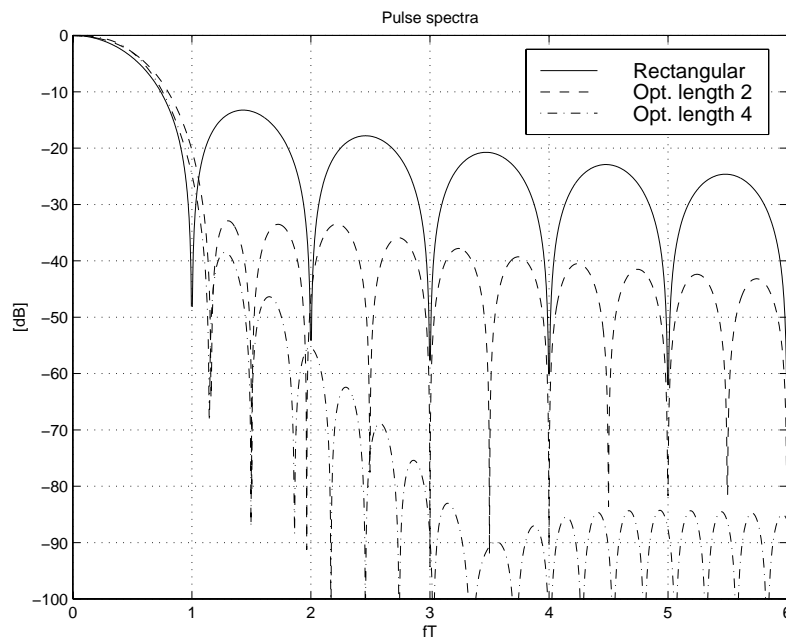
Figure 2.10. *Spectra of square pulse and optimized pulses of length 2T and 4T.*

Table 2.1 and show that the use of O-QAM and optimized pulses for OFDM systems with strong spectral requirements gives a significant reduction in the number of required channels compared to a QAM realization with square pulses.

	Rect. pulses	Opt. pulses $2T$	Opt. pulses $4T$
Sidelobe level $-30dB$	192	15	11
Sidelobe level $-40dB$	627	80	20

Table 2.1. *Number of channels necessary to achieve a given sidelobe level for 5% excess bandwidth.*

Increasing the length of the optimized pulses, decrease the sidelobe level, but increase the complexity of the receiver filters. But increasing the length of the pulses from $2T$ to $4T$ increase the complexity in each channel, but reduce the number of necessary channels according to Table 2.1. For sidelobe level $-40dB$ (Vahlin 96) has shown that the complexity measured in number of operations per output symbol is equal for the two optimized pulse systems, while the complexity for the 627 channel rectangular pulse system is approx. doubled.

2.5.2 Number of channels determined by delay spread

As described in Chapter 2.6 a transmission channel can be both time dispersive and time varying. In the frequency domain, this equals a non frequency flat, time varying transmission channel (Steele 92). Wideband SC systems must use equalizers in the receivers to compensate for the non frequency flat transmission channel (Lee and Messerschmitt 94). Using an OFDM system with a sufficient number of subchannels, the transmission channel experienced by the separate (narrowbanded) subchannels will be close to frequency flat, reducing the need of high complexity equalizers.

According to (Steele 92), a measure of the transmission bandwidth at which distortion due to time dispersion becomes appreciable, is often based on the transmission channels coherence bandwidth. The coherence bandwidth indicates the frequency separation at which the attenuation of the amplitudes of two frequency components becomes decorrelated such that the envelope correlation coefficient, $\rho(\delta f, \Delta t)$, reaches a predesignated value, ρ_{limit}. There have been several proposals for this value ranging from $1/e$ to 0.9. Systems applying different modulation formats, have different time dispersion sensitivities. A particular system might experience problems for a transmission bandwidth corresponding to a correlation coefficient of

0.9, where as more robust systems may perform satisfactorily on a transmission bandwidth corresponding to a correlation coefficient of $1/e$.

The envelope correlation coefficient of two signals separated by δf Hz and Δt seconds equals (Steele 92):

$$\rho(\delta f, \Delta t) = \frac{J_0^2\left(2\pi\frac{v}{c}\Delta t\right)}{1 + (2\pi\delta f)^2\zeta^2(t)} \tag{2.15}$$

J_0: Zero order Bessel function

v: Mobile speed

c: Speed of light

$\zeta(t)$: delay spread

Inserting $\Delta t = 0$, the (frequency) correlation coefficient equals:

$$\rho(\delta f) = \frac{1}{1 + (2\pi\delta f)^2\zeta^2(t)} \tag{2.16}$$

In an OFDM system the subchannel transmission bandwidth can be defined as $2/T$. Designing the system for a maximum delay spread, ζ_{max}, and a chosen ρ_{limmit} for the subchannel transmission bandwidth, the subchannel spacing equals:

$$\frac{1}{T} = \frac{1}{2\sqrt{1 + (2\pi)^2\varsigma_{max}^2\rho_{limmit}}} \tag{2.17}$$

2.6 Channel models

The transmission channel in Figure 2.1, has been assumed impairment free in the discussions above, but in general it will distort the signals and introduce noise and interference. The stationary transmission channel model described in Chapter 2.6.1 is used for calculations and simulations in Chapter 4, 5 and 6. The flat Rayleigh fading transmission channel model of Chapter 2.6.3 is used for calculations and simulations in Chapter 6.

2.6.1 Stationary additive white Gaussian noise channel

Several transmission channels exhibit extremely slow changes, or no changes at all as function of time. One example is the transmission channel of stationary line of sight radio links. The channels can thus be viewed as stationary. Despite stationarity, multipath propagation can generate time dispersion, described by the channel impulse response, $b(\tau)$.

In addition to time dispersion, the transmission channel introduce noise. For radio links the noise is usually modelled as additive white Gaussian noise (AWGN), (Lee and Messerschmitt 94). Unless other is stated the transmission channels in this work are assumed non time dispersive with AWGN.

$$b(\tau) = \delta(\tau) \tag{2.18}$$

$\delta(\ )$: Dirac function.

For testing of the proposed carrier frequency acquisition algorithms in Chapter 4, the two ray AWGN transmission channel of (Rummler et al. 86) is applied as well.

$$b(\tau) = \delta(\tau) + \alpha_D e^{j\theta_D}\delta(\tau - \tau_D) \tag{2.19}$$

α_D : Attenuation of the non direct path

θ_D : Phase shift of the non direct path

τ_D : Delay of the non direct path

2.6.2 Fading channels

In the mobile scenario the transmitter or receiver (or both) will be moving. In the case of multipath propagation, the transmission channel impulse response, $b(t, \tau)$, is a function of time, t, as the mobile moves relative to the base station and reflectors. This is the most general case with a time dispersive, time varying channel. The stationary channel $b(\tau)$, discussed in Chapter 2.6.1, can be viewed as a special case of the general channel, $b(t, \tau)$. Yet another special case is the non time dispersive, time varying channel, also known as the frequency flat fading channel:

$$b(t, \tau) = c(t)\delta(\tau) \tag{2.20}$$

$c(t)$: Time variation to be multiplied with the transmitted signal.

The channels applied in this work for use with mobile applications, is flat Rayleigh fading channels, which is discussed in further detail below. Similar to the stationary channel, the noise is assumed AWGN.

Flat Rayleigh fading channels

In a mobile radio channel there will be many paths between the base station and the mobile because of a multitude of reflectors. Compared to the direct path between base station and mobile the reflected paths are time delayed. Some reflectors are located far away from the mobile, typically being the origin to paths with delays longer than the time resolution of the receiver. This generates what the receiver detects as time dispersion. Other reflectors are located close to the mobile, these paths have delays shorter than the receiver's time resolution and can not be separated from each other. The delay difference between the different short delay paths is however large enough to give the paths different phase in addition to a phase shift in the reflection. The phase difference between non separable paths produces the fading.

First a time domain explanation of the flat fading channel is given. The limitation to flat channels equals excluding the paths with delay larger than the receiver time resolution. The total signal with amplitude and phase will be a sum of the short delay paths, where the paths have different amplitude and phase. As the mobile moves relative to the reflectors, the phase in each path will change and the total signal will exhibit random amplitude and phase variations. Assuming no direct path, Gaussian amplitude of the reflected paths and uniform distribution of the reflectors around the mobile, the amplitude of the total signal will be Rayleigh distributed and the phase will be uniformly distributed (Steele 92).

Alternatively the flat fading channel can be interpreted in the frequency domain. The mobile moves towards some reflectors and away from others, generating different doppler shifts in the different paths. The total signal will contain a sum of contributions with different doppler shifts resulting in a frequency dispersion of the signal. According to (Steele 92) the channel Fourier transformed with respect to the time variations is equal to the Doppler spread or frequency dispersion of the channel.

2.6.3 Fading channel model

The frequency flat fading channel model of (Jakes 74) is adopted in this work. The time variations are modelled as a complex multiplicative, time varying factor $c(t)$ as shown below in Figure 2.11
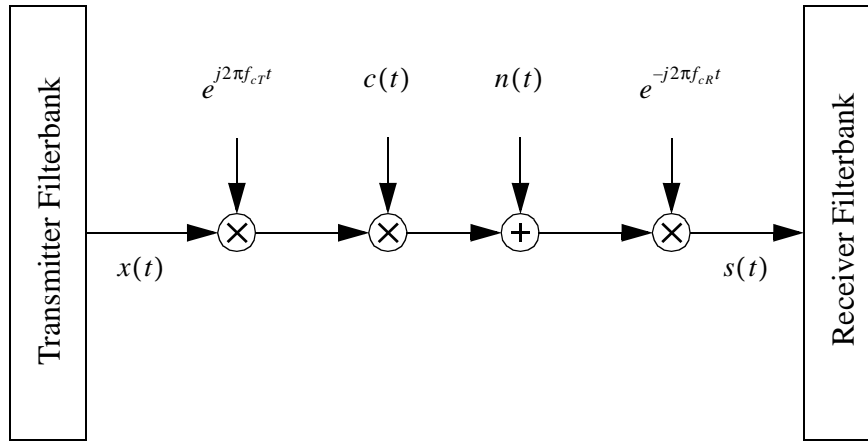
Figure 2.11. *OFDM on Rayleigh fading AWGN channel*

$c(t)$ has Rayleigh distributed amplitude and uniformly distributed phase and is modelled by independent low pass filtered Gaussian sources for the real and imaginary part.
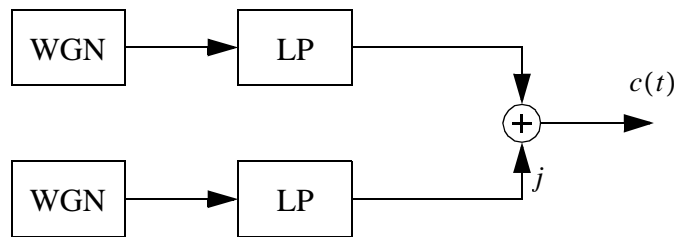
Figure 2.12. *Rayleigh fading model*

WGN: White Gaussian noise

LP: Butterwort low pass filter

The bandwidth of the low pass filters equal the doppler bandwidth of the channel.

$$f_D = \frac{v f_c}{c} \qquad\qquad (2.21)$$

f_D : Channel doppler bandwidth

Chapter 3
Synchronization in OFDM

The task of the receiver is to reconstruct the transmitted data sequence as accurately as possible. The reconstruction, i.e. detection, process needs synchronization information, i.g. timing, frame synchronization, carrier frequency and carrier phase. These synchronization parameters are unknown to the receiver, which must thus estimate them from the received signal. The number of synchronization parameters depend on the system. In differential encoded systems, it is not necessary to estimate the carrier phase.

This chapter contains the main principles of timing and carrier synchronization in OFDM. The effects of flat fading channels and carrier frequency offset (CFO) in OFDM systems are covered qualitatively. Timing and frame synchronization is briefly treated in this chapter, mainly by references to other work, but will not be pursued in later chapters of this thesis. Carrier synchronization, CFO consequences and fading channel consequences will be elaborated in later chapters.

The chapter is organized as follows: Chapter 3.1 contains references to earlier work in the area of carrier synchronization, Chapter 3.2, 3.3 and 3.4 looks at synchronizer structures and classes in general, while Chapter 3.5 looks at the special case of carrier synchronization in OFDM. References to timing is given in Chapter 3.6. In Chapter 3.7 and Chapter 3.8 the consequences of respectively CFO and flat fading channels in OFDM systems are discussed.

3.1 Previous work

Analysis of the effect of phase errors was carried out by (Chang and Gibby 68), while phase noise is treated by (Pollet et. al 95) and (El-Tanany and Wu 97). Analysis of the consequence of carrier frequency errors are found in (Moose 94), (Pollet et. al 95) and (Speth et. al 98).

Several algorithms for carrier synchronization / acquisition have been proposed in the literature. (Clasen and Meyr 94), (Lambrette et. al 97a) and (Speth et. al 98) use DA approaches with pilots, which gives fast acquisition at the cost of loss in capacity and non optimal tracking.

(Daffra and Chouly 93) use a non data aided (NDA) approach. This method includes double set of filter banks in the receiver. (Oh et. al 96) propose another NDA system which requires four sets of filterbanks and an oversampling factor of two in the receiver. The carrier synchronization algorithm in (Moose 94) also belong to the NDA algorithms and is based on transmitting the output of the filterbank twice and synchronize in front of the receiver filterbank. Another NDA system working only for square pulses with guard interval is proposed by (Van de Beek et. al 97).

A special carrier synchronization algorithm for constant envelope paired burst OFDM is given by (Dinis and Gusmao 97).

Maximum likelihood estimation of the phase error is treated in (Hirosaki 84).

3.2 Synchronization topologies

Both timing, carrier phase synchronization and carrier frequency synchronization can be divided into two operations: Estimation and Correction. The estimation algorithm use the received signal to estimate the error of a given sync parameter, this estimate is than used to correct the received signal. To improve the performance of the error estimate, it can be averaged or filtered in time before it is used for correction. For OFDM systems, the performance can also be increased by averaging across the subchannels. Knowing the effect or operation of an error, the correction equals the inverse operation based on the estimated error.

There exist several topologies for synchronization algorithms. With feed forward solutions the correction is made after the estimation in the signal path. The estimated error is used for correcting the signals from which the error was estimated. Two possible feed forward solutions for OFDM are shown in Figure 3.1.
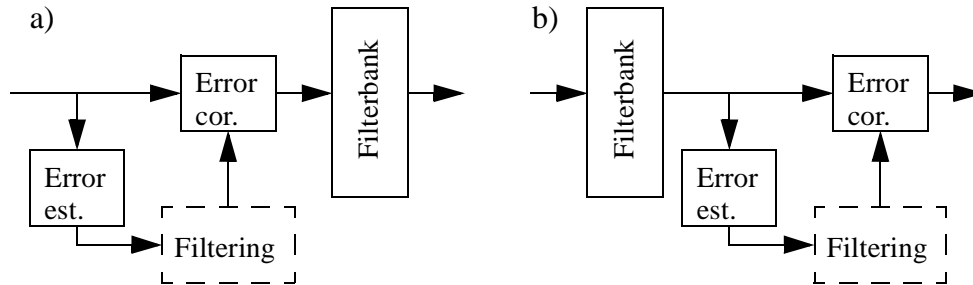
Figure 3.1. *Sketch of feedforward topologies with OFDM.*

Alternatively feedback solutions can be used, where the estimated error is used as correction to the signal in the consecutive frames. Three possible feedback solutions are shown in Figure 3.2. Note that the feedback loop must include a delay.
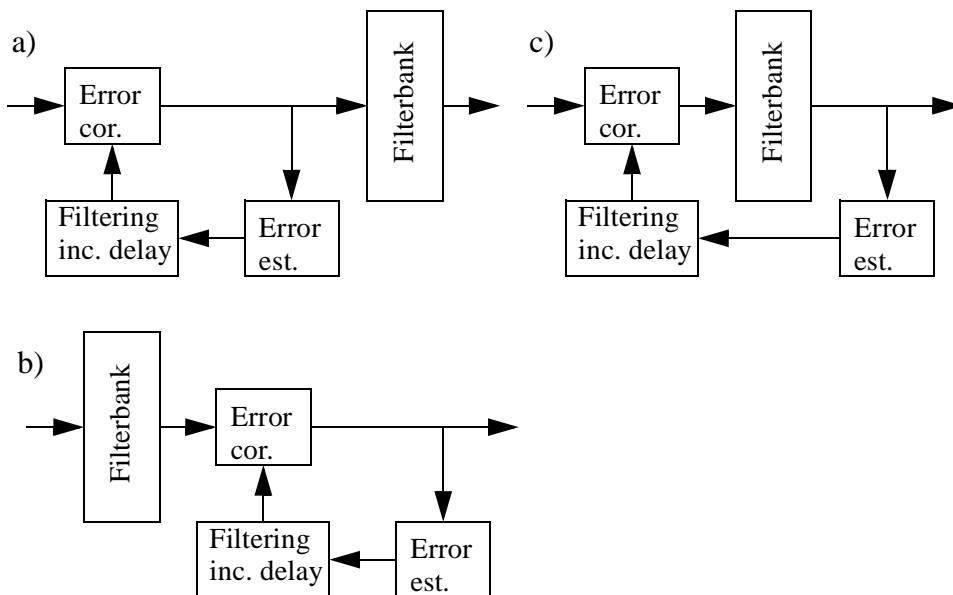
Figure 3.2. *Sketch of feedback synchronization loops in OFDM.*

Error estimate filtering is far more common for the feedback solution, than for the feed forward solution. To be able to perform synchronization operations after the filterbank, the sync parameter must be stable enough to be considered constant during at least one OFDM frame. Sufficient sync parameter stability for synchronization operations after the filterbank will be assumed throughout this work.

When deciding if the error estimation should be performed in front of or after the filterbank, the nature of the signal should also be considered. After the filterbank the signal is well defined as symbols belonging to a limited symbol alphabet plus noise. Estimation algorithms which in some manner utilize information about the symbol alphabet should thus be performed after the filterbank. The signal in front of the filterbank in an OFDM receiver is not well related to the symbol alphabet, but other features of the signal can be exploited. In the case of rectangular pulses with guard interval, the signal in front of the filterbank will contain repeated sequences, which can be used by estimation algorithms, Chapter 2.4.1.

One criterion for choosing correction before or after the receiver filterbank is complexity. Observing the received signal, the consequence of a sync parameter error can be modelled as a mathematical operation performed on the transmitted signal. This mathematical operation might differ for observation before and after the filterbank. The complexity of performing the inverse operation, i.e. correction, before or after the filterbank may thus differ, excluding one of the alternatives.

3.3 Synchronization modi

To optimize the synchronizer it can be advantageous to divide the synchronization into two steps or modi:

- Acquisition
- Tracking

After a total synchronization loss during operation or at system start-up, the carrier frequency is only known to be inside a specified frequency range, while carrier phase and timing are totally unknown. During acquisition mode these relatively large sync parameter errors are reduced to zero average. Tracking mode equals ordinary system operation where sync parameter deviations are tracked.

One synchronization algorithm can cover both modi, or specialized algorithms can be adopted for each mode. If separate algorithms area applied, the acquisition algorithms should be optimized for fast convergence and large lock-in range, i.e. the maximum error the synchronizer can correct. The steady state performance of the acquisition algorithms need only to be good enough to ensure that the residual parameter errors are inside the lock-in range of the tracking algorithms. The task of the tracking algorithms is then to reduce the errors to a level sufficiently low for average system operation, and track the deviations during system operation. The important features of the tracking algorithms are thus low residual error variance and ability to follow time variations in the sync parameters.

3.4 Synchronization algorithm classes

Both acquisition and tracking algorithms can be divided into three classes.

- Data Aided (DA): The error estimates is based on known symbols in the transmitted sequence, (pilot symbols).

- Decision Directed (DD): The transmitted symbols are unknown, but the decisions are used as estimates of the transmitted sequence in the error estimation.

- Non Data Aided (NDA): The error estimates are based on extraction of statistical properties from the received signal. Generally, there are made no assumption in NDA algorithms about other than statistical knowledge of the transmitted sequence.

When DD methods are used for acquisition, the decisions are generally erroneous and the algorithms will work based on statistical properties of the signal, it can thus be advocated that DD acquisition algorithms are NDA algorithms.

DA and DD methods exploits knowledge or estimations of the transmitted symbol sequence. In front of the receiver filterbank in OFDM systems, the signal is a complicated function of the transmitted symbols, thus excluding error estimation in front of the filterbank for DA and DD methods.

Introducing pilots will reduce system capacity or increase bandwidth and power consumption. But pilots will also decrease acquisition time considerably and increases the ability to follow time variations. During tracking, NDA algorithms will suffer from a higher residual error variance than DA and DD algorithms, (Mengali and D'Andrea 97).

3.5 Carrier synchronization

Receiver carrier and transmitter carrier are generated from local oscillators. The oscillators are not phase synchronous, creating an arbitrary phase error θ. At the same time, deviations from the nominal oscillators values will create a carrier frequency offset (CFO) (A pure Doppler shift generates the same effects.):

$$\Delta f = f_{Tc} - f_{Rc} \tag{3.1}$$

f_{cR} Receiver carrier frequency.

f_{cT} Carrier frequency of received signal.

Δf: Carrier frequency offset, CFO.

The maximum size of the CFO at start-up is given by the specification of oscillator accuracy in transmitter and receiver. For proper system operation, the receiver must synchronize/lock its carrier phase and frequency to the carrier of the transmitter.

Phase noise

In addition to frequency and phase error, there will be short time variations in transmitter and receiver oscillators creating phase noise, reducing system performance. This is not the scope of this work. The effect of phase noise in rectangular pulse OFDM systems is analysed in (Pollet et. al 95) and (El-Tanany and Wu 97).

3.5.1 Carrier phase acquisition

There is no difference in the principles of carrier phase synchronization for OFDM and SC systems, Chapter 5.3, and known algorithms for SC phase synchronization can be applied, (Meyr et. al 98), (Mengali and D'Andrea 97) and (Lee and Messerschmitt 94). Algorithms for carrier phase acquisition is not treated in detail in this work. Two observations are made. DA carrier phase tracking have a lock-in range of $\pm\pi$ and need no separate acquisition algorithm, Chapter 5.3.1. A NDA phase error estimator suitable for carrier phase acquisition is given by Equation 4.10. The error estimation is performed after the receiver filterbank and is suitable for feedback solutions.

3.5.2 Carrier phase tracking

Carrier phase tracking using pilots

As mentioned above, a DA carrier phase synchronization algorithm, will perform both acquisition and tracking. Since DA algorithms are symbol based, phase error estimation should be performed after the receiver filterbank. At the same time, phase error correction equals a complex multiplication independent of if it is performed before or after the filterbank, Chapter 5.3. DA phase tracking is thus well suited for feed forward solutions after the filterbank, Figure 3.1b. Due to multipath transmission channels, it is advantageous to perform phase correction after the receiver filterbank for feedback solutions as well, Chapter 5.3. The resulting feedback phase synchronizer is shown in Figure 3.2b. With DA phase tracking in OFDM, only a few

subchannels contain pilots. The correction for the intermediate subchannels must be interpolated from the pilot channels. DA carrier phase tracking is discussed in Chapter 5.3.1.

Carrier phase tracking without the use of pilots

During tracking, reliable decisions can be assumed available, making DD methods possible, NDA methods are excluded due to lower tracking performance, (Mengali and D'Andrea 97). While DA phase synchronization can be both feed forward and feedback, it is in the nature of DD solutions to be feedback (unless intermediate decisions are used). With the same arguments as for the DA algorithms, the preferred structure is the one of Figure 3.2b, a phase locked loop (PLL) placed after the filterbank. DD carrier phase tracking is covered in Chapter 5.3.2 through Chapter 5.3.5.

3.5.3 Carrier frequency acquisition

Before frequency acquisition, the CFO can be in the range of several subchannels in an OFDM system. It is the task of the acquisition algorithm to reduce the CFO to a fraction of a subchannel bandwidth.

Carrier frequency acquisition using pilots

Like any symbol based error estimation, DA carrier frequency acquisition must perform the error estimation after the receiver filterbank. The consequence of a CFO, observed after the filterbank, is inter channel interference (ICI), Chapter 3.7. The inverse operation would be quite complex. On the other hand the CFO can easily be corrected in front of the filterbank, either by adjusting the oscillator frequency or by time discrete complex exponential multiplication after the A/D conversion. The preferred DA carrier frequency acquisition structure, is thus the feedback synchronizer of Figure 3.2c. Assuming the tracking algorithm to be DA as well, the lock-in range of the tracking algorithm will almost be comparable with the subchannel spacing, allowing a quite high steady state variance of the DA acquisition algorithm. DA acquisition algorithms are not covered in this work, but examples are found in (Clasen and Meyr 94), (Lambrette et. al 97a) and (Speth et. al 98).

Carrier frequency acquisition without the use of pilots

Assuming no reliable decisions due to large CFO, this case is limited to NDA solutions. Similar to the DA case, correction should be made in front of the receiver filterbank due to complexity considerations. The error estimation can be performed both in front of and after the filterbank. Assuming low performance of the NDA error estimator, averaging over a large number of error estimates will be necessary.

The feedback solutions, i.e. frequency locked loops (FLL), of Figure 3.2 a) and c) will thus be suitable. Assuming the tracking algorithm to be DD, the acquisition algorithm must reduce the CFO to a small fraction of a subchannel bandwidth where reliable decisions are available. Examples of NDA acquisition according to Figure 3.2a is found in (Moose 94) and (Van de Beek et. al 97). Carrier frequency acquisition according to Figure 3.2c is found in (Daffra and Chouly 93), (Oh et. al 96) and Chapter 4 of this work.

3.5.4 Carrier frequency tracking

During carrier frequency tracking, it can be assumed that reliable decisions or pilots are available. Both solutions include the use of symbol based frequency error estimation, i.e. the frequency error estimation should be performed after the receiver filterbank. At the same time, the frequency error correction should be performed in front of the filterbank as discussed above. The resulting structure, is thus the structure of Figure 3.2c, independent of the use of pilots or not.

Since the carrier frequency is the derivative of the carrier phase with respect to time, it is possible to perform carrier tracking just by performing carrier phase tracking in SC systems. OFDM systems with estimation after the filterbank, will produce error estimates at maximum rate of $1/T$. If only phase synchronization was performed at this rate, the mean CFO could be removed, but the CFO in each frame would not be removed resulting in ICI, Chapter 3.7. Estimation after the filterbank in OFDM systems will thus enforce separate carrier phase and frequency tracking. Using a feedback frequency synchronization loop with correction in front of the filterbank, the phase synchronization will be placed inside the frequency loop. A sketch of a carrier synchronization solution with feedback phase loop is shown in Figure 3.3.
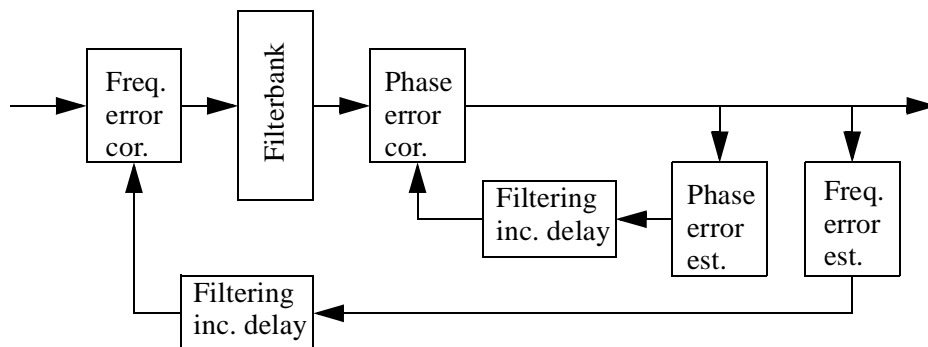
Figure 3.3. *Sketch of carrier phase and carrier frequency synchronization loops in OFDM.*

In differentially encoded systems phase synchronization will not be used.

Carrier frequency tracking using pilots

In DA carrier tracking, the CFO estimate will be averaged over the pilot channels, and used for correction in front of the filterbank. Due to correction in front of the filterbank and error estimation after the filterbank, feed forward solutions are not available. Since DA carrier tracking use known symbols, the lock-in range of the algorithm is comparable with the subchannel bandwidth of the OFDM system. A solution to DA carrier frequency tracking is found in (Clasen and Meyr 94). This is the same DA solution which is discussed in Chapter 5.4 of this work.

Carrier frequency tracking without the use of pilots

Due to the difference in performance, DD tracking is preferred compared to NDA tracking, (Mengali and D'Andrea 97). Comparing DD and DA tracking algorithms, the DA pilot sequences can be tailored to have good synchronization properties, which can not be done with the data sequence used for synchronization in DD algorithms. The strength of the DD algorithms comes from the possibility to average the error estimates over all subchannels, compared to a subset of channels, which is the case of the DA algorithms. The DD tracking is discussed in Chapter 5.4.

3.6 Timing recovery in OFDM

In OFDM systems with time discrete filtering, Figure 2.5, timing can be divided in sampling (instant) recovery and frame synchronization. Sampling recovery refers to the sampling instant in the high rate sampling process at the A/D converter, while frame synchronization refers to grouping samples belonging to one OFDM frame. It is important to note that the samples at this stage can not be viewed as symbols from the transmitter symbol alphabet plus noise. Frame synchronization (error) can be viewed as timing (error) with resolution T/N. For OFDM systems using square pulses and guard interval, frame synchronization errors smaller than the guard interval is tolerated, while sampling recovery is not necessary, (Speth et. al 98). The timing error will only result in a phase error which depends on the channel number. For systems without guard interval, the frame synchronization must be correct, while a sampling instant error will give a small amount of IBI in addition to a channel dependant phase error.

In OFDM systems with analog filtering in each subchannel, timing is performed at the low sampling rate with one sample per OFDM frame. The samples consist of symbols from the transmitter symbol alphabet plus noise. There is no frame synchronization in such a system.

(Van de Beek et. al 97) carries out frame synchronization for OFDM systems with guard interval by exploiting that a guard interval equals a cyclic extension of an OFDM frame. The synchronizer consists of a sliding correlator and a peak detector. Maximum correlation is obtained when correlating the cyclic extension at the front of the OFDM frame with the original data at the end of the frame, thus identifying start and stop of the frame. The method works both for acquisition and tracking. Several related methods based on guard intervals or other kinds of signal repetition are proposed, (Palin and Rinne 98), (Mochizuki et. al 98) and (Negi and Cioffi 98). Pilot based frame acquisition and tracking have been proposed by (Warner and Leung 93), (Schmidl and Cox 97), (Speth et. al 97) and (Speth et. al 98), while (Lambrette et. al 97b) have proposed both DA and NDA SC frame synchronization algorithms which can be modified for use with OFDM.

A decision directed symbol timing algorithm for tracking mode has been proposed by (Kang et. al 94). The algorithm is based on the observation that a small timing mismatch results in a phase error which is increasing with channel number. Estimates of the phase change between neighbouring channels can be used for calculating the timing error. An algorithm for maximum likelihood estimation of timing error with analog per channel filtering for O-QAM is found in (Hirosaki 84).

Analysis of the consequences of timing error is given by (Speth et. al 98), (Pollet and Moencleclaey 95) and (Chang and Gibby 68).

3.7 Effects of carrier frequency offset in OFDM

During the calculations of the received signal in Chapter 2 it was assumed flat channel, no noise and no CFO, $\Delta f = 0$. Under these conditions the received symbols are identical to the transmitted symbols, Equation 2.4, 2.9 and 2.10. In this chapter, the effect of $\Delta f \neq 0$ will be discussed qualitatively. Quantitative discussions are left for Chapter 6.

3.7.1 Phase slipping

In this work, phase slipping is used about phase errors, θ, large enough to create decision errors in even noiseless systems, i.g. for 4-QAM: $|\theta| > \pi/4$. One reason for phase slipping in coherent receivers is insufficient carrier phase synchronization. Another reason for phase slipping is to large CFO when using feedback carrier phase synchronization, i.g. for 4-QAM $|\Delta f| > 1/(8T)$. This is a problem even for differential encoded systems. The tolerated CFO with respect to phase slipping depends on

the inverse of the symbol length. Since OFDM systems have symbols lengths N times larger than SC systems, the tolerated CFO is reduced with a factor N in OFDM systems compared to tolerated CFO in SC systems.

3.7.2 Carrier offset with QAM and Rectangular pulses

The CFO behaviour of OFDM systems with QAM and rectangular pulses are similar for systems with and without guard interval, only systems without guard interval will be discussed. Including the CFO in Equation 2.4, neglecting the noise, the received signal with a non time dispersive channel is given by Equation 3.2

$$z_{k,m} = \frac{1}{T} \sum_{n=0}^{N-1} a_{k,n} \int_0^T e^{j\frac{2\pi}{T}(n-m+\Delta fT)\tau} d\tau \tag{3.2}$$

$$= \sum_{n=0}^{N-1} a_{k,n} \frac{\sin(\pi(n-m+\Delta fT))}{\pi(n-m+\Delta fT)}(-1^{(n-m)})e^{j\pi\Delta fT}$$

Like in the case of no CFO, the received symbols in frame k are only influenced by symbols transmitted in frame k. Since the pulse length equals just one symbol interval T no ISI can be created by a frequency shift.

For zero CFO there will be no ICI either, mathematically stated in Equation 2.4 with zero contribution for $m \neq n$. Studying Equation 3.2 reveals that this is not the case for $\Delta f \neq 0$. A related situation to no CFO is when ΔfT is an integer, i.e. the CFO equals an integer number of subchannel bandwidths. No ICI is created but the output has been moved ΔfT channels compared to the input (a subchannel offset of ΔfT channels)

$$z_{k,m} = a_{k,m-\Delta fT} \qquad \Delta fT \ Integer \tag{3.3}$$

Usually the carrier offset is not an integer number of subchannel bandwidths. In this case the integration in Equation 3.2 is not equal to zero for any value of n and the received symbol will be a sum of contributions from all the channels, generating ICI.

3.7.3 Carrier Offset with O-QAM

The received symbol in an O-QAM OFDM system is given by Equation 2.9 and 2.10. Inserting CFO gives a sampled real part equal to

$$Re\{z_{k,m}\} = \sum_{n=0}^{N-1} \sum_{l=0}^{\infty} \int_{-\infty}^{\infty} Re\{a_{l,n}\} h(t-lT) h(t-kT) \tag{3.4}$$

$$\cdot \cos\left(\left(\frac{2\pi}{T}t + \frac{\pi}{2}\right)(n-m) + 2\pi\Delta f t\right) dt$$

$$-\sum_{n=0}^{N-1} \sum_{l=0}^{\infty} \int_{-\infty}^{\infty} Im\{a_{l,n}\} h\left(t-lT+\frac{T}{2}\right) h(t-kT)$$

$$\cdot \sin\left(\left(\frac{2\pi}{T}t + \frac{\pi}{2}\right)(n-m) + 2\pi\Delta f t\right) dt$$

Similarly, the sampled imaginary part will be equal to

$$Im\{z_{k,m}\} = \sum_{n=0}^{N-1} \sum_{l=0}^{\infty} \int_{-\infty}^{\infty} \left(Im\{a_{l,n}\} h(t-lT+\frac{T}{2}) h(t-kT+\frac{T}{2}) \right. \tag{3.5}$$

$$\cdot \cos\left(\left(\frac{2\pi}{T}t + \frac{\pi}{2}\right)(n-m) + 2\pi\Delta f t\right) \Big) dt$$

$$+\sum_{n=0}^{N-1} \sum_{l=0}^{\infty} \int_{-\infty}^{\infty} Re\{a_{l,n}\} h(t-lT) h(t-kT+\frac{T}{2})$$

$$\cdot \sin\left(\left(\frac{2\pi}{T}t + \frac{\pi}{2}\right)(n-m) + 2\pi\Delta f t\right) dt$$

Before the introduction of a CFO, the integrands in Equation 2.9 and 2.10 with substitution of integration variable, where odd functions except for $(l = k) \wedge (n = m)$ and correct quadrature. Since the integration of odd functions from $-\infty$ to ∞ is zero there will be no ICI and no ISI. When the CFO equals an integer number of subchannel bandwidths, the integrands will still be odd functions avoiding both ISI and ICI, but the output will be shifted a number of channels compared to the input. This is the same behaviour as for QAM with rectangular pulses, Equation 3.3. With a CFO not equal to an integer number of subchannel bandwidths, the integrands will not be odd functions of time resulting in non zero integrals, i.e. each output symbol will be a sum of several input symbols. Since all the O-QAM pulse shapes which we are going to study are of length more than one symbol and bandwidth more than one subchannel bandwidth, they will all exhibit both ISI and ICI under the influence of a CFO.

3.7.4 Interference components due to CFO

How many symbols and channels which contribute to the interference in a given channel in a given frame, will differ between the different OFDM systems. A CFO in a QAM system with rectangular pulses will only generate ICI since the pulse duration is limited to one symbol interval. Rectangular pulses have infinite bandwidth and thereby ICI contributions from all the channels in the OFDM filterbank. In a practical context, contributions below a given level will not be of significance, but since the spectral sidelobes of the rectangular pulses are slowly decaying, the ICI contributions from a large number of channels must be accounted for.

In O-QAM systems, bandlimited pulses will receive ICI only from the closest channels, but the infinite extension of the pulses in time gives ISI from an infinite number of symbols. As in the case of the ICI for rectangular pulses, practical considerations will limit the number of symbols which give significant contributions to the ISI. O-QAM pulses of finite length will limit the number of symbols contributing to the ISI to a number similar to the pulse length, but finite pulse length gives infinite bandwidth and ICI from all the channels. Like in the case of QAM and rectangular pulses, practical considerations will limit the number of channels giving contributions to the ICI. Assuming that the spectra of the finite length O-QAM pulses are decaying faster than the spectra of the rectangular pulses, the ICI in an O-QAM system will be com-
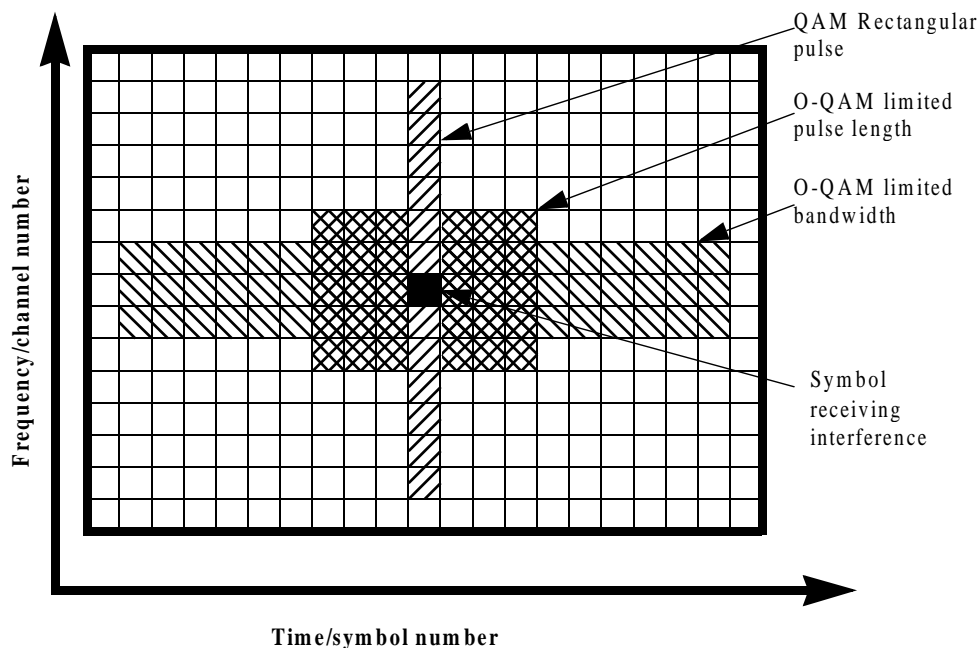
Figure 3.4. *Areas giving significant IBI contribution for different OFDM systems*

posed of contributions from less channels than in a rectangular pulse QAM system. A schematic illustration of where the IBI comes from is given in Figure 3.4.

To the receiver, interference is noise reducing the system performance.

3.8 OFDM on flat fading channels

The flat fading channel described in Chapter 2.6 can be viewed as a generalization of a CFO. A CFO viewed in the frequency domain equals a shift, or a convolution with a dirac, $\delta(f - \Delta f)$. A flat fading channel equals a convolution with the Doppler spectra of the time varying channel. While the CFO just shifts the signal spectra in the frequency domain, the fading channel creates a frequency dispersion, (Steele 92).

Including the time varying channel, neglecting the noise, the received signal in a rectangular pulse OFDM system equals

$$z_{k,m} = \frac{1}{T} \sum_{n=0}^{N-1} a_{k,n} \int_0^T c(t) e^{j\frac{2\pi}{T}(n-m+\Delta fT)\tau} d\tau \tag{3.6}$$

Even with no CFO $\Delta f = 0$, the integral will generally not equal zero creating ICI. In addition there will be a time varying signal power due to the fading channel. However if $c(t)$ is changing so slowly that it can be viewed as constant over one frame no ICI is created, but the OFDM receiver will still experience a slowly time varying or fading signal power.

For O-QAM systems, observations which are similar to the observations made for systems with QAM and rectangular pulses can be made.

Chapter 4
Carrier frequency acquisition in OFDM

During system start-up or after a total synchronization loss, the carrier phase is totally unknown while the carrier frequency is known to be inside a region given by receiver and transmitter oscillator accuracy. Typically this region can be several times larger than the subchannel spacing in an OFDM system. It is the task of the carrier acquisition algorithm to reduce the carrier error to a level where carrier tracking algorithms can operate. Carrier tracking algorithms are discussed in Chapter 5.

The acquisition methods presented in this work will be intended for high capacity, spectral efficient OFDM systems, for example fixed radio links. With strong spectral requirements, pilots and guard interval should, if possible, be avoided in order to achieve high bandwidth efficiency. During acquisition, reliable decisions do not exist, thus leaving us with NDA methods. The disadvantage of NDA compared to DA algorithms, is increased acquisition time, (Mengali and D'Andrea 97). NDA algorithms are thus best suited for systems with continuous time transmission, while other solutions should be sought for burst transmission systems. Most existing carrier acquisition algorithms for OFDM use pilots or other redundant signalling. In this work NDA acquisition algorithms will be developed. The focus is on carrier frequency acquisition, while only references to carrier phase acquisition are given. The algorithms are presented for use with QAM and square pulses, but they can be modified to operate with O-QAM and other pulse shapes.

In addition to spectral efficiency, low receiver complexity is an important issue. The few existing NDA carrier acquisition algorithms assume receivers with over sampling or double set of filterbanks. The algorithms developed in this work are blind acquisition algorithms with critically $(1/T)$ sampling both in front of and after a single receiver filterbank. All algorithms are feedback solutions with carrier estimation after the filterbank and carrier correction in front of the filterbank. The reference

carrier frequency acquisition algorithm in this chapter will be the blind ML algorithm by (Daffra and Chouly 93) with critically sampling and double set of filterbanks in the receiver. Algorithms related to the acquisition algorithms presented in this work, are found in (Remvik and Holte 96) and (Remvik and Holte 97a).

This chapter is organized as follows: Chapter 4.1 previous work. Chapter 4.2 discuss ambiguity when no pilots are used. In Chapter 4.3 a Maximum Likelihood based carrier frequency acquisition algorithm is presented as reference algorithm. A Mueller and Müller motivated carrier frequency acquisition algorithm is developed in Chapter 4.4, while a Bussgang motivated algorithm is developed in Chapter 4.5. In Chapter 4.6 the performance of the acquisition algorithms, measured in acquisition time, is simulated. Chapter 4.7 is an introduction to gear shift algorithms and Chapter 4.8 contains a summary.

4.1 Previous work

Pilot based carrier frequency acquisition in OFDM systems with square pulses are presented in the literature by (Clasen and Meyr 94), (Lambrette et. al 97a) and (Speth et. al 98). NDA algorithms for the same purpose are given by (Daffra and Chouly 93) and (Oh et. al 96). NDA algorithms with special demands to the transmitted OFDM signal is presented by (Moose 94), (Van de Beek et. al 97) and (Dinis and Gusmao 97).

4.2 Channel number ambiguity without pilots

4.2.1 Channel number offset

As stated in Equation 3.3, a carrier frequency offset equal to an integer number I of subchannel bandwidths will not create IBI, but rather result in a subchannel offset of I channels. This is a "legal" solution in the sense that the input to the decision devices equals transmitted symbols plus channel noise. This will be referred to as the carrier frequency being locked on to the frequency grid with a channel number offset. The frequency grid consists of the single correct carrier frequency and all frequencies an integer number of subchannel bandwidths away from the correct frequency. The reference carrier frequency acquisition algorithm in Chapter 4.3 is an example of an algorithm with all its lock points on the frequency grid. The locking points equals the zero crossings with positive gradient of the error function in Figure 4.2. So even though the algorithm may give "false locking" in the sense that it

locks on to an other frequency than the single correct carrier frequency, the algorithm will always lock on to the frequency grid. The other carrier frequency acquisition algorithms presented below will also lock on to the grid, but not necessarily at the single correct carrier frequency, and thus need channel number offset correction after frequency grid locking.

4.2.2 Methods to correct channel number offsets

Adopting the OFDM system of Chapter 2.4.3 with guard channels, the receiver should only observe channel noise in the guard channels. With N data channels and locking on to the frequency grid with an offset of I channels, data channel number 0 to $I-1$ will contain zero signal power, while the I guard channels outside data channel $N-1$ will contain signal power, assuming I to be positive. If it is possible to detect the number of data channels not containing signal power and the number of guard channels containing signal power, the carrier frequency can be corrected to remove the channel number offset. The "power measurement" is the same as the per channel power correction necessary for equalization in OFDM, (Sari et. al. 95), and the necessary information for channel number offset correction can thus be viewed as available.

Two alternative solutions are based on the observation that reliable detections are available despite of the channel number offset, i.e. the decisions are reliable but the correct subchannel number for the symbol is unknown. Channel number offset is thus similar to symbol stream synchronization in SC systems. One possibility is the use of unique words. The other one is use of error correcting channel coding with synchronization, (i.e. offset), information, (Ytrehus 97). Channel coding with synchronization information is error correcting coding with the additional property that it contains information about positioning in the symbol stream. When this is used for detection of channel number offsets in OFDM, the coding must be performed across the subchannels.

4.3 Maximum Likelihood carrier frequency estimation

A method for NDA ML estimation of carrier frequency offset in OFDM systems has been developed by (Daffra and Chouly 93). The method assumes the use of guard channels and two filterbanks in the receiver. The input to the extra filterbank is preprocessed while the output of the extra filterbank, $\dot{z}$, is correlated with the output of the ordinary filterbank, z, to generate the gradient ε of the likelihood function,

(Daffra and Chouly 93). The likelihood function is maximized by updating the CFO estimate by the use of a gradient algorithm, Equation 4.3. The preprocessing is made according to Figure 4.1
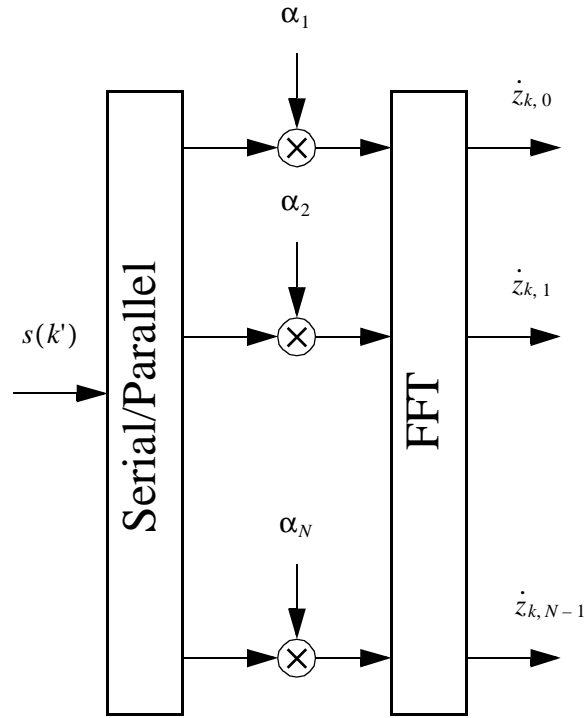
Figure 4.1. *The extra filterbank with preprocessing, used in the NDA carrier frequency acquisition technique of (Daffra and Chouly 93)*

The weight values equals:

$$\alpha_n = -j2\pi(n-1) \tag{4.1}$$

And the estimated gradient of the likelihood function equals:

$$\varepsilon_{D,k} = \sum_{m=0}^{N-1} Re\{z_{k,m}\dot{z}^*_{k,m}\} \tag{4.2}$$

$\varepsilon_{D,k}$: The estimated gradient of the likelihood function of frame k, from now on termed the Daffara error function of frame k

The S-curve of the error function, $E[\varepsilon_{D,k}]$, is calculated according to (Daffra and Chouly 93) and is plotted in Figure 4.2 for $N = 256$ channels.
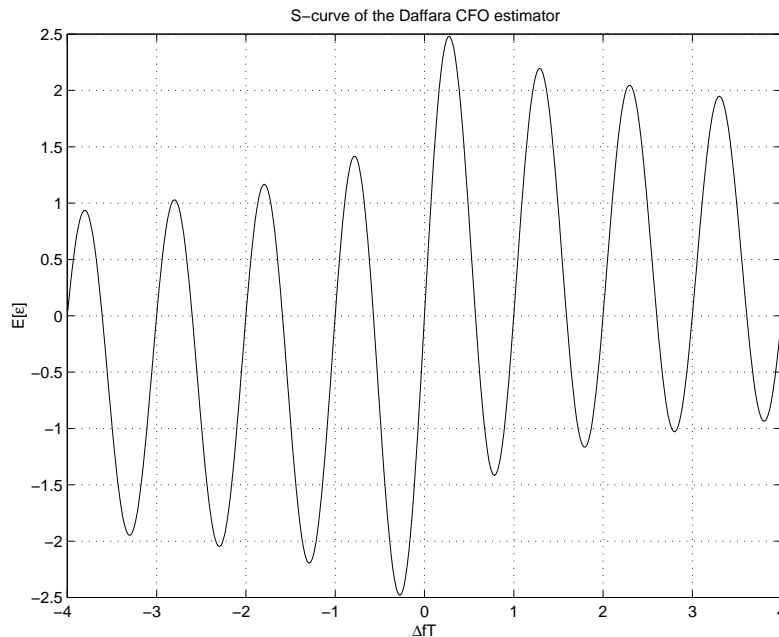
Figure 4.2. *S-curve of the Daffara CFO estimator for N=256 channels, unity transmitted power and unity symbol interval*

Possible lock points for the gradient algorithm of Equation 4.3 equals zero crossings with positive gradient in the S-curve. According to Figure 4.2 the lock-in range of the proposed acquisition algorithm is approx. $\Delta f = \pm 0.5/T$. Larger frequency errors will give locking on to other frequencies in the frequency grid. A modification of the error function by (Daffra and Chouly 93) has been proposed to obtain larger lock-in range at the cost of reduced performance measured as steady state variance. This modification is not discussed here, since the lock-in range can be increased by accepting locking to other frequencies in the frequency grid, and correcting the offset by the methods of Chapter 4.2.

The recursive CFO estimate updating equals:

$$\Delta \hat{f}_{k+1} = \Delta \hat{f}_k - \mu_D \varepsilon_{D,k} \tag{4.3}$$

μ_D: LMS algorithm step size for the Daffara algorithm

4.4 Mueller and Müller motivated carrier frequency synchronization

4.4.1 Properties of carrier offset generated inter bin interference

The received, sampled signal $z_{k,m}$ with CFO and no channel noise in an OFDM system using square pulses and QAM was given by Equation 3.2. Including AWGN on the channel and correcting the phase at the signal component $a_{k,m}$, the received sampled signal can be rewritten as:

$$z_{k,m} = \sum_{n=0}^{N-1} a_{k,n} \text{sinc}(n - m + \Delta fT)(-1)^{n-m} + n_{k,m} \tag{4.4}$$

Since this is pure ICI, the frame number index k can be dropped for convenience.

In the case of a SC system transmitting N symbols over a non time dispersive channel, the received symbol number m can be written as a function of the symbol timing error τ, (Lee and Messerschmitt 94):

$$z(m) = \sum_{n=0}^{N-1} a(n) p((m-n)T + \tau) + n(m) \tag{4.5}$$

$p(\ )$: Convolution of transmitter and receiver and should thus fulfill the Nyquist criterion, (Lee and Messerschmitt 94)

T: SC symbol interval

Recognising $\text{sinc}(-(m-n-\Delta fT))(-1)^{n-m}$ as a sampled version of a function fulfilling the Nyquist criterion, the correction of the frequency error $-\Delta fT$ in a critically sampled OFDM system equals the correction of a timing error τ in a baud rate sampled SC system. The same basic methods used for SC timing recovery can be used for carrier frequency correction in OFDM.

The output $z(m)$ equals the convolution of the transmitted sequence $a(m)$ and a filter $h(m)$ whose response is a function of the CFO. As an example $h(m)$ is plotted in Figure 4.3 for $N = 64$ with $\Delta fT = -0.05$ and $\Delta fT = 0.3$.
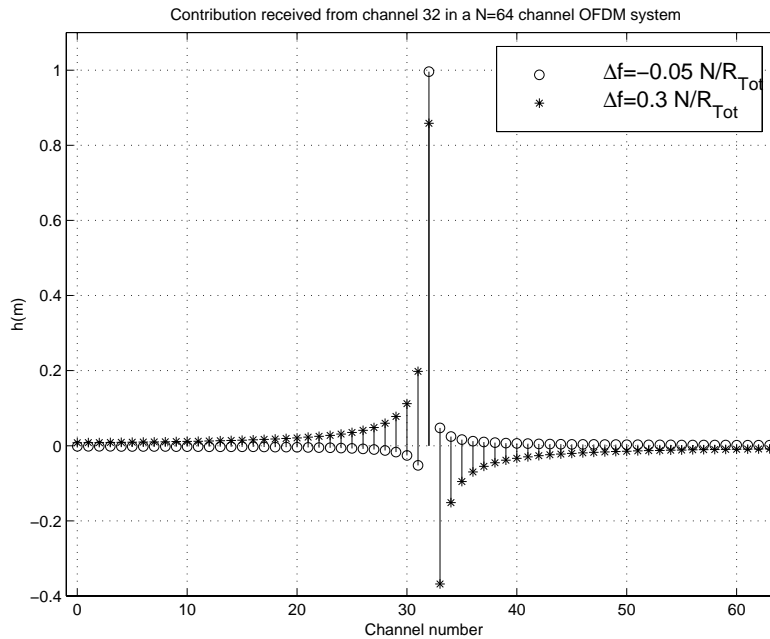
Figure 4.3. *IBI contribution from channel* 32 *in a N* = 64 *channel OFDM system with CFO of* −0.05 *and* 0.3 *subchannel bandwidths*

The results here are based on the continuous time square pulse filterbank, but the results are also valid for the symmetrical sampled IFFT/FFT given by Equation 2.14. Using the ordinary IFFT/FFT filterbanks, Equation 2.13, the unsymmetrical sampling will introduce an imaginary component in the output, $z(m)$, dependant on the number of channels N in the filterbank.

4.4.2 Mueller and Müller motivation

As pointed out in Chapter 4.4.1, critically carrier frequency synchronization in OFDM is related to baud rate timing correction in SC systems. One well known technique for time discrete baud rate timing in SC systems was developed by (Mueller and Müller 74), a method described in several other works, (Lee and Messerschmitt 94), (Mengali and D'Andrea 97). The method is based on a LMS algorithm for timing estimate updating, with an error function rewritten for OFDM systems. The error function is equal to:

$$\varepsilon_{M,k,m} = Re\{\hat{a}_{k,m}{}^* z_{k,m-1} - \hat{a}_{k,m}{}^* z_{k,m+1}\} \tag{4.6}$$

$\varepsilon_{M,k,m}$: Mueller and Müller based error function, channel m, frame k

In a SC timing problem, the timing estimate would be updated for each increment of m. For carrier synchronization in OFDM, a carrier estimate update for each m, or channel, would require N calculations of the receiver filterbank output per frame. Instead of per channel updating, the carrier frequency estimate is updated once per frame with an error function averaged over all subchannels:

$$\varepsilon_{M,k} = \frac{1}{N} Re \left\{ \sum_{m=0}^{N-1} \hat{a}_{k,m}{}^* z_{k,m-1} - \hat{a}_{k,m}{}^* z_{k,m+1} \right\} \tag{4.7}$$

$\varepsilon_{M,k}$: Mueller and Müller based error function, frame k

The sign of the error function is reversed compared to the original algorithm of (Mueller and Müller 74) to keep the gradient positive at the zero crossing similar to the error function of the Daffara algorithm, Chapter 4.3. The error function, or S-curve, is plotted below in Figure 4.4 under the assumption of correct decisions and zero phase error.
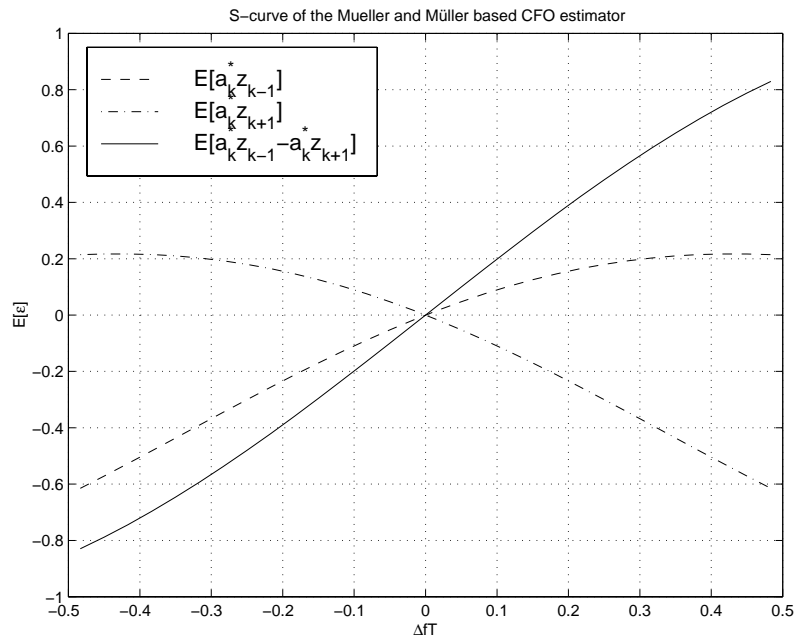
Figure 4.4. *S-curve of the Mueller and Müller based CFO estimator for* $-0.5 < \Delta fT < 0.5$ *with perfect decisions and zero phase error*

Using a LMS algorithm for CFO estimate updating, the estimated CFO equals:

$$\hat{\Delta f}_{k+1} = \hat{\Delta f}_k - \mu_M \varepsilon_{M,k} \tag{4.8}$$

μ_M : Step size with Mueller and Müller based acquisition

In the area of $-0.5 < \Delta fT < 0.5$ there will be an unique locking point, which make the LMS algorithm drive the CFO to zero.

4.4.3 Acquisition with erroneous decisions

The S-curve of Figure 4.4 assumed perfect decisions and zero phase error. Usually these assumptions are not valid during carrier frequency acquisition. Before the acquisition algorithm has brought the CFO close to the frequency grid the decisions will be unreliable due to a high level of IBI and random phase errors. Random phase errors and erroneous decisions are included in Figure 4.5. The zero crossings with positive gradient of the S-curve are still located at CFO's equal to an integer number of subchannel bandwidths, placing its lock points on the frequency grid.
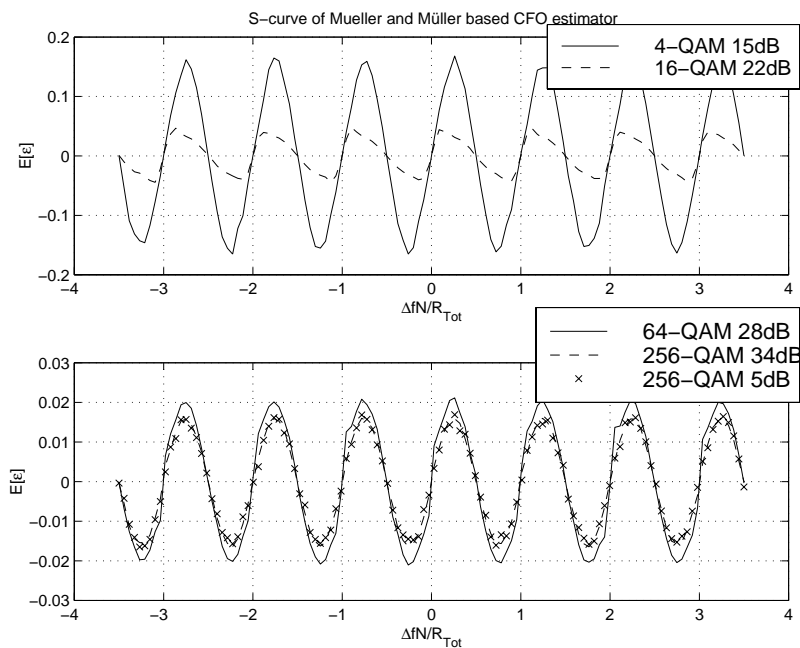
Figure 4.5. *S-curve of the Mueller and Müller based CFO estimator with non perfect decisions and random phase error, N = 256 channels*

The distance between the true transmitted sequence and the output of the decision device depends on constellation size and SNR, and the S-curves may thus be changing with these parameters. The amplitude of the S-curve, Figure 4.5, is decreasing with increasing constellation size. For the given example, variations in the SNR have little influence on the S-curve amplitude. Assuming N is large, the S-curve of the proposed estimators in this chapter is close to periodic around the correct carrier frequency, with period $1/T = R_{Tot}/N$. This is in opposition to the S-curve of the estimator of (Daffra and Chouly 93), Figure 4.2. Due to the periodicity, only one period of the S-curves will be plotted for the rest of Chapter 4.

4.4.4 Acquisition with erroneous decisions and phase correction

The S-curves of Figure 4.5 is produced with random phase error in front of the decision device, corrupting the decisions even at small and zero CFO. Correcting the phase error in a feed forward manner in front of the decision device, will make the S-curve more similar to the S-curve with perfect decisions in the areas with CFO close to the frequency grid. As shown in Equation 5.10, the influence of a phase error θ in an OFDM system with QAM, rectangular pulses, flat channel and zero CFO is equal to the influence of a phase error in a SC system:

$$z_{k,m} = a_{k,m}e^{j\theta} + n(m) \tag{4.9}$$

Well known methods for NDA SC phase correction can thus be applied, one possible estimator is (Mengali and D'Andrea 97):

$$\hat{\theta}_k = \frac{1}{4}\angle\left\{\sum_{m \in \varsigma} z_{k,m}^4\right\} \tag{4.10}$$

ς: The L channels used for averaging

The estimator is unbiased for QAM modulation, with phase ambiguity of multiples of $\pi/2$. The phase ambiguity is identical to phase ambiguity during phase tracking, Chapter 5.3.2. With 4-QAM the estimator obtains Cramer Rao bound (CRB) at high SNR, while the distance to the bound increase with increasing constellation size, (Mengali and D'Andrea 97) and Chapter 5.2.

The S-curve of Equation 4.7 with phase correction in front of the estimator is shown in Figure 4.6. Correction based on the phase estimator of Equation 4.10. Averaging over a larger number of channels, the phase estimate improves and the CFO area with low SER decisions increase, Figure 4.7. In the case of time dispersive channels,
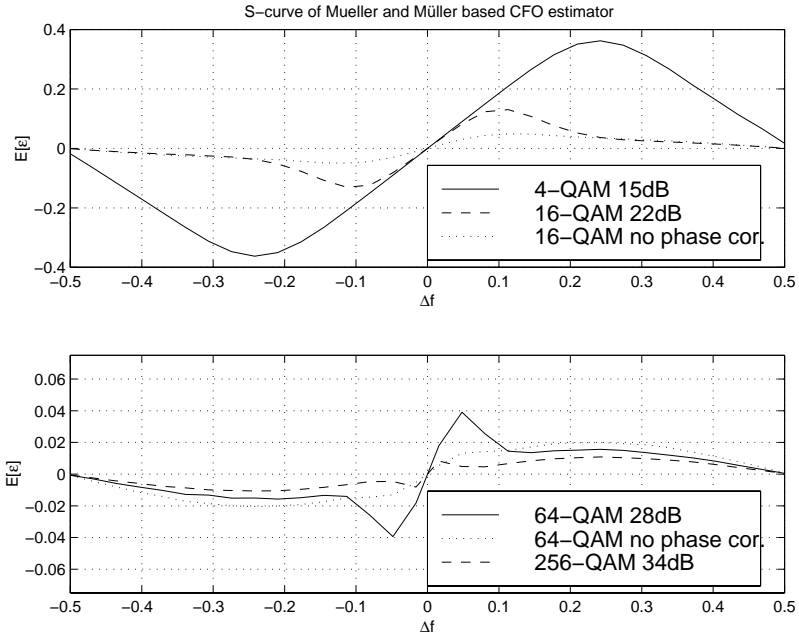
Figure 4.6. *S-curve of the Mueller and Müller based CFO estimator with phase correction in front of the decision device and non perfect decisions,* 16 *channels*
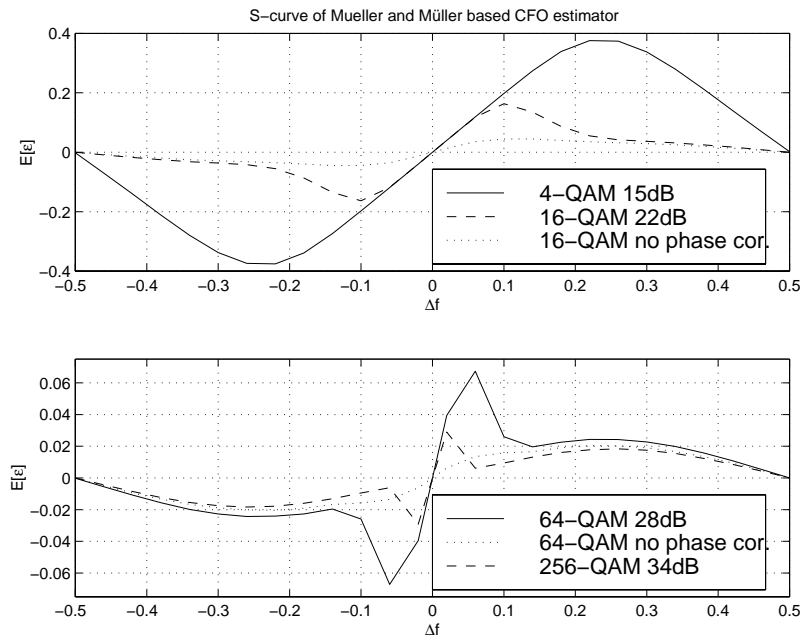
Figure 4.7. *S-curve of the Mueller and Müller based CFO estimator with phase correction and non perfect decisions,* 256 *channels*

the number of channels used for phase averaging must be limited according to the coherence bandwidth of time dispersive channels, (Steele 92).

4.5 Bussgang motivated carrier frequency synchronization

For low signal to noise plus interference ratio, transmitted symbol estimates, $\hat{a}$, will be of low quality, if generated by processing the received signal, z, with an ordinary decisions device, i.e. a slicer. During carrier frequency acquisition in OFDM the signal to noise plus interference ratio will be low due to large IBI. A better alternative under these conditions is a Bayes estimate of a, optimized for minimum mean squared error between actually transmitted symbols, a, and estimated symbols, $\hat{a}$. This yields the conditional mean estimator of Equation 4.11, (Haykin 96). It is the same estimator which is used for transmitted symbol estimation in bussgang algorithms during SC blind equalization.

$$\hat{a} = E[a|z] \tag{4.11}$$

$\hat{a}$ is not limited to the transmitted symbol alphabet in this case. Knowing the transmission alphabet and the noise statistics, $\hat{a}$ can be calculated as a function of z. Unfortunately the calculations assume knowledge about the total signal to noise plus interference ratio. Both IBI level during carrier frequency acquisition in OFDM and ISI level during blind equalization in SC are unknown. The mapping from z to $\hat{a}$ is recognized as a memoryless non linearity, several alternative memoryless nonlinearities, not depending on signal to noise plus interference ratio, have been proposed for use with bussgang algorithms. One of these proposed nonlinearities is tested in this chapter for transmitted symbol estimation during carrier frequency acquisition in OFDM.

The bussgang algorithm most widely tested, (Nikias and Petropulu 93), is the equalizer of (Godard 80). The memoryless nonlinearity, termed $g(\ )$, equals:

$$\hat{a}(m) = g(z(m)) = \frac{z(m)}{|z(m)|}(|z(m)| + R_p|z(m)|^{p-1} - |z(m)|^{2p-1}) \tag{4.12}$$

$$R_p = \frac{E[|a(m)|^{2p}]}{E[|a(m)|^p]} \tag{4.13}$$

$p \in \{1, 2\}$: Order of the Godard algorithm

Including the frame number index k and inserting the nonlinearity of the Godard algorithm, Equation 4.12, into the error function for adaptive LMS frequency estimation algorithm, Equation 4.6, the new error function based on the first order Godard algorithm equals:

$$\varepsilon_{G1, k, m} = Re\left\{\left(\frac{z_{k, m}}{|z_{k, m}|}\right)^* z_{k, m-1} - \left(\frac{z_{k, m}}{|z_{k, m}|}\right)^* z_{k, m+1}\right\} R_p \qquad (4.14)$$

The error function of the second order Godard algorithm equals:

$$\varepsilon_{G2, m} = Re\{-z_{k, m}^{*2} z_{k, m} z_{k, m-1} + z_{k, m}^{*2} z_{k, m} z_{k, m+1}\} \qquad (4.15)$$

From Equation 4.14 and 4.15 it can be observed that both Godard motivated error functions are insensitive to constant phase errors. Phase estimation during carrier frequency acquisition using the Godard motivated error functions will thus have no effect. Averaging over all subchannels in the OFDM system with one estimate update per frame, the error functions equals:

$$\varepsilon_{G1, k} = \frac{R_p}{N} \sum_{m = 0}^{N-1} Re\left\{\left(\frac{z_{k, m}}{|z_{k, m}|}\right)^* z_{k, m-1} - \left(\frac{z_{k, m}}{|z_{k, m}|}\right)^* z_{k, m+1}\right\} \qquad (4.16)$$

$$\varepsilon_{G2, k} = \frac{1}{N} \sum_{m = 0}^{N-1} Re\{-z_{k, m}^{*2} z_{k, m} z_{k, m-1} + z_{k, m}^{*2} z_{k, m} z_{k, m+1}\} \qquad (4.17)$$

The error function motivated by the second order Godard algorithm equals an unbiased estimate of the difference of two fourth order cumulants as defined by (Nikias and Petropulu 93):

$$E[\varepsilon_{G2, k, m}] = -c(z_{k, m}^{*2} z_{k, m} z_{k, m-1}) + c(z_{k, m}^{*2} z_{k, m} z_{k, m+1}) \qquad (4.18)$$

$z(m)$ can be viewed as a random white sequence, $a(m)$, filtered by an all pass filter, $h(m)$, Chapter 4.4.1. Since second order statistics, i.e. the auto correlation function, is phase insensitive, second order statistics give no information about the all pass filter $h(m)$. Fourth order cumulants on the other hand is phase sensitive and will thus contain information about the all pass filter and thus the CFO. The S-curve of the

second order Godard CFO error function is plotted below in Figure 4.8, normalized with $\left| c(a_m^4) \right|$.
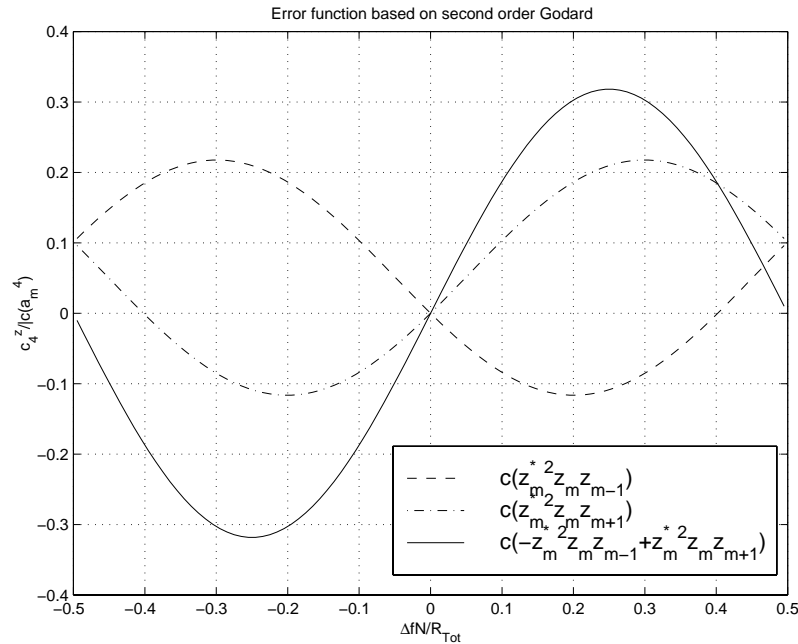
Figure 4.8. *S-curve of the second order Godard based error function*

$\left| c(a_m^4) \right|$ depends on the constellation size, $\left| c(a_m^4) \right| = 1$ for 4-QAM, $\left| c(a_m^4) \right| = 0.68$ for 16-QAM, $\left| c(a_m^4) \right| = 0.62$ for 64-QAM and $\left| c(a_m^4) \right| = 0.60$ for 256-QAM. The cumulants, and thus the S-curve of the second order Godard error function, does not depend on the SNR. The S-curve of the error function based on the first order Godard is simulated and plotted in Figure 4.9

The S-curves of first an second order Godard do have a single zero crossing with positive gradient in the area $-0.5 < \Delta fT < 0.5$, the zero crossings being located at $\Delta f = 0$. The algorithms will thus lock at the frequency grid. In contrast to the second order Godard and the Mueller and Müller based algorithms, the amplitude of the S-curve for first order Godard is reduced at low SNR.
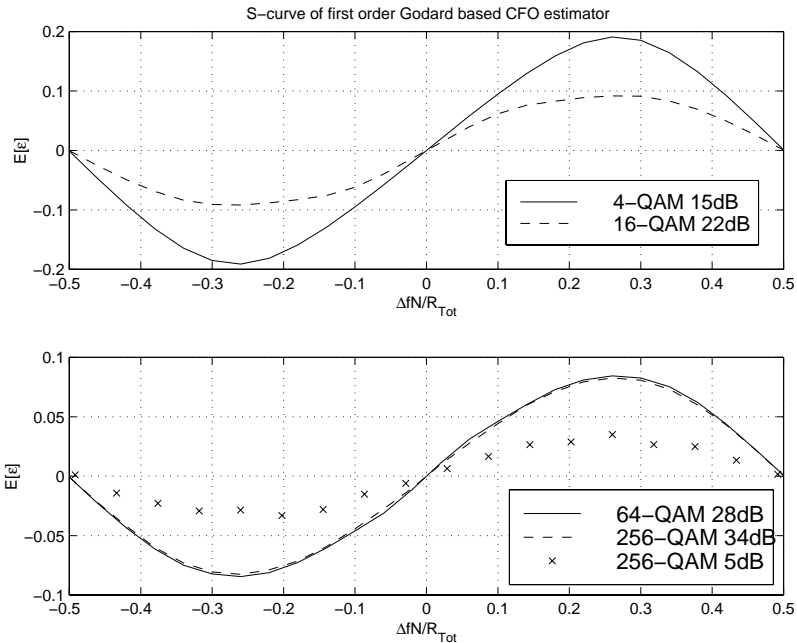
Figure 4.9. *S-curve of the first order Godard based CFO estimator, $N = 256$ channels*

4.6 Performance of the acquisition algorithms

The performance of the acquisition algorithms can be measured in number of iterations needed to reduce a CFO to an average of zero with a given steady state variance, i.e. closed loop residual CFO variance. The number of iterations needed is termed the acquisition or convergence time. Rewriting the LMS algorithms of Equation 4.3 and 4.8 for the general case, the result equals:

$$\hat{\Delta f}_{k+1} = \hat{\Delta f}_k - \mu \varepsilon_k \tag{4.19}$$

Both acquisition time and steady state variance is influenced by the error function ε and the size of the step size parameter μ. The error function behaviour is given by the working conditions like SNR, number of channels in the system, constellation size, time dispersion in the transmission channel and choice of error function algorithm, which is the only free parameter. For a given error function algorithm, the steady state variance is assumed to be a strictly monotone raising function of the step size parameter. The step size parameter is thus an unambiguous function of the

steady state variance. Steady state variance decrease with decreasing step size parameter while acquisition time increase with decreasing step size. The connection between step size parameter and steady state variance in this work is found by closed loop simulations for different step sizes.

As mentioned above, one of the parameters that steady state variance depends on, is time dispersion in the transmission channel. In Chapter 4.6.1 and 4.6.2, non time dispersive channels will be discussed, while the steady state performance for some two ray channels will be discussed in Chapter 4.6.3.

4.6.1 Performance without channel number offset

As discussed in Chapter 4.2 the carrier acquisition algorithms discussed in this work can either lock on to the single correct carrier frequency or lock on to another frequency in the frequency grid. In this sub chapter it will be assumed that the carrier locks on to the single correct carrier frequency, while in Chapter 4.6.2 the performance consequences of locking to another frequency in the grid will be discussed.

Daffara algorithm

Steady state variance for LMS carrier frequency acquisition is plotted in Figure 4.10.
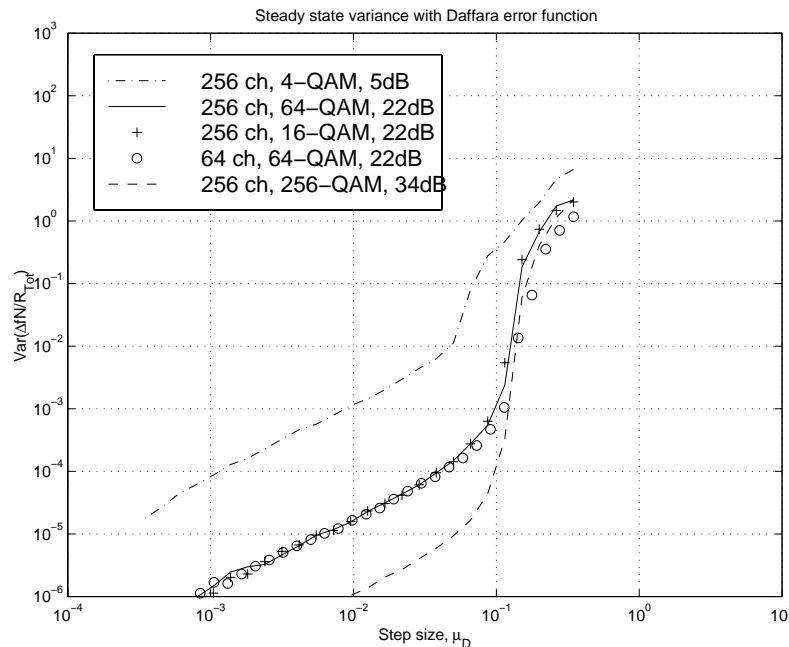
Figure 4.10. *Steady state variance as function of step size parameter with the error function of (Daffra and Chouly 93)*

The variance is given as function of step size parameter μ_D, with the error function ε_D of Equation 4.2 proposed by (Daffra and Chouly 93).

Figure 4.10 indicates that the steady state variance depends little on constellation size and number of subchannels in the OFDM system, on the other hand is it heavily dependant on SNR. At high steady state variance, the performance is close to equal for $SNR = 22dB$ and $SNR = 34dB$, while at lower steady state variance the higher SNR is superior allowing a larger step size parameter. Average acquisition is plotted below for steady state variance of 10^{-3} and 10^{-4}.
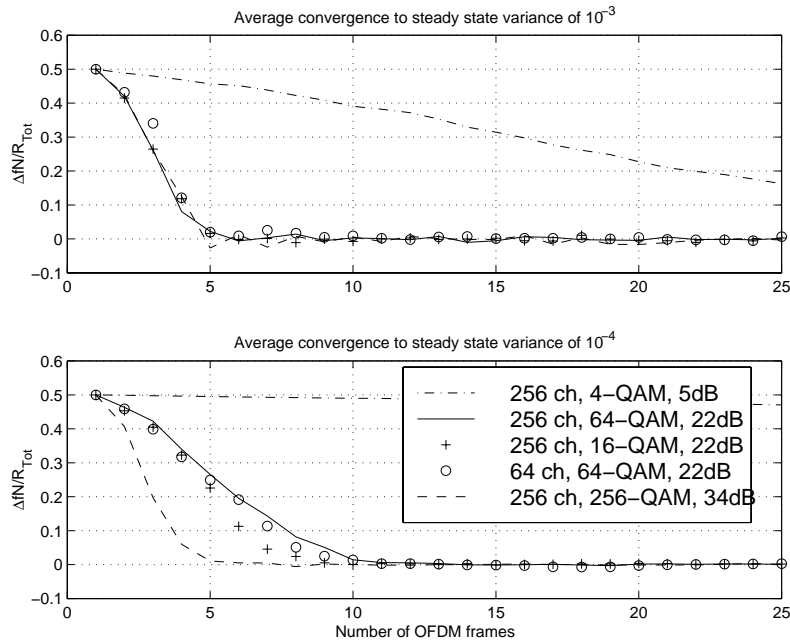
Figure 4.11. *Average Acquisition for steady state variance of 10^{-3} and 10^{-4} with the error function of (Daffra and Chouly 93), Average over 20 realizations*

The performance independency of number of subchannels in the OFDM systems, makes the error function of (Daffra and Chouly 93) unique compared to the other error functions in this work. For non time dispersive channels the Daffara algorithm gives fast acquisition compared to the other algorithms in systems with low and moderate number of channels. Measuring the acquisition time in number of data symbols, the acquisition time with the Daffara error function increase with the same factor as the number of subchannels in the OFDM system.

First order Godard algorithm

Steady state variance as function of step size parameter is plotted below for the first order Godard error function, Equation 4.16.
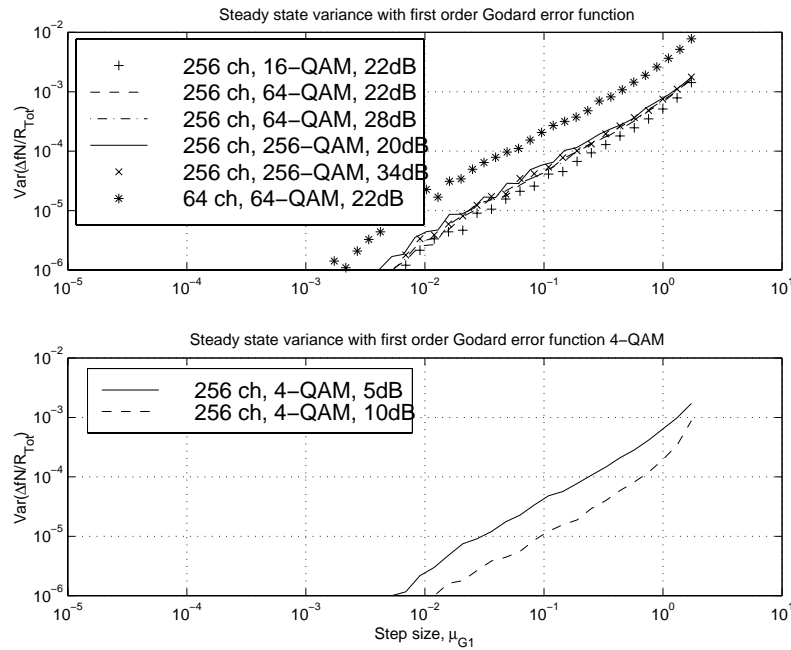
Figure 4.12. *Steady state variance as function of step size parameter with the first order Godard error function*

The steady state variance differs little with changing SNR and constellation size, with the exception of 4-QAM where the variance decrease with increasing SNR. The steady state variance decreases also with increasing number of subchannels in the OFDM system. At higher order modulation, the step size parameter is thus only dependant on number of channels, while with 4-QAM the SNR must be considered as well. Plotting the acquisition time in a 256 channel system, the difference in acquisition time is moderate for different SNRs and constellation sizes, with a tendency of decreasing acquisition time with increasing SNR and decreasing constellation size. The SNR and constellation size dependency is larger for the steady state variance of 10^{-4} than 10^{-3}, Figure 4.13,.

With 4-QAM, the steady state variance dependency on the SNR in Figure 4.12 is also visible at the acquisition time.
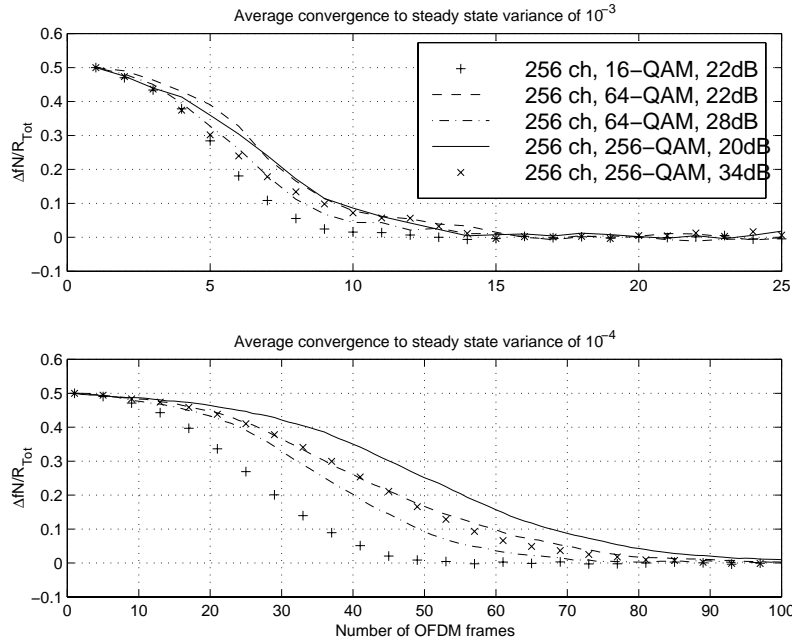
Figure 4.13. *Average Acquisition for steady state variance of 10^{-3} and 10^{-4} with the first order Godard error function, Average over 20 realizations*
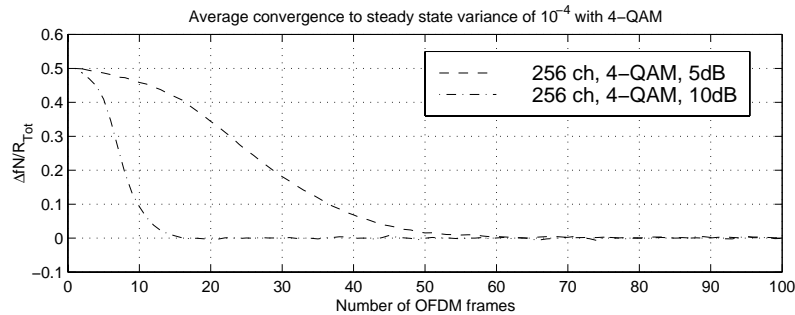
Figure 4.14. *Average Acquisition for steady state variance of 10^{-4} with the first order Godard error function and 4-QAM, Average over 20 realizations*

With the Daffara error function, comparing a $N = 256$ channel system with a $N = 64$ channel system, the number of frames used for acquisition was constant, Figure 4.11. In the case of the first order Godard error function, the acquisition time measured in number of frames decreases with increasing number of subchannels in the system, but the decay is not strong enough to avoid a small increase in acquisition time measured in number of data symbols, Figure 4.15.
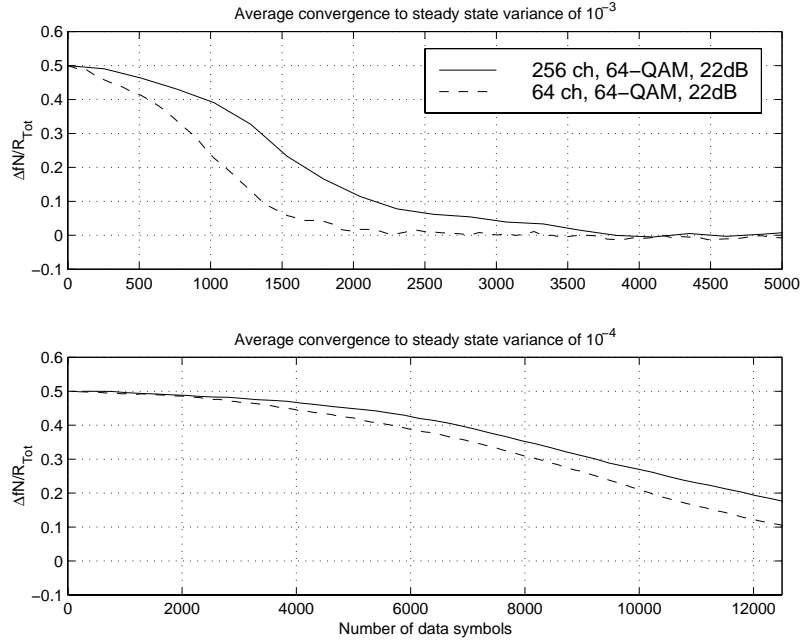
Figure 4.15. *Average acquisition time in number of data symbols, for steady state variance of 10^{-3} and 10^{-4}, 1.order Godard error func, 20 realizations*
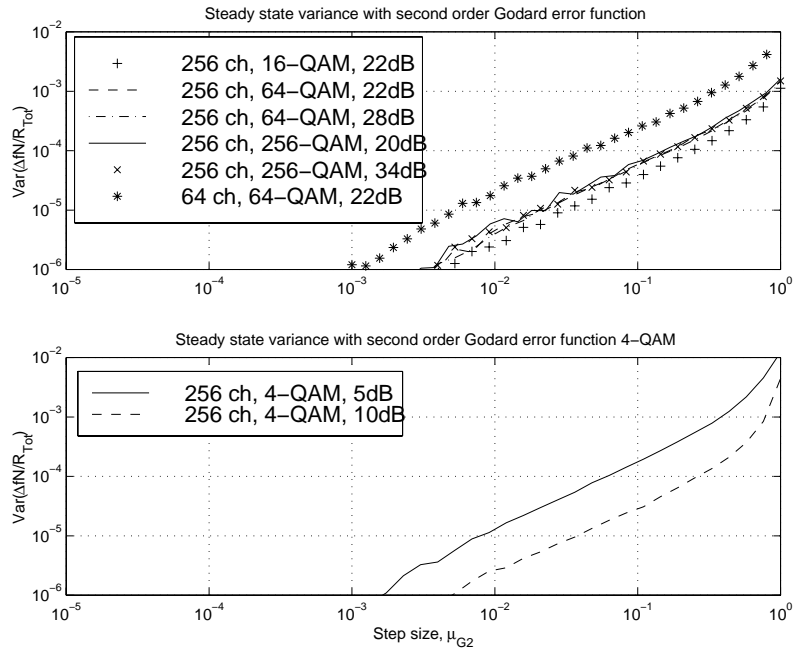
Figure 4.16. *Steady state variance as function of step size parameter with the second order Godard error function*

Second order Godard algorithm

Similar to the first order Godard algorithm, the steady state variance with second order Godard algorithm depends heavily on number of channels and little on SNR and constellation size, except for 4-QAM modulation where the variance also depends on the SNR.

Plotting the acquisition time in a 256 channel system reveals the same pattern for the second order Godard error function as for the first order error function.
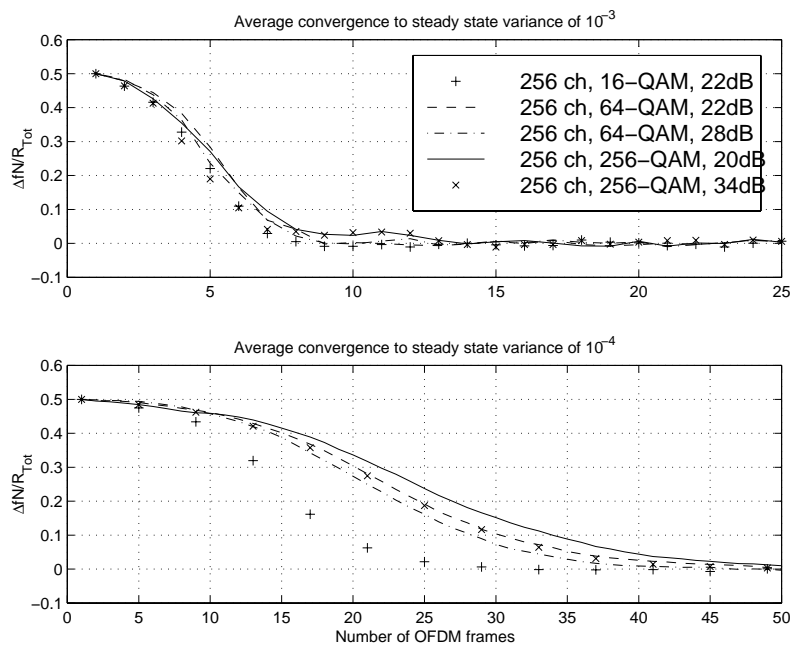
Figure 4.17. *Average Acquisition for steady state variance of* 10^{-3} *and* 10^{-4} *with the second order Godard error function, Average over 20 realizations*

There is a tendency of increasing acquisition time for increasing constellation size. This might be expected since Figure 4.16 indicates close to equal step size parameter for 16-QAM, 64-QAM and 256-QAM, while the amplitude of the second order Godard error function decays with increasing amplitude, Chapter 4.5. For 16-QAM and larger constellations there is even smaller dependency on SNR for second order Godard error function than for first order, while with 4-QAM the acquisition time still depends on the SNR, Figure 4.18.

Looking at the acquisition time measured in number of data symbols, the $N = 256$ channel do have larger acquisition time than a $N = 64$ channel system for a steady
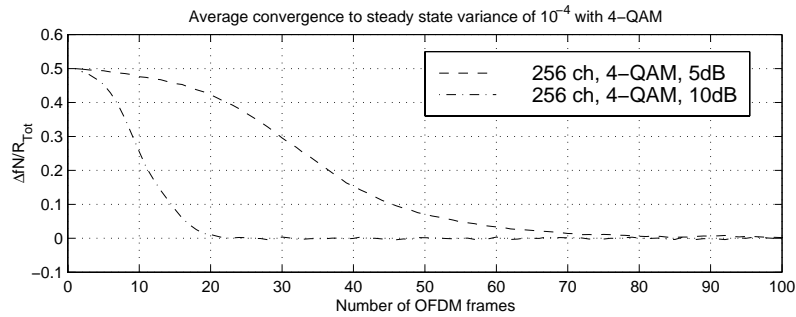
Figure 4.18. *Average Acquisition for steady state variance of 10^{-4} with the second order Godard error function and 4-QAM, Average over 20 realizations*

state variance of 10^{-3}, while the difference is almost negligible for a steady state variance of 10^{-4}.
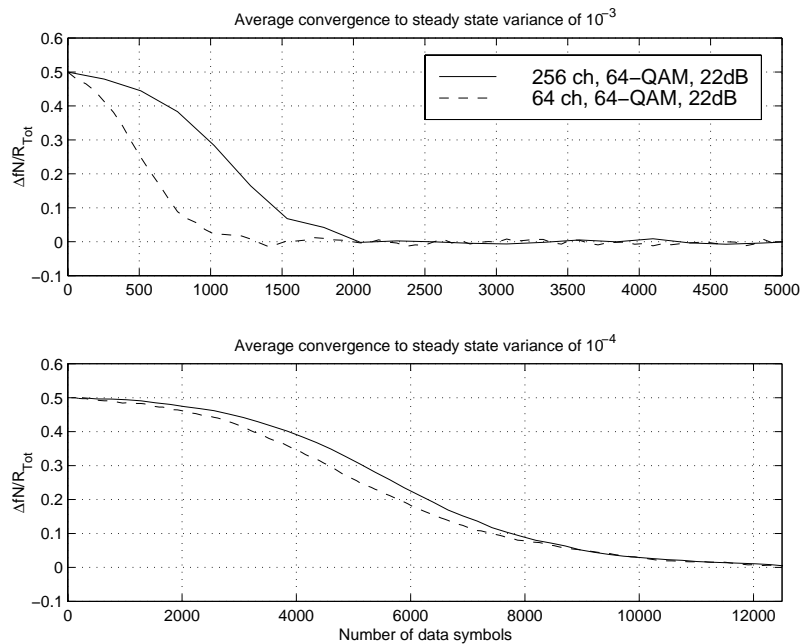
Figure 4.19. *Average Acquisition measured in number of data symbols, for steady state variance of 10^{-3} and 10^{-4} with the second order Godard error function, Average over 20 realizations*

Comparing the performance of the first and second order Godard error function, the first order function is slightly better for 4-QAM constellation, while for larger constellations the second order error function performs better. The difference is small

for acquisition to a steady state variance of 10^{-3}, while the acquisition time is reduced with approx. 50% for the second order Godard error function compared to the first order function for a steady state variance of 10^{-4}.

Mueller and Müller based algorithm with phase correction

The steady state variance and thus the step size parameter for the Godard error functions was little influenced by constellation size and SNR for constellations larger than 4-QAM. This is not the case for the Mueller and Müller based error function with phase correction as shown below.
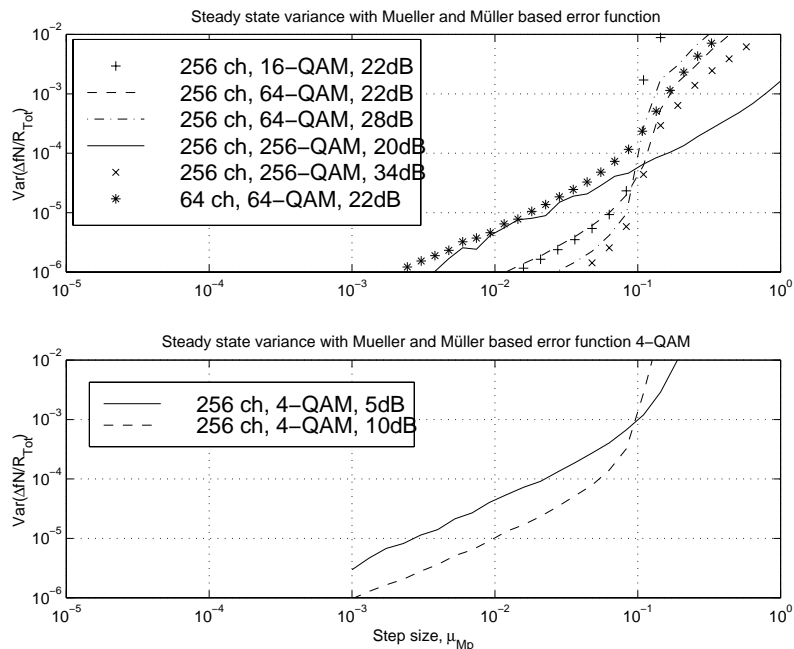
Figure 4.20. *Steady state variance as function of step size parameter, Mueller and Müller based error function with phase correction*

The steady state variance depends on the SNR, but is independent of the constellation size. For low steady state variance, the allowed step size parameter increases with the SNR, while at higher allowed steady state variance this is reversed. One should also note the small difference in allowed step size parameter for the $N = 64$ channel system and the $N = 256$ channel system.

The average acquisition is plotted below in Figure 4.21.

Figure 4.21. *Average Acquisition for steady state variance of 10^{-3} and 10^{-4} with the Mueller and Müller based error function, Average over 20 realizations*

For higher order modulation the acquisition time apparently increases with the SNR due to decreased allowed step size parameter. With lower order modulation the acquisition time decrease with SNR.
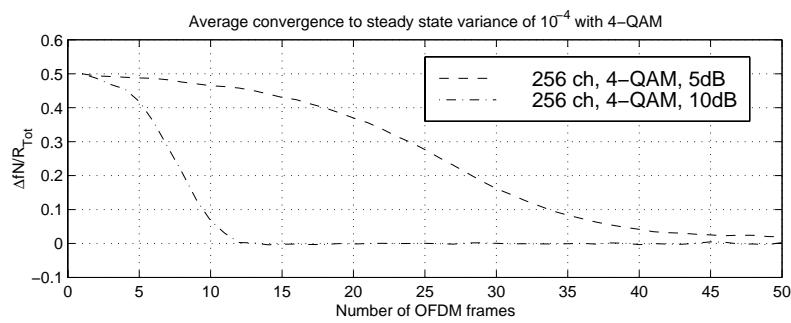
Figure 4.22. *Average Acquisition for steady state variance of 10^{-4} with 4-QAM and Mueller and Müller based error function, Average over 20 realizations*

Higher order modulation with high SNR do not fully gain on averaging over several subchannels either, Figure 4.23.
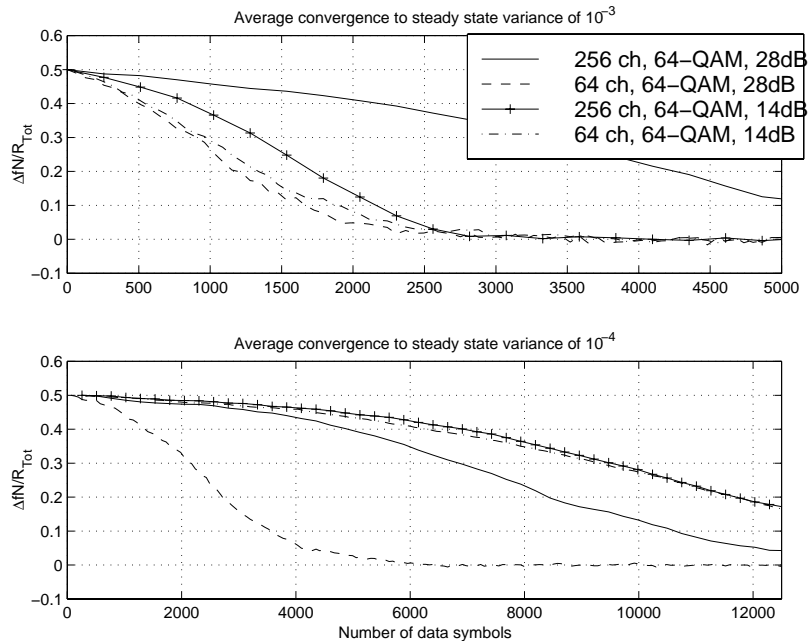
Figure 4.23. *Average Acquisition measured in number of data symbols, for steady state variance of 10^{-3} and 10^{-4} with the Mueller and Müller based error function, Average over 20 realizations*

Mueller and Müller based algorithm without phase correction

The SNR influence on the steady state variance is similar in shape but reduced for a system without phase correction compared to a system with phase correction using the Mueller and Müller based error function. At high steady state variance the allowed step size parameter for low SNR parameters grows larger than the allowed step size parameter for high SNR. Comparing systems with and without phase correction, the difference in allowed step size parameter is smaller for the system without phase correction. The intersection point after which high SNR systems get smaller step size parameter than low SNR systems, is moved to a higher steady state variance for the non phase correcting algorithm, Figure 4.24.

The acquisition time is little influenced by SNR and constellation size for higher order constellations and steady state variance of 10^{-4}. At steady state variance of 10^{-3} there is a small penalty for high SNR and small constellations, Figure 4.25.
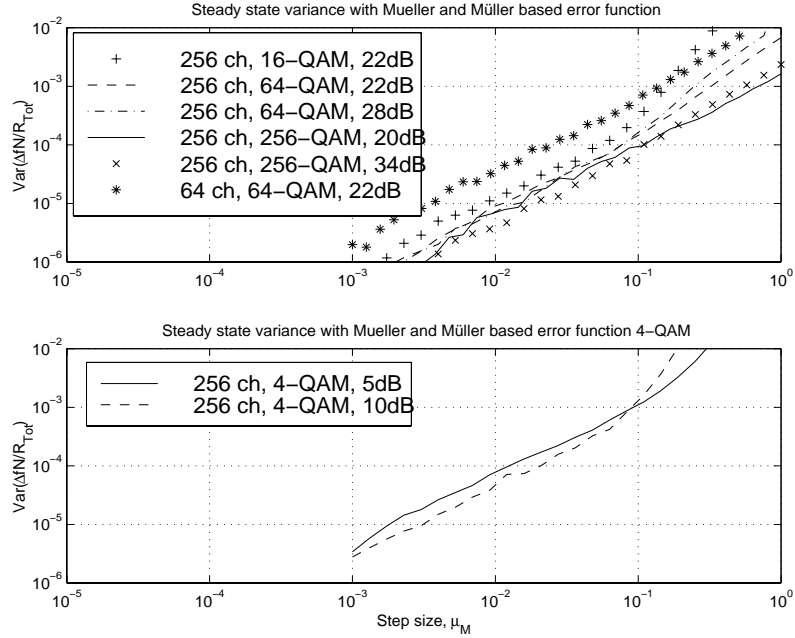
Figure 4.24. *Steady state variance as function of step size parameter, Mueller and Müller based error function without phase correction*
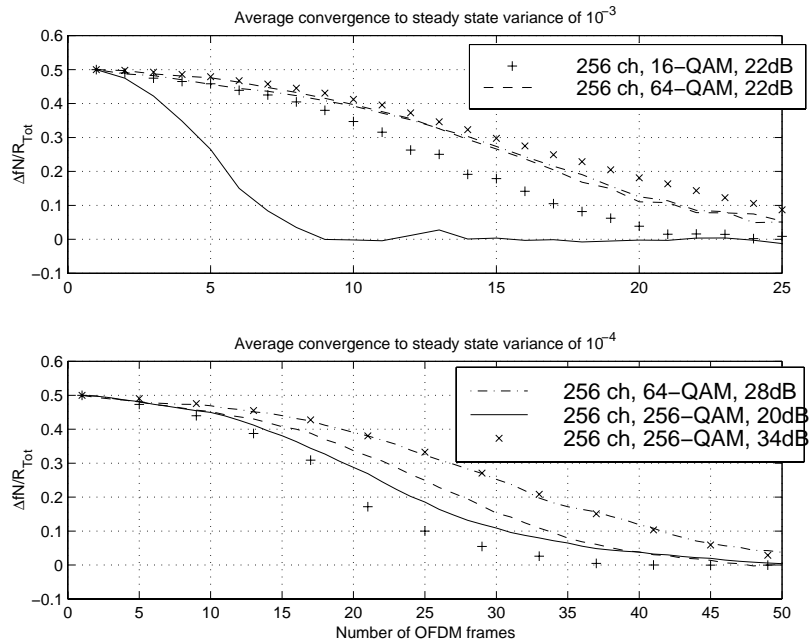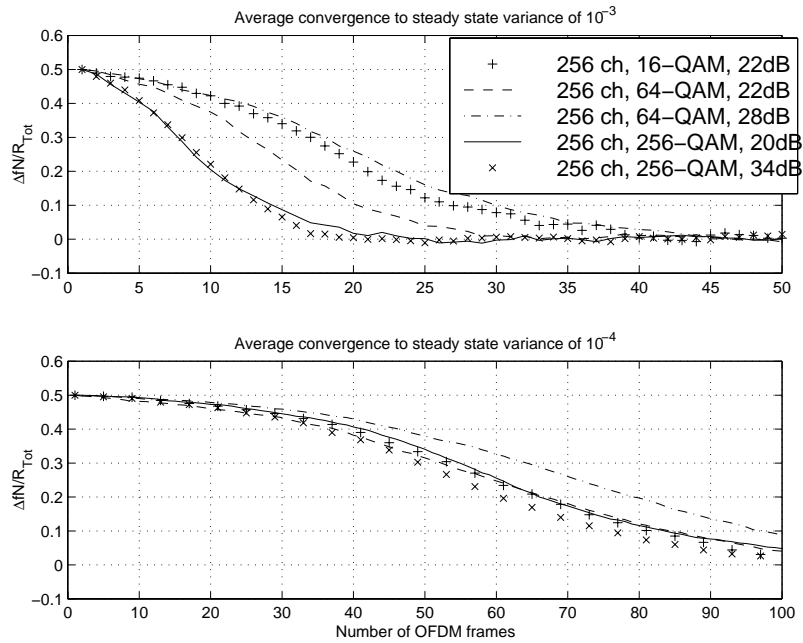

Figure 4.25. *Average Acquisition for steady state variance of 10^{-3} and 10^{-4}, Mueller and Müller based error func. no phase cor. Average over 20 realizations*

Comparison of algorithms

Comparing the algorithms for 64-QAM and $N = 256$ channels, the acquisition time of the Mueller and Müller based algorithms is several times larger than the acquisition time of the other algorithms at high SNR and steady state variance of 10^{-3}, Figure 4.26a. The Daffara error function performs best, while for the second order Godard error function there is a factor of approx. 1.5 in increased acquisition time compared to Daffara. For the first order Godard error function there is a factor of two in acquisition time compared to Daffara.

Reducing the SNR from $28dB$ to $14dB$, Figure 4.26b, the Godard algorithms are close to unchanged, while the Daffara algorithms get closer to the second order Godard error function, but is still a little better. The Mueller and Müller based algorithms with phase correction become equal to the first order Godard algorithm, while dropping the phase correction increases the acquisition time between 50% and 100%.

For steady state variance of 10^{-4} and SNR of $28dB$, Figure 4.26c, the acquisition time of Daffara out performs the second order Godard algorithm with a factor of four, Mueller and Müller with phase correction with a factor of six, first order Godard with a factor of seven and Mueller and Müller without phase correction with a factor larger than ten.

Reducing the SNR to $14dB$, Figure 4.26d, does not alter the performance of the second order Godard and the Mueller and Müller based algorithms with phase correction. The acquisition time of the Daffara algorithm increase to close to the acquisition time of the second order Godard algorithm, while both first order Godard and Mueller and Müller without phase increase their acquisition time as well.

Summarizing, the Daffara algorithm performs best, followed by the second order Godard algorithm. The difference in acquisition time depends on SNR and steady state variance with a maximum of a factor four to a minimum of close to equal performance.

4.6.2 Locking on to an incorrect frequency in the frequency grid

As discussed in Chapter 4.2 the acquisition algorithms might lock on to another frequency in the frequency grid than the single correct carrier frequency. Some of the methods proposed in Chapter 4.2.2 to correct channel number offsets after locking on to another frequency in the frequency grid, assumed decisions with ordinary operational quality, which assumes the tracking algorithm to work. The goal of the acqui-
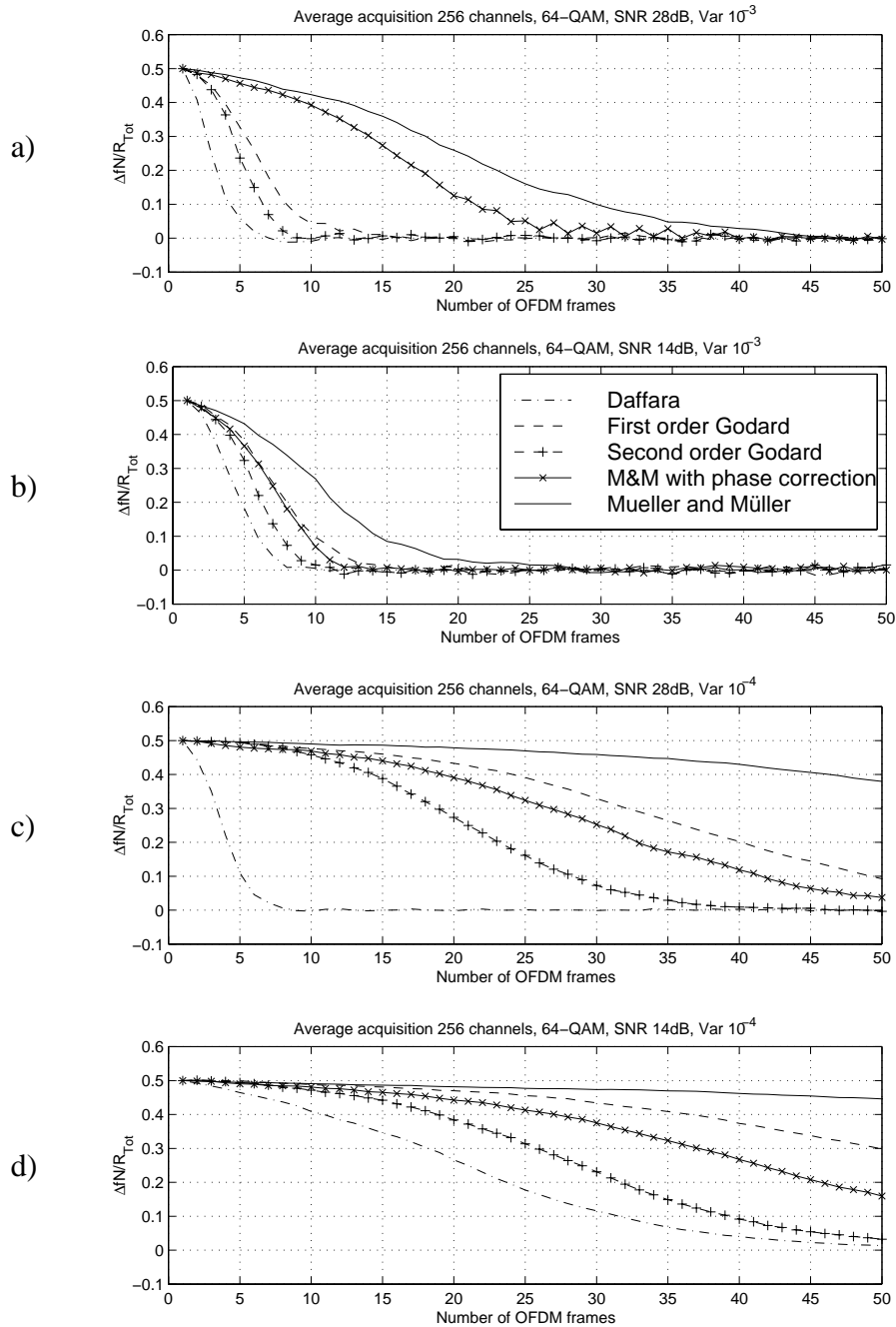
Figure 4.26. *Comparison of average acquisition for different error functions with a 256 channel OFDM system and 64-QAM, Average over 20 realizations*

sition algorithm is thus to produce a carrier estimate good enough for the tracking algorithm to start to operate independent of which of the allowed frequencies in the grid the acquisition algorithm locks on to. I.e. the steady state variance demand is the same for locking to all allowed frequencies in the grid. The allowed frequencies equals the frequencies in the grid centred around the correct carrier frequency with a width / number of grid frequencies, given by the maximum deviation of the oscillator frequencies.

Channel number offset influence on μ

Plotting steady state variance as function of step size for different channel number offsets, reveals that the only algorithm where steady state variance is influenced by a channel number offset is the Daffara algorithm. In Figure 4.27 steady state variance is plotted for a channel number offset of 0, 5 and 20 channels, in an OFDM system with $N = 256$ channels, 64-QAM and $SNR = 28dB$.
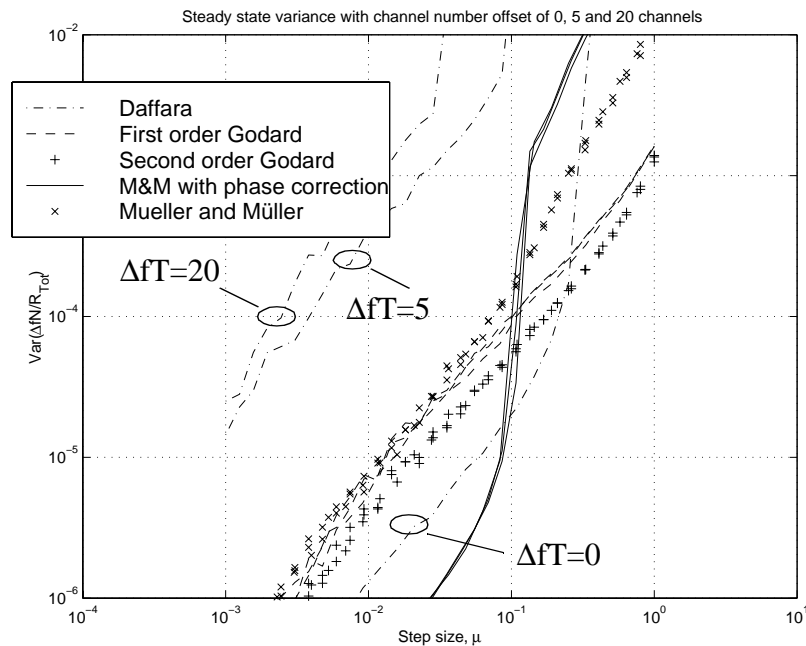
Figure 4.27. *Steady state variance as function of step size parameter with channel number offset of 0, 5 and 20 channels, $N = 256$, $SNR = 28dB$, 64-QAM*

While the step size parameter is close to unchanged by the channel number offset for all the other algorithms, the allowed step size is reduced with one to two decades for the Daffara algorithm, moving from a channel number offset of 0 channels to 5

channels. Increasing the channel number offset to 20 channels the tolerated step size factor is further decreased, but at a much slower rate.

Average acquisition time with a channel number offset

Comparing Figure 4.26a with Figure 4.28.   the acquisition time for the Daffara error function increases approx. with a factor seven due to a channel number offset of 5 channels, assuming a SNR of $28dB$ and a steady state variance of 10^{-3}. The acquisition time of the other error functions are not significantly altered by the channel number offset.
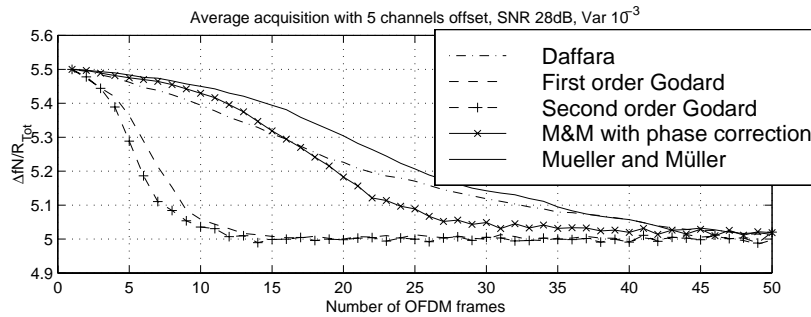
Figure 4.28. *Comparison of average acquisition for different error functions with a channel number offset of 5 channels, $N = 256$, 64-QAM, $SNR = 28dB$ and steady state variance of 10^{-3}, Average over 20 realizations*

Increasing the channel number offset from 5 to 20 channels does not alter the acquisition time of the other algorithms, but the acquisition time with the Daffara error function will increase to a level substantially higher than any of the other algorithms.

Figure 4.29. *Comparison of average acquisition for different error functions with a channel number offset of 20 channels, $N = 256$, 64-QAM, $SNR = 28dB$ and steady state variance of 10^{-3}, Average over 20 realizations*

Decreasing the tolerated steady state variance to 10^{-4}, the Daffara algorithm will exhibit larger acquisition time than all the other algorithms even for a channel number offset of 5 channels.
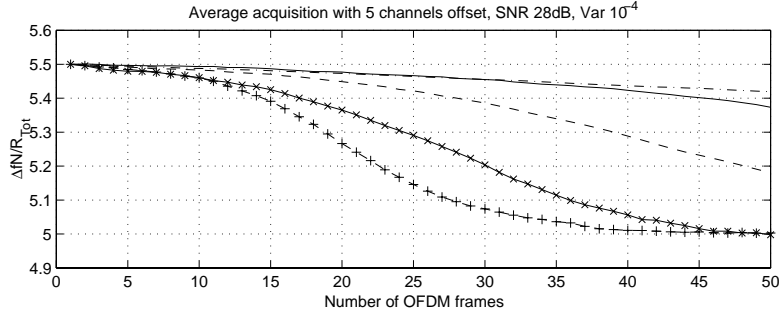
Figure 4.30. *Comparison of average acquisition for different error functions with a channel number offset of* 5 *channels,* $N = 256$, *64-QAM, SNR* = 28*dB and steady state variance of* 10^{-4}, *Average over 20 realizations*

4.6.3 Time dispersive transmission channels

So far only the performance on ideal transmission channels have been examined. In many applications, the channel has multipath characteristics introducing inter symbol interference. To discuss the performance of the proposed carrier frequency acquisition algorithms on time dispersive channels, a two-ray channel is used. This is a commonly used model of e.g. line-of-sight microwave radio channels, (Rummler et al. 86). The first ray or path is assumed to reach the receiver without attenuation or delay, while the second path is attenuated with a factor α_a, delayed τ_D seconds and shifted in phase by θ Rad. In this work the discussions are limited to the case of $\theta = \pi$ and $\tau_D N / T$ integer. The received sampled signal in front of the receiver filterbank can then be written as:

$$s(k') = x(k') - \alpha_a x(k' - \tau_D) + n(k') \tag{4.20}$$

Step size factor μ **with two ray channel**

The influence of two different two ray channels will be discussed. First a channel with a long delay on the second path, $\tau_D = T/4$ and an attenuation of 0.4. The second channel exhibits a much shorter delay, $\tau_D = 2T/N$ and no attenuation of the second path, $\alpha_a = 1$. The first transmission channel gives rapid amplitude and phase variations in the frequency spectra and thus between the subchannels in the receiver, while the second transmission channel gives zeros in the frequency spectra

close to subchannel number 0, $N/2$ and $N-1$. Steady state variance on the two transmission channels is plotted as function of step size parameter for the Daffara algorithm and the second order Godard algorithm, Figure 4.31.
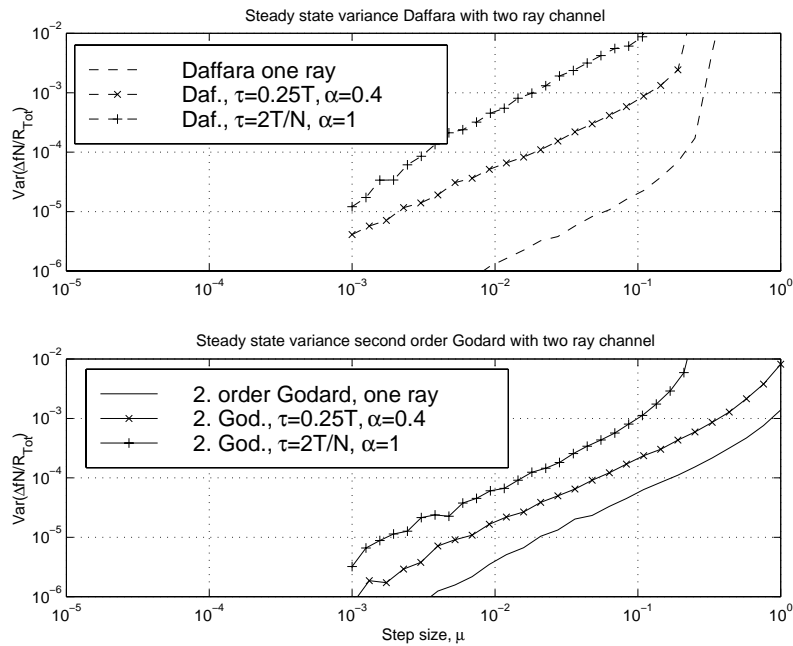
Figure 4.31. *Steady state variance as function of step size parameter for one ray (ideal) and two ray channel, $N = 256$, $SNR = 28dB$, 64-QAM*

For both algorithms a two ray channel gives a reduction of allowed step size parameter, with the largest reduction for the channel with a short, strong delay.

Acquisition time with two ray channel

In a $N = 256$ channel OFDM system with 64-QAM, $SNR = 28dB$ and a two ray transmission channel with $\alpha_a = 0.4$ and $\tau_D = T/4$, the first order Godard and the Daffara algorithms are close to equal in performance for a steady state variance of 10^{-3}, Figure 4.32.

Comparing Figure 4.26a and Figure 4.32. , both the Daffara algorithm and the two Godard algorithms suffer from an increased acquisition time. For Mueller and Müller, the two ray channel give an increase in acquisition time similar to a reduction in SNR. Decreasing the tolerated steady state variance to 10^{-4}, the pattern is repeated, Figure 4.33
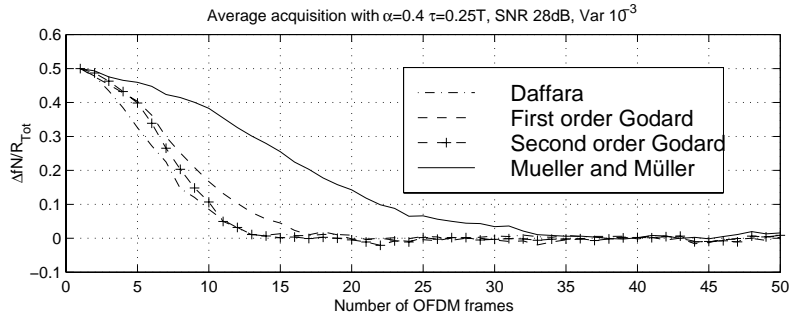
Figure 4.32. *Comparison of average acquisition for different error functions with a two ray channel, $N = 256$, 64-QAM, $SNR = 28dB$ and steady state variance of 10^{-3}, Average over 20 realizations*
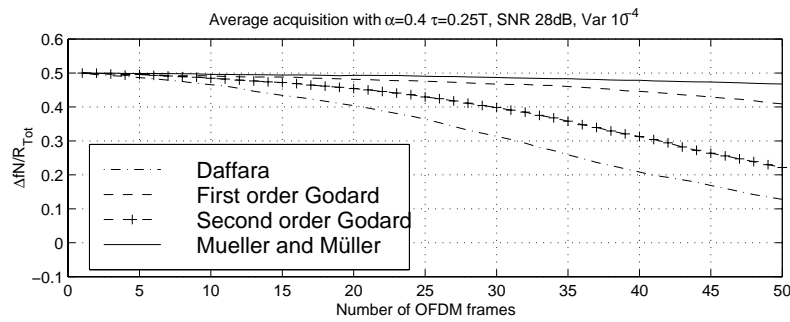
Figure 4.33. *Comparison of average acquisition for different error functions with a two ray channel, $N = 256$, 64-QAM, $SNR = 28dB$ and steady state variance of 10^{-4}, Average over 20 realizations*
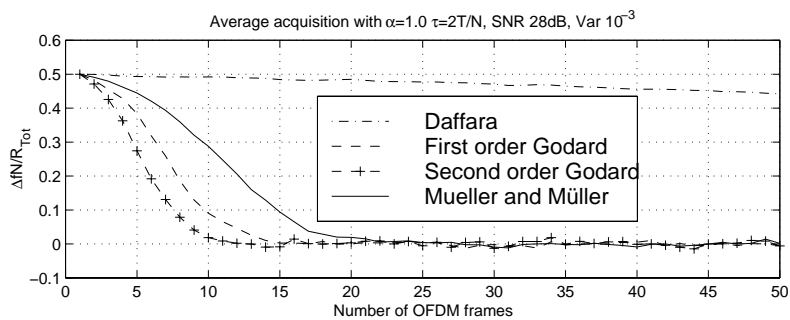
Figure 4.34. *Comparison of average acquisition for different error functions with a two ray channel, $N = 256$, 64-QAM, $SNR = 28dB$ and steady state variance of 10^{-3}, Average over 20 realizations*

For the transmission channel with a short powerful reflection, the Daffara algorithm exhibits a large increase in acquisition time to a level far beyond any of the other algorithms, while the other algorithms perform a little better than for the two ray channel with long delay and more attenuation of the second ray, Figure 4.34.

Two ray channel and channel number offset

Introducing a channel number offset in addition to the two ray channel gives little difference in performance compared to the system with two ray channel and no channel number offset.
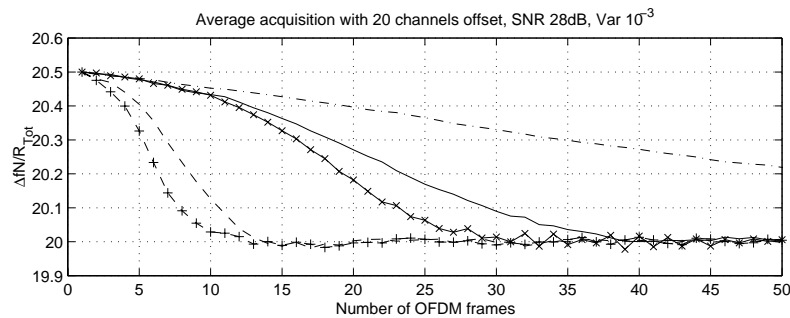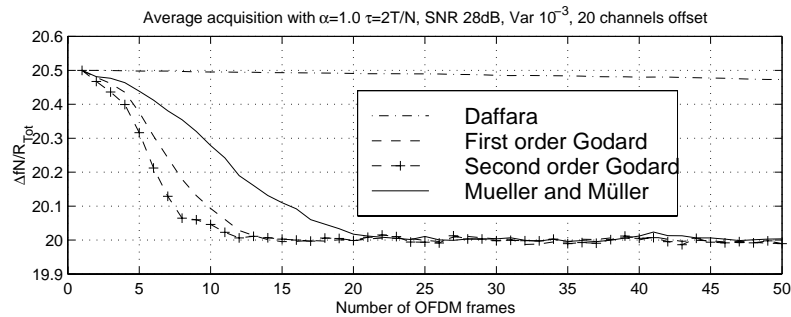

Figure 4.35. *Comparison of average acquisition for different error functions with a two ray channel and a channel number offset of 20 channels, $N = 256$, 64-QAM, $SNR = 28dB$ and steady state variance of 10^{-3}, Average over 20 realizations*

4.6.4 Carrier frequency acquisition time with timing error

The proposed carrier frequency algorithms have been investigated under the assumption of no timing error. The consequences of a timing error is not treated in depth, but simulations for two examples are shown below.

For both examples the following is valid: $N = 256$ channels, 64-QAM, $SNR = 28dB$, non time dispersive transmission channel and step size parameter which would give steady state variance of 10^{-3} for no timing error. The results are averaged over 1000 realizations. In the first example there is a timing error of $0.2T$, Figure 4.36.
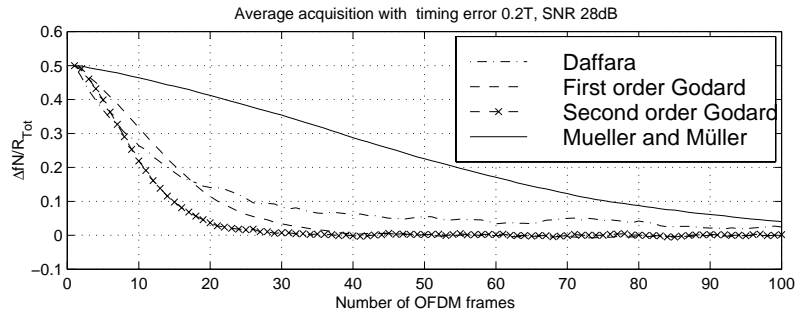
Figure 4.36. *Comparison of average acquisition for different error functions with a timing error of* $0.2T$*,* $N = 256$*, 64-QAM and SNR* $= 28dB$*. Average over 1000 realizations*

All algorithms converge, with the second order Godard algorithm performing best. Compared to the case of no timing error Figure 4.26a, the acquisition time is approx. doubled for the second order Godard algorithm with timing error of $0.2T$. Increasing the timing error to $0.3T$, the algorithms do not converge to zero CFO, Figure 4.37.
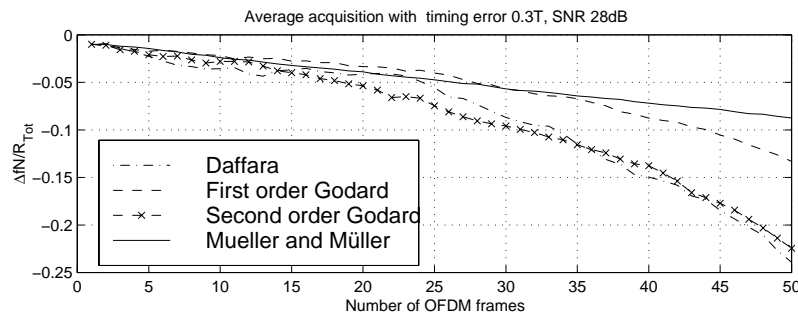
Figure 4.37. *Comparison of average acquisition for different error functions with a timing error of* $0.3T$*,* $N = 256$*, 64-QAM and SNR* $= 28dB$*. Average over 1000 realizations*

Carrier frequency acquisition, using the proposed algorithms, can thus not be performed before the timing acquisition. On the other hand, tolerating a timing error of $0.2T$ in the given example, there is no need for a complete timing recovery to make the proposed carrier frequency acquisition algorithms converge. Possible solutions are thus timing acquisition before carrier frequency acquisition or simultaneous carrier and timing acquisition.

4.7 Gear shift algorithms in carrier frequency acquisition

As discussed in Chapter 4.6, there is a trade off between steady state variance and acquisition or convergence time when choosing step size parameter μ. A large step size parameter gives fast convergence and high steady state variance, while a small step size parameter gives slow convergence and low steady state variance. Assuming a decision directed carrier frequency tracking algorithm and higher order signal constellations, the steady state variance of the acquisition algorithm must be small to make the tracking algorithm start working. Since steady state variance is only of interest after convergence, it is possible to obtain both fast convergence and low steady state variance by switching the step size parameter during operation, i.e. using a gear shift algorithm, (Lee and Messerschmitt 94). During the first stage of the acquisition a step size parameter corresponding to a high steady state variance, e.g. 10^{-3}, can be used. After reaching steady state for the large step size parameter, the gear shift algorithm switches to a smaller step size factor with a lower corresponding steady state variance. The total acquisition time will then be heavily reduced compared to only applying the small step size parameter.

4.8 Summary

This chapter was devoted to carrier frequency acquisition in OFDM without the use of pilots or guard intervals. The transmission channel is assumed stationary. The methods have been presented for use with QAM systems and rectangular pulses, but can be modified for use with other pulse shapes as well.

Critically sampled LMS carrier frequency acquisition algorithms have been developed for OFDM systems with a single filterbank in the receiver to maintain minimum complexity. The algorithms have been developed by recognizing similarities between NDA carrier frequency acquisition for OFDM on one hand and SC timing and SC blind equalization on the other hand. The error function of the SC timing algorithm of (Mueller and Müller 74) has been adapted to LMS carrier acquisition in OFDM. The symbol estimation used in the SC blind equalization algorithms of (Godard 80) have been adopted as well for development of alternative error functions used in LMS algorithms for carrier acquisition. The carrier acquisition algorithms in this work are developed by viewing each OFDM frame as one sequence, but the resulting LMS algorithms are block oriented, updating the carrier estimate once per frame.

The performance of the developed algorithms have been compared to each other and to the performance of the ML carrier frequency acquisition algorithm of (Daffra and Chouly 93). The Daffara algorithm is also critically sampled, but applies two filter-banks in the OFDM receiver. Comparing the Mueller and Müller based algorithms with the Godard based algorithms, the Godard algorithms always give the best performance measured in acquisition time. For the investigated OFDM systems, depending on SNR, constellation size, number of channels in the OFDM system, time dispersion in the channel and steady state variance requirements, the difference in performance varies with a factor between two and ten when comparing the best Godard algorithm and Mueller and Müller. Two Godard based algorithms have been investigated, first order Godard and second order Godard. The second order Godard performs better than the first order Godard except for 4-QAM where the performances are close to equal. The performance of the Daffara algorithm is heavily dependant on the SNR and little dependant on the number of subchannels in the OFDM system. For the second order Godard algorithm it is the other way around. For moderate SNR and low number of subchannels in the OFDM system, the Daffara algorithm outperforms the second order Godard algorithm, while for a high number of channels and low SNR the second order Godard algorithm outperforms the Daffara algorithm. In an example system with 256 channels, $SNR = 28dB$ and steady state variance of 10^{-3}, there is a factor of 1.5 in favour of the Daffara system comparing acquisition times. Introducing a channel number offset or a time dispersive channel with zeros in the frequency spectrum close to channel number 0 and $N-1$, the acquisition time of the Daffara algorithm increases rapidly to a level far beyond the second order Godard algorithm. The second order Godard algorithm is little influenced by neither channel number offset nor time dispersive transmission channels.

The second order Godard based algorithm is robust against low SNR, high CFO and time dispersive transmission channels. The algorithm also give low receiver complexity and high spectral efficiency.

Chapter 5
Algorithms for carrier tracking in OFDM

After the carrier acquisition algorithm, Chapter 4, has reduced the carrier error to a sufficiently low level, the carrier tracking algorithm starts to work. As mentioned in Chapter 3, the main task of carrier tracking is to track the deviations in carrier phase and frequency during system operation. The carrier tracking is not perfect because of noise and other impairments. The quality of the algorithms can thus be measured by the variance of the carrier estimate, assuming the estimators to be unbiased. Consequences, i.e. system degradation, due to non perfect carrier frequency tracking are analysed in Chapter 6.

One of the features of OFDM is spectral efficiency, which is important for several systems, e.g. fixed radio links. Focusing on the example of fixed radio links, these systems can be described by good SNR, low SER, high capacity, strong spectral requirements, stable oscillators and slowly changing transmission channel. Strong spectral requirements enforce higher order modulation at the same time as the use of guard interval and pilot/DA based algorithms should be avoided. To maintain high SNR, CFO generated IBI must be kept at a minimum, $\Delta f \ll 1/T$. This requires high performance tracking algorithms. Choosing between DD and NDA algorithms, DD algorithms should be used due to better performance, (Mengali and D'Andrea 97). According to Chapter 3.5.4, separate carrier phase and carrier frequency tracking is necessary. A DD carrier tracking structure is suggested in Figure 3.3 with a feedback phase synchronizer placed inside a feedback frequency synchronizer.

It is the task of the tracking algorithms to keep phase error and CFO/IBI at a minimum. Analysing the algorithms under the assumption of proper operation, the Inter Bin Interference can thus be neglected. This gives a situation where each channel in the OFDM system can be viewed as similar to Single Carrier systems, allowing the use of known algorithms and theory for carrier tracking in SC systems.

The carrier synchronization algorithms presented in this work are intended for carrier tracking in spectral efficient OFDM systems. Earlier methods for carrier frequency tracking in OFDM are mainly based on pilots or other redundant signalling. This chapter will look into one family of possible decision directed high performance carrier frequency tracking algorithms and a related decision directed carrier phase tracking algorithm, neither of them requiring redundant signalling. The carrier estimators are known from SC systems, and are tested her for performance in OFDM systems with: averaging both in time and across sub channels, higher order modulation and DD input to the estimator. The algorithms are presented for use with QAM systems, but can be modified to work with O-QAM systems.

In the case of separate algorithms for tracking and acquisition, the tracking algorithm will sometimes also perform the last part of the acquisition. I.e. the acquisition algorithm does not need to reduce the carrier error to a level with satisfactory system operation, but rather reduce the error to a level good enough for the tracking algorithms to start to work. The lock-in range of the tracking algorithm should thus be investigated to find a minimum quality limit of the carrier estimate produced by the acquisition algorithm. For the tracking algorithm presented in this chapter, only a coarse estimate of the lock-in range is given. On the other hand, the acquisition algorithms presented in Chapter 4 are shown to be able to produce arbitrarily good estimates by reducing the algorithm step size parameters. Cooperation of the proposed tracking and acquisition algorithms are thus guaranteed.

The chapter is organized as follows: Chapter 5.1 contains references to earlier work in the area of carrier tracking, fundamental limits are given in Chapter 5.2, Chapter 5.3 describes a decision directed phase tracking algorithm, Chapter 5.4 describes a decision directed carrier frequency tracking algorithm and analyses it's performance and the consequences of constellation size, time averaging and channel averaging, Chapter 5.5 is a summary.

5.1 Previous work

There exist several references to carrier synchronization in OFDM as mentioned in Chapter 3.1, (Hirosaki 84), (Clasen and Meyr 94), (Lambrette et. al 97a), (Speth et. al 98), (Daffra and Chouly 93), (Oh et. al 96), (Moose 94), (Van de Beek et. al 97) and (Dinis and Gusmao 97). The assumption about negligible IBI in tracking mode makes it possible to adopt carrier tracking algorithms and theory from SC systems. SC carrier tracking is a well documented area, examples of textbooks covering the subject are (Meyr and Ascheid 90), (Meyr et. al 98), (Mengali and D'Andrea 97) and (Lee and Messerschmitt 94).

5.2 Cramer Rao Bounds for phase and frequency estimators

Comparing different synchronizers, the optimum synchronizer performance is of interest. As discussed in Chapter 3, a synchronizer consists of estimation and correction, with the performance of the synchronizer as a whole given by the estimator performance (including filtering/averaging as a part of the estimator). The minimum attainable variance for an unbiased estimator is given by the Cramer Rao Bound (CRB). This makes CRB to a performance threshold, with which estimators can be compared. CRB for the different synchronization parameters depend on signals statistics, knowledge about the other synchronization parameters and knowledge about the transmitted data (Mengali and D'Andrea 97).

The bounds for carrier estimation in a SC system with additive white Gaussian noise (AWGN) are found in (Meyr et. al 98). Sufficient SNR and averaging over some symbols with random data is assumed. In this work unity amplification trough the system and no timing error is assumed. CRB for the phase estimator equals:

$$CRB_{\hat{\theta}} = \frac{1}{2K\frac{A^2}{\sigma^2}} \tag{5.1}$$

While CRB for the frequency estimator equals:

$$CRB_{\hat{\Delta f}} = \frac{6}{(2\pi T)^2 \frac{A^2}{\sigma^2} K(K^2 - 1)} \tag{5.2}$$

σ^2 : Noise power

K : Number of frames used for estimation

For unity bandwidth and symbol duration $T = 1$, the signal power A^2 equals:

$$A^2 = E[|a|^2] \tag{5.3}$$

Averaging over L independent channels, which is the case of OFDM when the ICI is small enough to be neglected, the Cramer Rao bounds equals:

$$CRB_{\hat{\theta}} = \frac{1}{2LK\frac{A^2}{\sigma^2}} \tag{5.4}$$

$$CRB_{\hat{\Delta f}} = \frac{6}{(2\pi T)^2 L\frac{A^2}{\sigma^2}K(K^2-1)} \tag{5.5}$$

The use of signal power A^2 in the SC case of Equation 5.1 and 5.2 is based on the approximation (Meyr et. al 98):

$$\sum_{k=1}^{K}\sum_{l=1}^{K} a_k^* a_l = \sum_{k=1}^{K} E[a_k^* a_k] \tag{5.6}$$

For the OFDM case of Equation 5.4 and 5.5, this equals:

$$\sum_{m=0}^{L-1}\sum_{n=0}^{L-1}\sum_{k=1}^{K}\sum_{l=1}^{K} a_{k,m}^* a_{l,n} = \sum_{n=0}^{L-1}\sum_{k=1}^{K} E[a_{k,n}^* a_{k,n}] \tag{5.7}$$

This is a consequence of the strong law of large numbers for large $L \cdot K$, but for small $L \cdot K$ the approximation is not valid. As an example, the extreme case of $LK = 1$ for phase estimation is discussed. Assuming unity bandwidth and symbol duration, the signal power equals:

$$A_{LK=1}^2 = |a|^2 \tag{5.8}$$

For constant amplitude modulation $A_{LK=1}^2 = A^2$, and Equation 5.4 and 5.5 are still valid. For non constant amplitude modulation, the signal power, $A_{LK=1}^2$ depends on the transmitted symbol. Averaging over all possible symbols the average CRB equals:

$$CRB_{\hat{\theta}} = \frac{1}{2\frac{1}{\sigma^2}} E\left[\frac{1}{A_{LK=1}^2}\right] \tag{5.9}$$

With unity transmitted signal power, $E[A^2] = 1$, $E[1/A_{LK=1}^2]$ equals 1 for 4-QAM, 1.9 for 16-QAM, 2.7 for 64-QAM and 3.4 for 256-QAM.

5.3 Carrier phase tracking algorithms

For an OFDM system with QAM, rectangular pulses, flat channel, zero CFO and a phase error θ between the carrier oscillators in transmitter and receiver, the received signal in channel m, frame k, equals:

$$z_{k,m} = \frac{1}{T} \sum_{n=0}^{N-1} a_{k,n} \int_0^T e^{j\left(\frac{2\pi}{T}(n-m)\tau + \theta\right)} d\tau + n(m) = a_{k,m} e^{j\theta} + n(m) \qquad \textbf{(5.10)}$$

θ : Phase error

The received signal equals the transmitted symbol with a phase rotation (equal to the phase error) plus channel noise, no IBI has been created. For systems with coherent detection, the phase error must be tracked and compensated.

5.3.1 Data aided carrier phase estimation

Concentrating on OFDM systems with phase error estimation after the filterbank, the phase error can be estimated by removing the modulation from the received signal and extracting the phase.

$$\hat{\theta}_{k,m} = \angle(z_{k,m} a_{k,m}{}^*) \qquad \textbf{(5.11)}$$

$\hat{\theta}_{k,m}$: Estimated phase error, frame k, channel m

The DA phase error estimator given by Equation 5.11 is a Maximum Likelihood (ML) estimator obtaining CRB, (Mengali and D'Andrea 97). Assuming good SNR and Gaussian additive noise, the noise of the phase estimate can also be assumed Gaussian. Phase errors in the range $\pm\pi$ can be detected and the estimator can be used for correction both in feed forward and feedback systems. In feed forward systems, Figure 5.1, the variance of the phase error after correction equals the variance of the phase estimate.
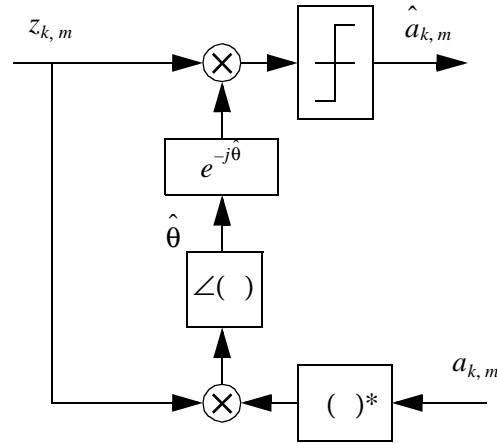
Figure 5.1. *DA feed forward phase synchronization solution. Channel and/or frame averaging can be performed before phase extraction or directly on the phase estimate.*

To increase the accuracy of the estimate it can be averaged over K frames and L channels, assuming the phase error to be constant over the frames and channels used for averaging.

$$\hat{\theta} = \angle \sum_{l=k-K+1}^{k} \sum_{m \in \varsigma} (z_{l,m} a_{l,m}{}^{*})$$
(5.12)

ς : The L channels used for averaging

In a pilot based system, only the pilot channels are used for averaging.

5.3.2 Decision directed phase error estimation

In Equation 5.11 the receiver is assumed to know the transmitted sequence, which is the case for systems using pilots. In spectral efficient systems where pilots are avoided the true transmitted symbols must be interchanged with decisions, creating a DD estimator for tracking:

$$\hat{\theta}_{k,m} = \angle(z_{k,m} \hat{a}_{k,m}{}^{*})$$
(5.13)

The decision directed estimator, Equation 5.13, will behave similar to the pilot based estimator under the assumption of low SER. For this to be true, phase slipping must

be avoided. For 16-QAM the maximum tolerated phase error in front of the decision device is approx. $\pm 0,075\pi$. Since the phase error before correction can be anywhere in the range of $\pm\pi$, DD phase tracking must be limited to feedback structures where the phase error is corrected in front of the decision device, Figure 5.2. The estimator of Equation 5.13 is sensitive to CFO, (Mengali and D'Andrea 97), however during tracking the CFO can be assumed small. Two equivalent implementations of the feedback phase synchronizer are shown below in Figure 5.2
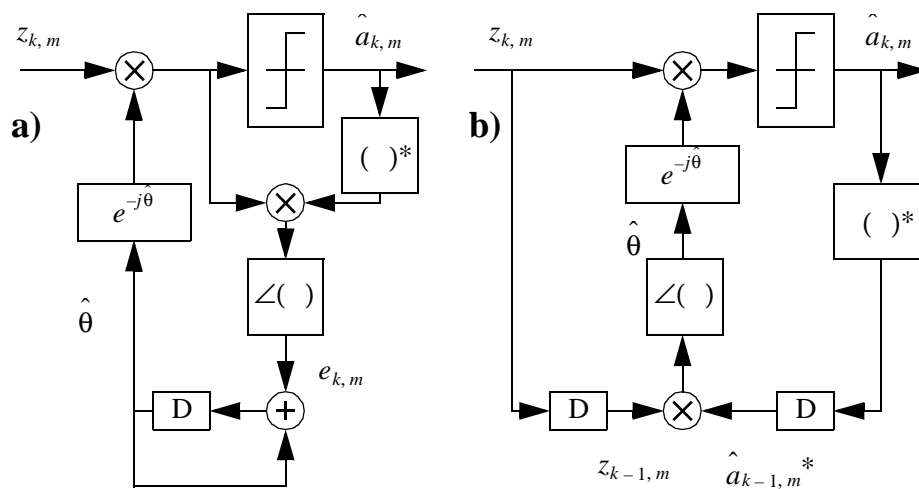
Figure 5.2. *Two equivalent DD feedback phase synchronization solutions. Channel and/or frame averaging can be performed before phase extraction or directly on the phase estimate.*

D: Time delay of length one symbol interval

To increase estimator accuracy, the estimate can be averaged over several channels and frames. Both in Figure 5.2a) and Figure 5.2. b) the averaging can be performed in front of the phase extraction or directly on the phase estimate $\hat{\theta}$.

The contributions from the different frames and channels can be given equal or different weights. In this work the phrase "windowing" is used for weights applied in the time direction, while the phrase "weighting" is used for the weights applied in the frequency direction. Multiplying the error signal $e_{k,m}$ in Figure 5.2a) with a constant smaller than unity, equals time averaging with an infinitely long windowing function using decaying weights for older frames. This equals a first order Phase Locked Loop (PLL).

An alternative is averaging over a finite number of frames and channels. The estimator using uniform time windowing and uniform channel weighting is given in Equation 5.14. With non constant amplitude modulation, there is an implicit weight for each contribution to the phase error estimate. It is easy to show that these implicit weights give optimum performance. With uniform windowing and weighting all frames and channels used per estimate must have the same phase error. The rate must thus be decimated with a factor K in the phase correction feedback loop of Figure 5.2.

Due to rotational symmetry of QAM constellations, there will be a phase ambiguity of $\pi/2$ for DD carrier phase synchronizers. This can be solved by rotational invariant coding, which produce the same information sequence independent of rotations with a multiple of $\pi/2$. Alternatively differential encoding can be used of the two bits identifying the quadrature of the symbol. Other special algorithms are found in (Mengali and D'Andrea 97).

5.3.3 Decision directed phase error estimator performance

Assuming correct decisions, the DD phase synchronization circuit in Figure 5.2b) is identical to a DA feed forward phase synchronizer except for a delay introduced in the feedback structure. With a constant phase error, i.e. no CFO, the performance of the feed forward and the feedback synchronizers will thus be identical, obtaining CRB. As mentioned above, increased performance of the DD phase tracking can be achieved by averaging the phase estimate. With uniform weighting this equals:

$$\hat{\theta} = \angle \sum_{l=k-K+1}^{k} \sum_{m \in \varsigma} (z_{l,m} \hat{a}_{l,m}{}^*) \tag{5.14}$$

In opposition to pilot based systems, all channels can be used for phase error estimation. Averaging across the subchannels with a non flat transmission channel, one should pay attention to the coherence bandwidth of the transmission channel and limit the number of subchannels used for averaging. In the same manner, averaging in time must be limited according to coherence time of a time varying channel and oscillator stability, (Steele 92). If per channel equalization is used in connection with non flat channels, the phase correction can be included in the equalizer.

The phase estimator in Equation 5.14 is unbiased under the assumption of negligible SER. At low SNR this will not be the case, Figure 5.3

.

Estimator bias with phase error 0.02π, 4–QAM and 64–QAM

Variance with phase estimate averaged over 64 channels
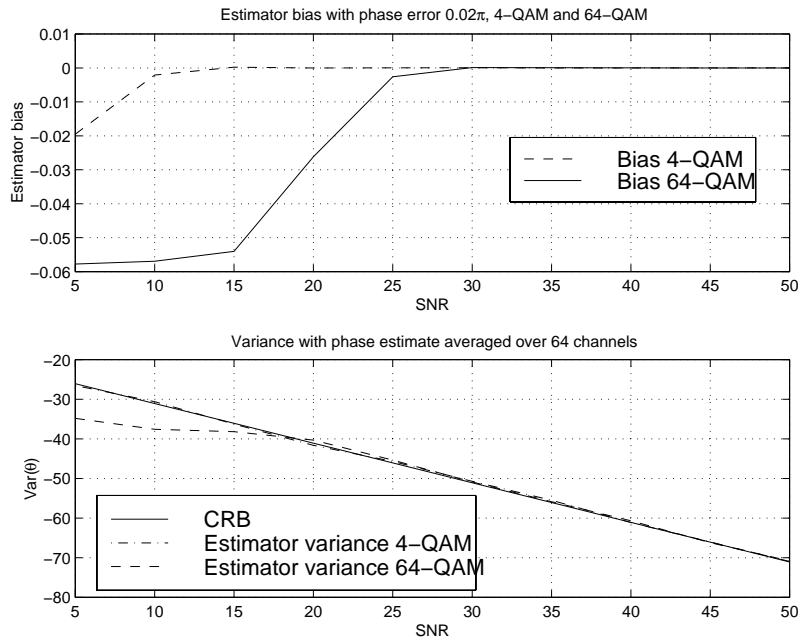
Figure 5.3. *DD phase estimator bias (linear) and variance (dB) as function of SNR, K = 1 and N = 64, all channels used for averaging phase estimate. SNR and variance in dB.*

Due to significant SER at low SNR the phase estimate becomes biased, explaining why the estimator variance can become lower than CRB. Since the algorithm is intended for systems with low SER and thus high SNR, the phase estimator bias at low SNR will not be of interest during tracking. Larger constellations need a higher SNR to obtain low SER. This can be observed in Figure 5.3 as a difference between SNR sensitivity for 4-QAM and 64-QAM.

The results shown in Figure 5.3 are obtained by averaging across 64 channels in one frame before phase extraction, giving equal performance for constant and non constant amplitude modulations. According to Equation 5.9 there is a penalty using non constant amplitude modulation if no averaging is performed during phase estimation. The performance loss can be observed in the upper part of Figure 5.4. On the other hand averaging before phase extraction over only six symbols, the performance difference between constant and non constant amplitude modulation is negligible, as observed in the lower part of Figure 5.4.
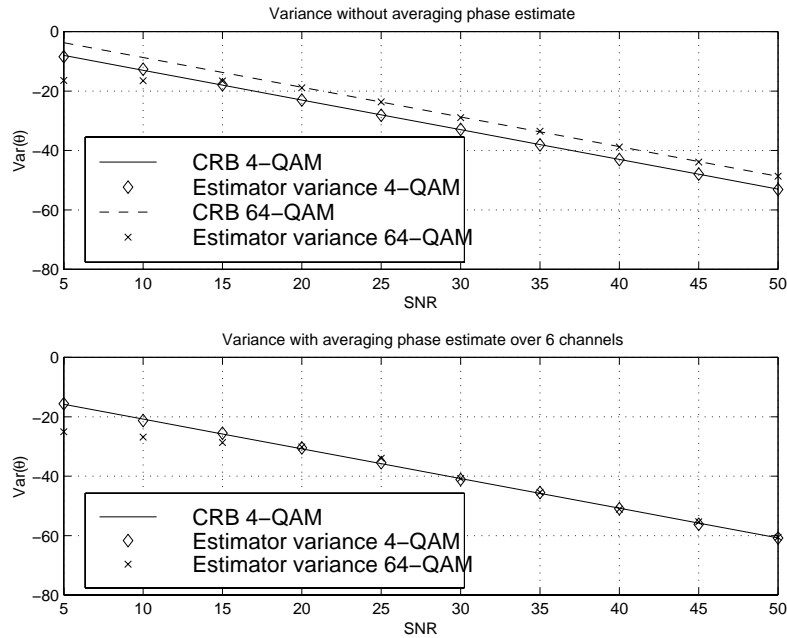
Figure 5.4. *DD phase estimator variance (dB) with and without averaging (before phase extraction) across the channels. Constant amplitude modulation, 4-QAM and non constant amplitude modulation, 64-QAM, $K = 1$ frame*

Generally, the performance of the proposed phase estimator follows CRB for 4-QAM, Equation 5.4, at sufficiently high SNR.

5.3.4 Phase error estimator performance requirements

A phase error will rotate the symbol constellation in the receiver, reducing the distance between the constellation points and the decision borders, resulting in a reduced noise immunity in the system, (Mengali and D'Andrea 97). Using QAM modulation with constellation size larger than 4, the symbols with the highest amplitude will obtain the largest noise immunity reduction due to a phase error. In this work the noise immunity reduction is defined as the reduction of distance to the closest decision border for the most phase error sensitive symbol in the symbol alphabet. The maximum tolerated noise immunity reduction due to phase error is a part of the system specifications. On the other hand with a stochastic Gaussian distributed phase error after correction in the synchronizer, there will always exist a possibility to exceed the tolerated immunity reduction. The probability to exceed a noise immunity reduction of $0,5dB$ is plotted in Figure 5.5 as function of number of symbols

used for phase averaging. The number of symbols equal the number of frames multiplied with the number of channels KL. $SNR = 10(M - 1)$, where M equals the constellation size. With the chosen SNR and no other impairments than AWGN, the SER equals 10^{-7}, (Pollet et. al 95).
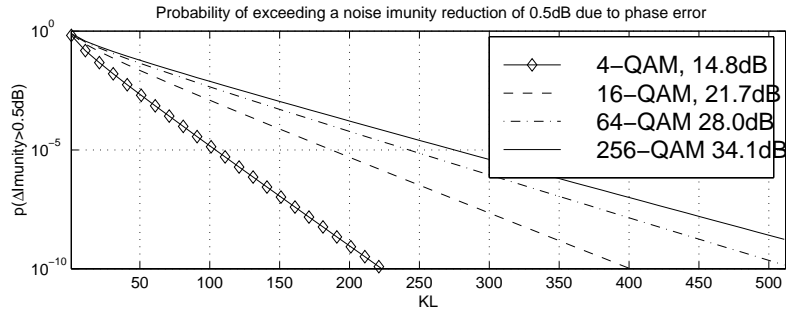
Figure 5.5. *Probability to exceed a noise immunity reduction of* 0.5dB *due to phase error, as function of number of frames and channels used for phase averaging.*

To obtain a given probability for exceeding the noise immunity reduction limit, the number of symbols needed for averaging increase with increasing constellation size. The difference in number of symbols needed for averaging is approx. a factor of 1.8 between 4-QAM and 16-QAM, a factor of 2.3 between 4-QAM and 64-QAM an a factor of 2.6 between 4-QAM and 256-QAM.

Comparing DD and pilot based systems, both of them must use the same number of symbols for averaging to obtain the same performance. But unlike the pilot based estimator, the DD estimator can use all channels for averaging. Compared to DD systems the number of channels used for phase averaging in pilot based systems will be reduced with a factor equal to the pilot spacing, increasing the required number of frames with the same factor. Pilot based phase tracking will thus be more sensitive to time variations in the phase error.

5.3.5 Lock-in range of the DD carrier phase tracking algorithm

With pilots and feed forward structures, the lock-in range equals $\pm\pi$ with unbiased estimators giving fast synchronization for the whole range of phase errors. Hence no separate carrier phase acquisition algorithm is needed.

The proposed DD phase tracking algorithm has lock-in range of $\pm\pi$, but if the initial phase error is large enough to create phase slipping, the phase estimator gets unbi-

ased and the algorithm use a large number of frames to obtain synchronization (Mengali and D'Andrea 97). To speed up synchronization, specialized acquisition algorithms should be used.

The proposed DD algorithm is sensitive to CFO. This is not a large problem during ordinary system operation, since the frequency tracking algorithm will keep the CFO at a low level. The CFO sensitivity is more critical in the period of time just after the transition between acquisition and tracking. Other more CFO robust algorithms could be considered at this stage. Examples of such algorithms are found in (Mengali and D'Andrea 97) and (Meyr et. al 98).

5.4 Decision directed carrier frequency tracking algorithms

A frequency estimator which attains Cramer Rao bound (CRB) has been proposed by (Kay 89). To obtain CRB, it is assumed AWGN and constant amplitude modulation for the symbols used for frequency estimation, (Kay 89), (Clasen and Meyr 94) and (Mengali and D'Andrea 97). The estimator has been used for carrier frequency tracking in pilot based OFDM systems (Clasen and Meyr 94), with CFO estimation after the receiver filterbank and feedback with carrier correction in front of the filterbank.

With the assumption of small CFO, the IBI can be ignored and the received signal can be approximated with (Mengali and D'Andrea 97):

$$z_{k,m} = a_{k,m} e^{j(2\pi\Delta fkT + \theta)} + n(m) \tag{5.15}$$

The frequency estimator equals the phase error difference between two subsequent symbols in time divided by the symbol duration. The phase difference is found by phase extraction after multiplication of subsequent symbols and removal of symbol modulation. In DA based OFDM systems, the estimate is averaged across the pilot channels, Equation 5.16

$$\hat{\Delta f}_{k+1} = \frac{1}{2\pi TL} \sum_{m=\varsigma} \angle(z_{k+1,m} z^*_{k,m} a^*_{k+1,m} a_{k,m}) \tag{5.16}$$

$\hat{\Delta f}_k$: Estimated frequency offset at frame k

If the performance of the CFO estimate produced from two frames with channel averaging is not good enough for proper system operation, i.e. the variance is too high, the CFO estimate must be averaged in time as well. This can be done by a FLL with a loop filter in the feedback, similar to a PLL, or it can be done by explicit averaging in time over K frames like it is proposed by (Kay 89). It is the last method which is investigated here.

Performing time averaging during CFO estimation on a non stationary channel one should pay attention to the oscillator stability and coherence time of the channel, (Steele 92).

Averaging over several frames, both estimate $\Delta \hat{f}_k$ and estimate $\Delta \hat{f}_{k+1}$ contains z_k. The noise of the two estimates is thus not independent and a time windowing function should be included, (Kay 89). The phrase "windowing" is used for weights applied in the time direction, while the phrase "weighting" is used for the weights applied in the frequency direction, i.e. across channels. Averaging across subchannels weighting is not necessary for constant amplitude modulation, assuming the subchannels to be independent. Equation 5.16 equals estimation over 2 frames which is the lowest number of frames possible. Using K frames and performing averaging, the estimator equals:

$$\Delta \hat{f}_{k+1}^K = \frac{1}{2\pi TL} \sum_{m=\varsigma}^{k} \sum_{l=r} w(l-r) \angle (z_{l+1,m} z^*_{l,m} a^*_{l+1,m} a_{l,m}) \qquad (5.17)$$

$$r = k - (K-2) \qquad (5.18)$$

$\Delta \hat{f}_k^K$: Estimated frequency offset at frame k, based on K frames

The time windowing function for constant amplitude modulation is given by Equation 5.19.

$$w(k) = \frac{\frac{3}{2}K}{K^2-1} \left\{ 1 - \left[\frac{k - \left(\frac{K}{2}-1\right)}{\frac{K}{2}} \right]^2 \right\} \qquad (5.19)$$

In DD systems the pilots are replaced with decisions:

$$\Delta \hat{f}_{k+1}^{K} \; = \; \frac{1}{2\pi TN} \sum_{m=0}^{N-1} \sum_{l=r}^{k} w(l-r) \angle (z_{l+1,m} z^{*}_{l,m} \hat{a}^{*}_{l+1,m} \hat{a}_{l,m}) \tag{5.20}$$

Replacing the pilots with decisions, the number of channels used for CFO estimation is increased from the fraction of subchannels used for pilots to all the subchannels in the system, improving the quality of the CFO estimate for a given number of frames. On the other hand the decisions will contain some errors, reducing the performance of the CFO estimate, but with sufficiently low SER during tracking, the performance loss due to SER will be smaller than the performance gain due to averaging over a increased number of channels. Unlike the phase estimate of Equation 5.14, the frequency estimate of Equation 5.20 can be averaged over all the channels used for estimation independent of time dispersion in the transmission channel.

With the proposed tracking scheme, both DA an DD carrier frequency tracking make use of feedback solutions. Assuming no decision errors and the same number of symbols used for CFO estimation, there will be no difference between the two systems. The performance of the synchronizer in Figure 5.6 thus equals the performance of the open loop CFO estimator.

To improve the frequency estimate, time and channel averaging can be performed in front of or after the phase extraction in the frequency correction feedback loop, Chapter 5.4.1. If averaging in the phase correction loop, special care must be taken not to corrupt the frequency estimate.

The down sampling in the frequency correction feedback loop is done to keep the frequency correction, and thus the frequency error in front of the filterbank, constant over the frames used for each CFO estimate.

In the further discussions about frequency tracking, perfect phase correction in front of each decision is assumed, i.e. no phase errors which reduce the noise resistance at the decision. The performance of the proposed synchronizer structure is given as a function of SNR in this chapter. As discussed in Chapter 6, even a small CFO will reduce the SNR at the receiver. The results presented here are valid for zero CFO. For non zero values of Δf the SNR axis must be shifted with the SNR degradation introduced by the actual Δf. The only exception from zero CFO, is found in Figure 5.9 when analysing the bias of the CFO estimator.
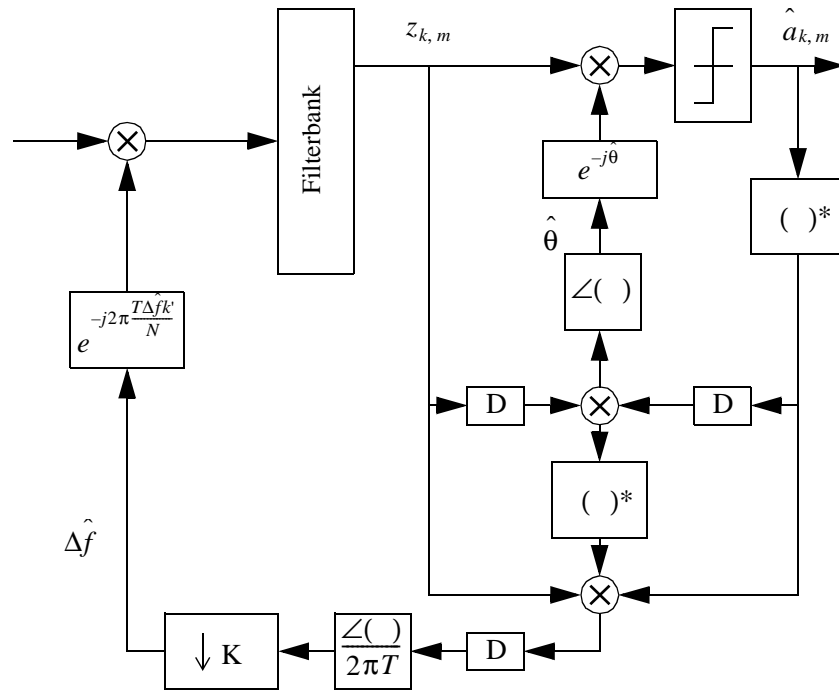
Figure 5.6. *DD feedback phase and frequency synchronization solutions. Channel and/or frame averaging can be performed before or after phase extraction.*

5.4.1 Alternative frequency estimators

The CFO estimator in Equation 5.20 is one of several possible CFO estimators which are unbiased at low SER. Other unbiased estimators may be found by rearranging the order of operations in the estimator, estimator one to six in Table 5.1, where:

$$p_{k,m} = (z_{k+1,m} z^*_{k,m} \hat{a}^*_{k+1,m} \hat{a}_{k,m}) \tag{5.21}$$

$$o_{k,m} = (z^*_{k,m} \hat{a}_{k,m}) \tag{5.22}$$

The time windowing function $w(k)$ can be square, i.e. $w(k) = 1/(K-1)$, or Equation 5.19 can be used for constant amplitude modulation. Square window is referred to as "no win" in the figures. For negligible SER, the estimators will be unbiased both with and without windowing. Interchanging the order of the opera-

	Frequency estimator	**Referred to in figures as:**
1	$\Delta\hat{f}_{k+1}^{K} = \dfrac{1}{2\pi TN} \displaystyle\sum_{m=0}^{N-1} \sum_{l=r}^{k} w(l-r)\angle p_{l,m}$	Phase, time, channel
2	$\Delta\hat{f}_{k+1}^{K} = \dfrac{1}{2\pi TN} \displaystyle\sum_{l=r}^{k} \sum_{m=0}^{N-1} w(l-r)\angle p_{l,m}$	Phase, channel, time
3	$\Delta\hat{f}_{k+1}^{K} = \dfrac{1}{2\pi T}\angle \displaystyle\sum_{m=0}^{N-1} \sum_{l=r}^{k} w(l-r)p_{l,m}$	Time, channel, phase
4	$\Delta\hat{f}_{k+1}^{K} = \dfrac{1}{2\pi T}\angle \displaystyle\sum_{l=r}^{k} \sum_{m=0}^{N-1} w(l-r)p_{l,m}$	Channel, time, phase
5	$\Delta\hat{f}_{k+1}^{K} = \dfrac{1}{2\pi TN} \displaystyle\sum_{m=0}^{N-1} \angle \sum_{l=r}^{k} w(l-r)p_{l,m}$	Time, phase, channel
6	$\Delta\hat{f}_{k+1}^{K} = \dfrac{1}{2\pi T} \displaystyle\sum_{l=r}^{k} w(l-r)\angle \sum_{m=0}^{N-1} p_{l,m}$	Channel, phase, time
7	$\Delta\hat{f}_{k+1}^{K} = \dfrac{1}{2\pi T}\left(\angle \displaystyle\sum_{m=0}^{N-1} \sum_{l=r}^{k} w(l-r)o_{k+1,m} \right.$ $\left. - \angle \displaystyle\sum_{m=0}^{N-1} \sum_{l=r}^{k} w(l-r)o_{k,m} \right)$	Time, channel phase diff.
8	$\Delta\hat{f}_{k+1}^{K} = \dfrac{1}{2\pi TN} \displaystyle\sum_{m=0}^{N-1} \left(\angle \sum_{l=r}^{k} w(l-r)o_{k+1,m} \right.$ $\left. - \angle \displaystyle\sum_{l=r}^{k} w(l-r)o_{k,m} \right)$	Time, phase diff, channel

Table 5.1. *Unbiased CFO estimators*

tions and dropping the window function will inflict on both estimator computational complexity and estimator performance.

Performing time averaging before phase extraction, (Kay 89) has shown that the SC estimator asymptotically obtain the CRB for constant amplitude with increasing SNR. Dropping time windowing this will increase the variance with a factor, (Kay 89):

$$\frac{Var(\Delta\hat{f})_{nowindow}}{Var(\Delta\hat{f})_{window}} = \frac{K(K+1)}{6(K-1)} \approx \frac{K}{6} \tag{5.23}$$

The last approximation in Equation 5.23 will not be valid for averaging over a small number of frames. Assuming independent subchannels, these results will also be valid for the estimators of Table 5.1 for a N channel OFDM system.

An alternative to the frequency estimators discussed so far, is to extract the phase before taking the phase difference between two subsequent frames, estimator seven and eight in Table 5.1. Unlike estimator one to six, estimator seven is not valid for non frequency flat transmission channels. In this case the number of subchannels used for each phase estimate must be limited, Chapter 5.3.3. Despite that the phase differs between the subchannels for non flat transmission channels, the CFO is identical over all the subchannels. This makes it possible to average the CFO estimates produced from subsets of channels. Estimator eight in Table 5.1 is the extreme case with per channel CFO estimation.

One problem in general with estimator seven and eight of Table 5.1, is the need of performing phase unwrapping. This is due to the fact that the output of the phase extraction operator is limited to $\pm\pi$. If the phase crosses π or $-\pi$ between frame k and $k+1$ this must be detected and the phase must be unwrapped. If the unwrapping fails, a phase difference close to zero will appear to be close to $\pm 2\pi$. However assuming a small phase error and a small CFO during tracking with coherent detection, the phases to detect will be close to zero and phase unwrapping will not be necessary. For frequency tracking with differential detection, phase unwrapping will be necessary. Non of the CFO estimators from one to six in Table 5.1 need to perform phase unwrapping. A tracking structure for estimator seven is shown below in Figure 5.7 for the special case of $K = 2$ frames. Channel averaging may be performed in front of the phase extraction.
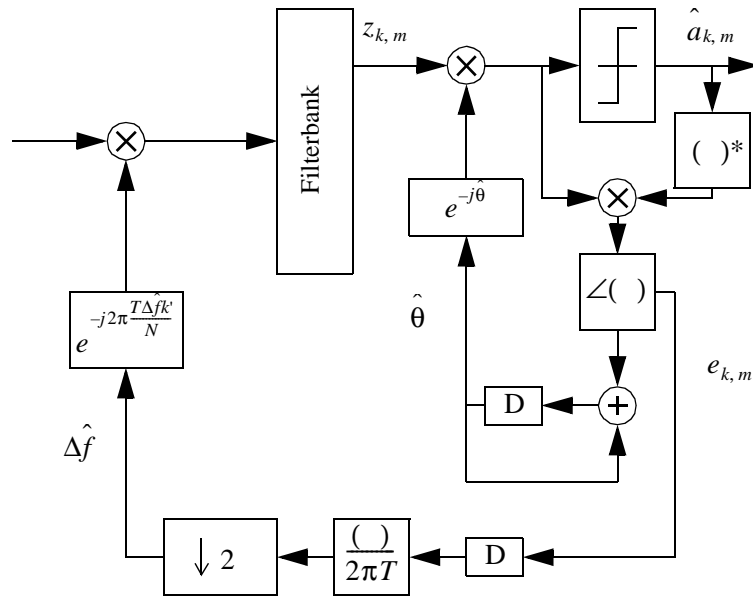
Figure 5.7. *Alternative DD feedback phase and frequency tracking solution. Averaging across subchannels is possible in front of phase extraction*

With phase extraction, time averaging and channel averaging the order of operations will inflict on the complexity of the estimator as shown in Table 5.2

First the estimators one to six in Table 5.2 are compared, these estimators don't need phase unwrapping. If phase extraction is the first or last operation, time and channel averaging can be interchanged freely producing identical results. If windowing is included channel averaging before time averaging will reduce the number of multiplication, excluding the first and the third estimator of Table 5.2. The estimator with lowest complexity is number four, with operation order channel averaging, time averaging and phase extraction. Assuming the phase extraction to be at least as complex as a multiplication, the second estimator will be the most complex estimator of interest with phase extraction before averaging.

If phase unwrapping is no problem, estimator seven and eight in Table 5.2 can be applied. The number of additions are doubled compared to the first six estimators. Compared to estimator four, the number of multiplications are increased with a factor of approx. $4/3$ with windowing and reduced with a factor of approx. $2/3$ without windowing. Estimator seven, which is valid for flat channels, performs two phase extractions while estimator eight which is valid also for non flat channels performs N phase extractions. Assuming phase extraction to be the computational

	Order of operators	**Additions**	**Multiplications**	**Phase extractions**
1	$\sum_m \sum_k \angle(\ )$	$N(K-1)-1$	$N(K-1)(3+w)$	$N(K-1)$
2	$\sum_k \sum_m \angle(\ )$	$N(K-1)-1$	$(K-1)(3N+w)$	$N(K-1)$
3	$\angle\sum_m \sum_k (\ )$	$N(K-1)-1$	$N(K-1)(3+w)$	1
4	$\angle\sum_k \sum_m (\ )$	$N(K-1)-1$	$(K-1)(3N+w)$	1
5	$\sum_k \angle\sum_m (\ )$	$N(K-1)-1$	$(K-1)(3N+w)$	$K-1$
6	$\sum_m \angle\sum_k (\ )$	$N(K-1)-1$	$N(K-1)(3+w)$	N
7	$\angle\sum_m \sum_{k+1}(\ ) - \angle\sum_m \sum_k (\ )$	$2N(K-1)-1$	$2N(K-1)(1+w)$	2
8	$\sum_m\left(\angle\sum_{k+1}(\ ) - \angle\sum_k (\ )\right)$	$2N(K-1)-1$	$2N(K-1)(1+w)$	$2N$

Table 5.2. *Number of operations per CFO estimate with averaging over N channels and K frames. $w = 1$ with windowing, $w = 0$ without windowing*

demanding task, the flat channel frequency estimator is comparable to estimator four in complexity, while the non flat channel estimator number eight will be more complex than estimator number two due to the increased number of phase extractions. Some of the calculations made for phase tracking may be reused for frequency tracking, this can alter the relation of complexity between the different estimators.

5.4.2 Non constant amplitude modulation

In high capacity transmission systems, symbol constellations larger than 4-QAM is often used. For DD systems, the data channels are used for synchronization, i.e. there will not be constant amplitude modulation in the channels used for frequency estimation. As discussed in Chapter 5.2, averaging over a small number of symbols during frequency estimation, CRB for non constant amplitude modulation will be higher than CRB for constant amplitude modulation. In this work the number of symbols used for averaging will however be assumed large enough to approximate the higher order modulation CRB with the constant amplitude modulation CRB.

Using non constant amplitude modulation, the different transmitted symbols have different SNR. For estimators averaging over several frames and/or channels, each term in the estimator have symbol dependant SNR. To obtain maximum performance, symbol dependant weights should be used for each term. The non constant amplitude modulation give implicit weights to the terms. For phase error estimation with non constant amplitude modulation, Chapter 5.3.3, the implicit weights were equal to the optimum weights (Mengali and D'Andrea 97). The estimator attains CRB independent of constellation size without explicit weights. Similar, the explicit phase difference based frequency estimators, seven and eight Table 5.1, also achieve CRB independent of constellation size if a sufficient number of symbols are averaged before the phase extraction.

With frequency estimators based on complex multiplication of succeeding symbols before the phase extraction, estimator one to six Table 5.1, special care must be taken for non constant amplitude modulation, i.e. use of explicit weights, since the implicit weights are not optimal. If no explicit weights are used there will be a performance loss.

Once more the phrase "windowing" is used for weights applied in the time direction, while the phrase "weighting" is used for the weights applied in the frequency direction, i.e. across channels. Assuming the subchannels to be independent, windowing can be performed in each subchannel before weighting across the subchannels. Both optimal windowing and optimal weighting will be symbol dependant. With this approach only estimators with time averaging before channel averaging are available. The estimators with weights investigated for non constant amplitude modulation are:

$$\Delta \hat{f}_{k+1}^{K} = \frac{1}{2\pi TN} \sum_{m=0}^{N-1} u(m) \sum_{l=r}^{k} w(l-r, m) \angle p_{l, m} \qquad (5.24)$$

$$\Delta \hat{f}_{k+1}^{K} = \frac{1}{2\pi T} \angle \sum_{m=0}^{N-1} u(m) \sum_{l=r}^{k} w(l-r,m) p_{l,m} \tag{5.25}$$

$$r = k - (K-2) \tag{5.26}$$

$w(l-r,m)$: Weight due to windowing, channel m , frame l

$u(m)$: Weight due to weighting, channel m

Frequency estimation from two frames

CRB for the frequency estimate is given by Equation 5.5. For $K = 2$ frames, averaging over N channels and normalized power, $E[|a|^2] = 1$, CRB equals:

$$CRB = \left(\frac{1}{2\pi T}\right)^2 \frac{\sigma^2}{N} \tag{5.27}$$

In the case of $K = 2$ frames there is no windowing, only weighting. Using uniform, non optimal, weighting, the estimator with channel averaging before phase extraction, Equation 5.25, has variance equal to (Equation A.11):

$$Var(\Delta \hat{f}_{Ch,phase}) \approx \left(\frac{1}{2\pi T}\right)^2 \frac{\sigma^2}{N} E_a[|a|^4] \tag{5.28}$$

An increase in variance of $E_a[|a|^4]$ equals a loss of 1.2dB for 16-QAM, and 1.4dB for 256-QAM compared with CRB. To improve the performance of the estimator symbol dependant weighting should be applied to each subchannel. The optimal weights are given by (Equation A.13), the focus is put on frame $k = 1$ and $k = 2$ without loss of generality.

$$u(m) = \frac{1}{|a_{1,m}|^2 + |a_{2,m}|^2} \tag{5.29}$$

Inserting the optimal weights from Equation 5.29 into the estimator of Equation 5.25, the variance equals (Equation A.14):

$$Var(\Delta \hat{f}_{Ch,phase}) \approx \left(\frac{1}{2\pi T}\right)^2 \frac{\sigma^2}{N} \frac{1}{2E_a\left[\frac{|a_1|^2|a_2|^2}{|a_1|^2+|a_2|^2}\right]} \tag{5.30}$$

a_1 : Data symbol in frame 1

Even with optimal weighting, there is a loss compared to CRB. The loss equals 0.8dB for 16-QAM, and 1.0dB for 256-QAM., i.e. a weighting gain of only 0.4dB .

Performing phase extraction before channel averaging, Equation 5.24, with uniform non optimal weighting, the estimator variance equals (Equation A.15):

$$Var(\Delta \hat{f}_{Phase, Ch}) = \left(\frac{1}{2\pi T}\right)^2 \frac{\sigma^2}{N} E_a\left[\frac{1}{|a|^2}\right] \tag{5.31}$$

Compared to CRB, there is a loss of 2.8dB for 16-QAM, and 5.4dB for 256-QAM. The optimum weighting factors with phase extraction before channel averaging equals (Equation A.17):

$$u(m) = \frac{\dfrac{|a_{1,m}|^2|a_{2,m}|^2}{|a_{1,m}|^2 + |a_{2,m}|^2}}{\dfrac{1}{N}\displaystyle\sum_{n=0}^{N-1}\dfrac{|a_{1,n}|^2|a_{2,n}|^2}{|a_{1,n}|^2 + |a_{2,n}|^2}} \tag{5.32}$$

Inserting the optimal weights of Equation 5.32 into the estimator of Equation 5.24, the estimator variance equals (Equation A.19):

$$Var(\Delta \hat{f}_{Phase, Ch}) \approx \left(\frac{1}{2\pi T}\right)^2 \frac{\sigma^2}{N} \frac{1}{2E_a\left[\dfrac{|a_1|^2|a_2|^2}{|a_1|^2 + |a_2|^2}\right]} \tag{5.33}$$

This is the same performance as the estimator with channel averaging before phase extraction and optimal weighting, Equation 5.30. With phase extraction before channel averaging the weighting gain equals 2dB for 16-QAM and 4.4dB for 256-QAM. Compared to CRB there is still a small loss of approx. 1dB even with optimal weighting.

Frequency estimation from more than two frames

For $K > 2$ frames, the complexity of both weighting and windowing factors increase. As an example, optimal weighting factors and optimal time windowing for the estimator in Equation 5.25 is given for $K = 3$. The results are found by maximizing SNR. Details are left out and only the answers are presented. The optimal time windowing function in channel m, equals:

$$w_m(k) = \begin{cases} 1 & k = 0 \\ \dfrac{A_m D_m + B_m C_m}{A_m E_m + B_m D_m} & k = 1 \end{cases}$$
(5.34)

Looking at the case of frequency estimation based on frame 1, 2 and 3:

$$\begin{aligned} A_m &= |a_{1,m}|^2 |a_{2,m}|^2 \\ B_m &= |a_{2,m}|^2 |a_{3,m}|^2 \\ C_m &= |a_{1,m}|^2 |a_{2,m}|^2 (|a_{1,m}|^2 + |a_{2,m}|^2) \\ D_m &= |a_{1,m}|^2 |a_{2,m}|^2 |a_{3,m}|^2 \\ E_m &= |a_{2,m}|^2 |a_{3,m}|^2 (|a_{2,m}|^2 + |a_{3,m}|^2) \end{aligned}$$
(5.35)

The optimal weighting factor of channel m equals:

$$u(m) = \frac{A_m + w_m(1)B_m}{C_m - 2w_m(1)D_m + w_m^2(1)E_m}$$
(5.36)

Looking at the estimator given by Equation 5.25, the performance gain due to optimal weighting and windowing (compared to uniform) equals 1.6dB for $K = 3$ and 16-QAM. The estimator with optimum weighting and windowing suffers from a loss of 1.2dB compared to CRB.

The complexity of the windowing functions and weighting factors are quite high for $K = 3$ and increase rapidly with increasing K. The gain due to time windowing and channel weighting (relative to uniform windowing and weighting) are calculated up to $K = 6$ for 16-QAM. Similar the loss relative to CRB is calculated for 16-QAM with optimal windowing and weighting, Table 5.3

Number of frames	$K = 2$	$K = 3$	$K = 4$	$K = 5$	$K = 6$
$\dfrac{Var(\hat{\Delta f})_{\text{Uniform weights}}}{Var(\hat{\Delta f})_{\text{Optimal weights}}}$	0.4dB	1.6dB	3.0dB	4.2dB	5.4dB
$\dfrac{Var(\hat{\Delta f})_{\text{Optimal weights}}}{CRB}$	0.8dB	1.1dB	1.2dB	1.3dB	1.4dB

Table 5.3. *Gain due to time windowing and channel weighting and loss for optimum weighting relative to CRB, 16-QAM and frequency estimator given by Equation 5.25*

Estimator variance without weighting

Generally both windowing and weighting is needed to optimize estimator performance when averaging over several frames and subchannels. If windowing and/or weighting is dropped (uniform weights), the performance of the estimators are reduced.

For constant amplitude modulation however, CRB is achieved for the frequency estimators in Table 5.1 without use of weighting, but using windowing. CRB decreases with increasing number of frames used for averaging according to $1/K^3$. If the estimators are used without time windowing there will be a loss equal to $K/6$ compared to CRB, resulting in an estimator variance proportional to $1/K^2$, (Kay 89).

Averaging over a sufficient number of symbols before phase extraction, frequency estimators seven and eight of Table 5.2 (explicit phase difference) behave similarly for constant and non constant amplitude modulation, obtaining CRB without weighting, but with time windowing.

As discussed above, the estimators given by Equation 5.24 and 5.25 need high complexity weighting and windowing functions with non constant amplitude modulation to maximize performance. Weighting and windowing can be dropped to reduce the estimator complexity at the cost of a performance loss.

The performance of the estimator given by Equation 5.25, without windowing or weighting, is simulated and plotted in Figure 5.8 as function of number of frames for 16-QAM. Similarly, the performance of the estimator given by Figure 5.24 is simulated and plotted, without channel weighting, but with and without constant amplitude time windowing. CRB is plotted as well.
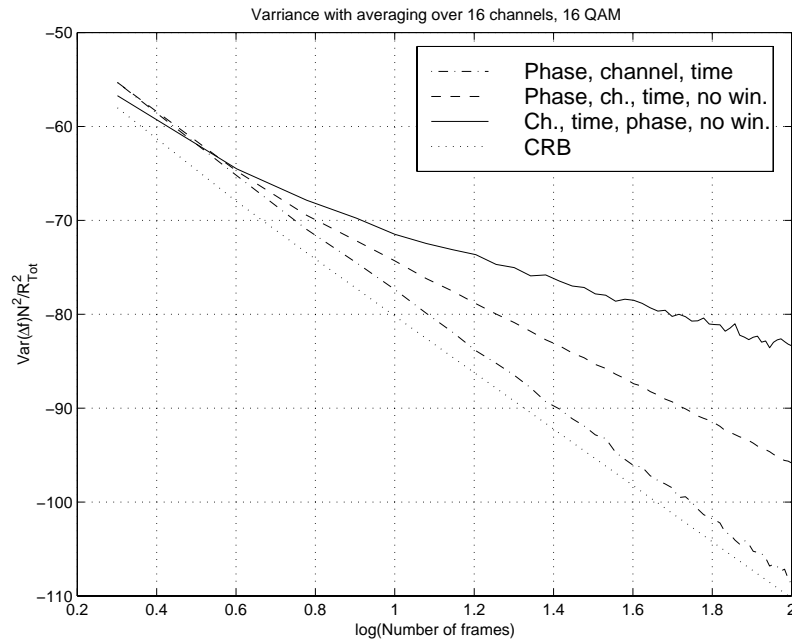
Figure 5.8. *Simulated values for CFO estimate variance (dB) for DD tracking with, $N = 16$, $SNR = 30dB$, 16-QAM, and different permutations of phase extraction, time averaging and channel averaging*

For estimator two, phase extraction before time and channel averaging, using constant amplitude modulation time windowing, there is a close to constant loss compared to CRB. This loss was calculated above to be 2.8dB for $K = 2$. The variance is thus proportional to $1/K^3$. Removing the time windowing, the inclination of the curve equals $-20dB$ per decade for high K, i.e. estimator variance proportional to $1/K^2$. With estimator four, channel and time averaging before phase extraction, without any weighting or windowing, the curve has an inclination of approx. $-10dB$ per decade for high K, i.e. estimator variance proportional to $1/K$. For estimator four, the constant amplitude time windowing has no value.

Avoiding weighting due to complexity, the choice of frequency estimator will thus affect the performance for non constant amplitude modulation. In the rest of this work, the only weighting function considered is the constant amplitude time windowing, due to the complexity of the other weighting functions.

5.4.3 Bias of frequency estimate

Similar to the DD phase error estimator, Chapter 5.3.3, the proposed frequency off-set estimators are unbiased under the assumption of negligible SER. At low SNR where the SER is not negligible, the estimators will be biased. Estimator seven and eight are based on the assumption of two phase estimates to be unbiased, at low SNR this is not the case, Figure 5.3. Estimator one to six are all based on Equation 5.21. In Figure 5.10. the mean and variance are plotted for estimator four with $\Delta f = 10^{-2}$, $N = 16$, 256-QAM and $K = 2$ (no time averaging)
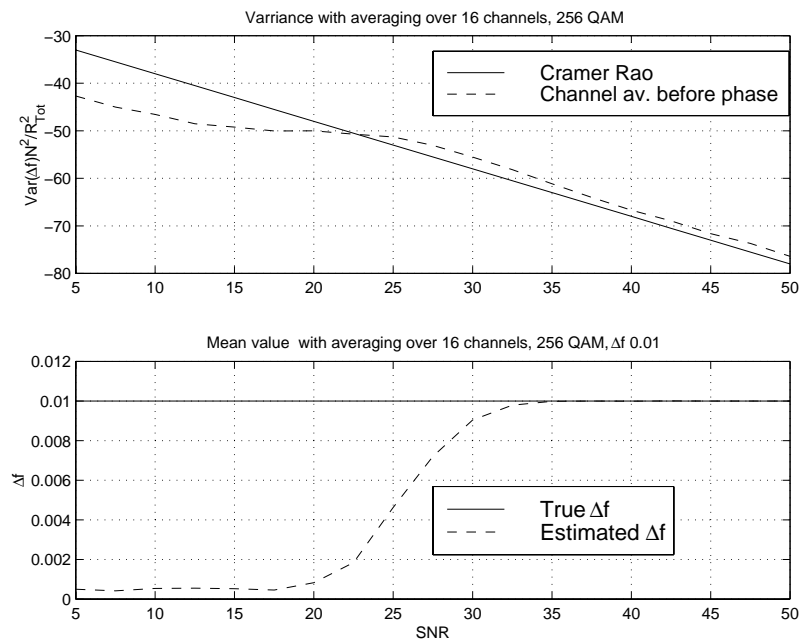
Figure 5.9. *CRB and simulated values for CFO estimate variance (dB) at top, $\Delta f = 10^{-2}$ and estimator mean value at bottom. DD tracking, $N = 16$, $K = 2$ (no time averaging) and 256-QAM.*

Similar to phase estimation, the frequency estimate becomes biased for low SNR due to a significant SER. This explains why the estimator variance can grow lower than CRB. Since the algorithm is intended for systems with low SER and thus high SNR, the phase estimator bias at low SNR will not be of interest during tracking.

5.4.4 Simulated variance of frequency estimate

In this chapter the estimator variance is simulated as a function of SNR for the different frequency estimators. Where available, the results are compared with calculated values. The estimator quality demands are treated in Chapter 6 together with a discussion of the consequences of a small CFO during tracking. Estimators two, four, five and six which all are guaranteed against the need of phase unwrapping will be discussed first. Afterwards estimators seven and eight will be discussed under the assumption of no need of phase unwrapping.

5.4.4.1 Constant amplitude modulation

Variance with channel averaging

As discussed above, the frequency estimators attain CRB with uniform channel weighting for constant amplitude modulation. In pilot based systems no data is transferred in the pilot channels. These systems should thus always base the synchronization on constant amplitude signals, independent of modulation in the data channels. The performance of DA frequency tracking is compared here with constant amplitude DD tracking and CRB. The number of channels used for averaging differs between DA and DD estimation. With CRB dependant on the number of channels used for averaging, Equation 5.5, CRB for DA and DD estimation will differ with a factor equal to the pilot spacing in the DA system, assuming CFO estimation over the same number of frames.

As an example, the performance of the DA frequency estimator, Equation 5.16, is compared to the DD frequency estimator, Equation 5.20, with 4-QAM, $N = 64$ channels, no time averaging, $K = 2$, and pilot spacing equal to 8, Figure 5.10.

As can be seen from Figure 5.10, both the DD and the pilot based CFO estimate do perform close to the CRB except for low SNR. The small number of decision errors at medium and high SNR gives thus no significant degradation of the DD estimator performance. With constant amplitude modulation, the DD estimator will be superior to the pilot based estimator measured in variance of the estimate. The variance of the estimators differ with a factor equal to the pilot spacing.

Equal power in all channels is assumed in this work. In the case of pilot based systems, or other systems using a subset of the channels for synchronization, a synchronization performance gain can be achieved by increasing the power in the synchronization channels, (Clasen and Meyr 94). This will be at the cost of reduced SNR in the other (data) channels.
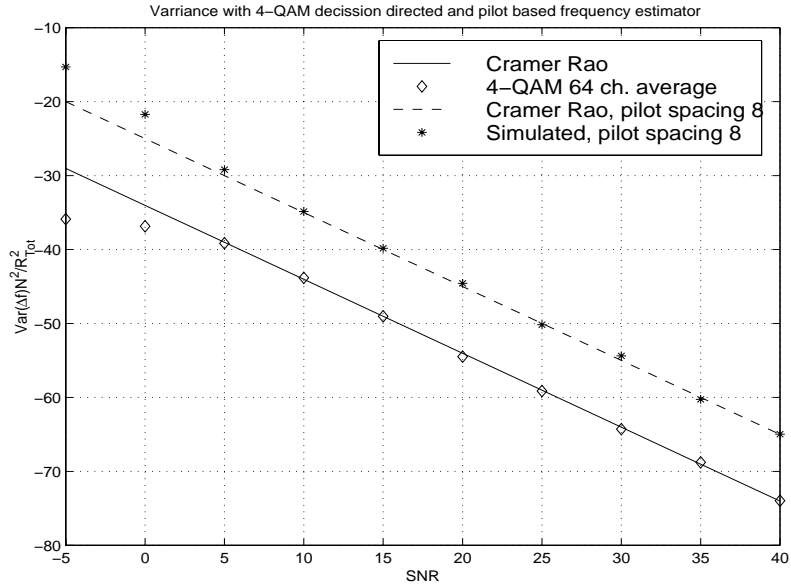
Figure 5.10. *CRB and simulated values for CFO estimate variance (dB) for DD tracking and pilot based tracking with pilot spacing equal to* 8*, N = 64, K = 2 (no time averaging) and 4-QAM, i.e. constant amplitude modulation*

.
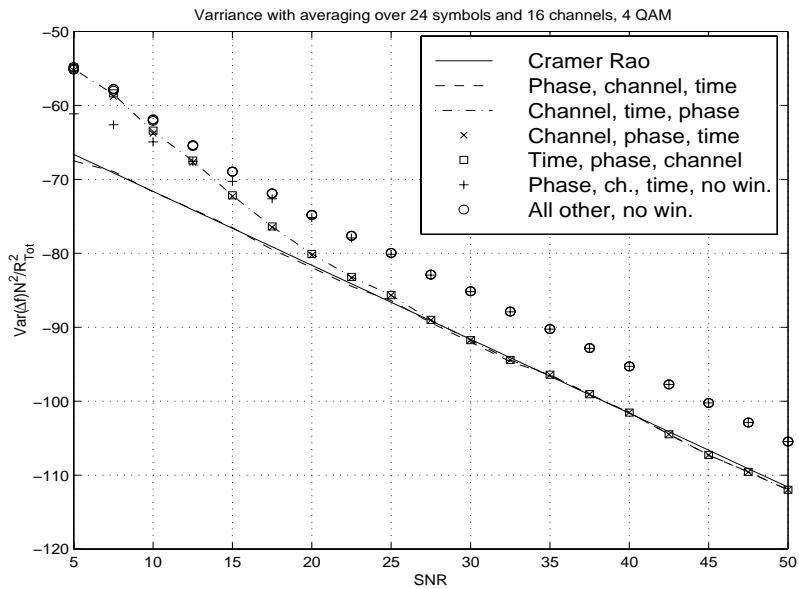
Figure 5.11. *CRB and simulated values for CFO estimate variance (dB) for DD tracking with, N = 16, K = 24, 4-QAM (constant amplitude), and different permutations of phase extraction, time averaging and channel averaging*

Time and channel averaging

CRB and simulated DD estimator performances are shown in Figure 5.11 for averaging over $N = 16$ channels and $K = 24$ symbols with and without time windowing

Using phase extraction before averaging with time windowing, the estimator obtains CRB even at low SNR, Figure 5.11. Any averaging before phase extraction will make the estimator approach CRB asymptotically (still using time windowing). This reduces the distance between the estimators with and without time windowing at low and moderate SNR. With time averaging over $K = 24$ symbols, the estimator performances with and without windowing differs with approx. $2dB$ at $SNR = 15dB$, which is a sufficient SNR for operation with 4-QAM. If averaging is performed before phase extraction, the value of time windowing must thus be considered for the actual averaging length and SNR used for system operation. Without windowing the performance is similar for all estimators.

Considering complexity and performance for constant amplitude modulation, this excludes all solutions with phase extraction in the middle and the solution with phase extraction before averaging and no windowing.

5.4.4.2 Non constant amplitude modulation

Variance with channel averaging

With channel averaging, the phase extraction can be performed before or after the channel averaging. Simulated values of the two alternatives are plotted in Figure 5.12 for 16-QAM and 256-QAM together with CRB. There is no time averaging, i.e. $K = 2$, $N = 16$ channels and no channel weighting.

At medium and high SNR where the SER is small, the estimators show a loss compared to CRB as calculated in Equation 5.28 and 5.31. For the worst case, 256-QAM DD frequency estimator with phase extraction before channel averaging, the loss equals $5.4dB$. This performance is slightly better than the performance of a pilot based system with pilot spacing equal to 4 channels. Including weighting, the performance at medium and high SNR becomes close to similar for both estimators and for 16-QAM and 256-QAM as calculated in Chapter 5.4.2, Figure 5.13.

CFO estimation for non constant amplitude modulation and no time averaging, channel averaging without weighting before phase extraction gives low complexity with only a small performance loss.
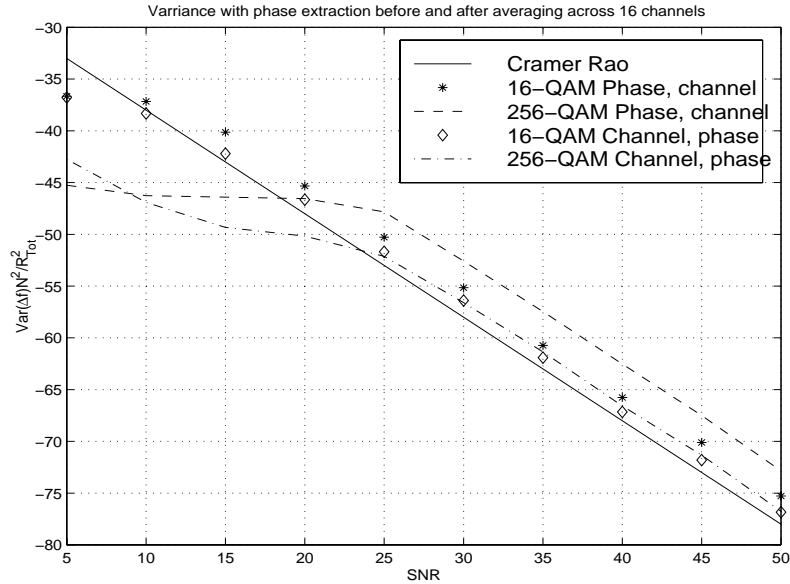
Figure 5.12. *CRB and simulated values for CFO estimate variance (dB) for DD tracking with, $N = 16$, $K = 2$ (no time averaging) and no weighting for 16-QAM and 256-QAM, with phase extraction before and after channel averaging*
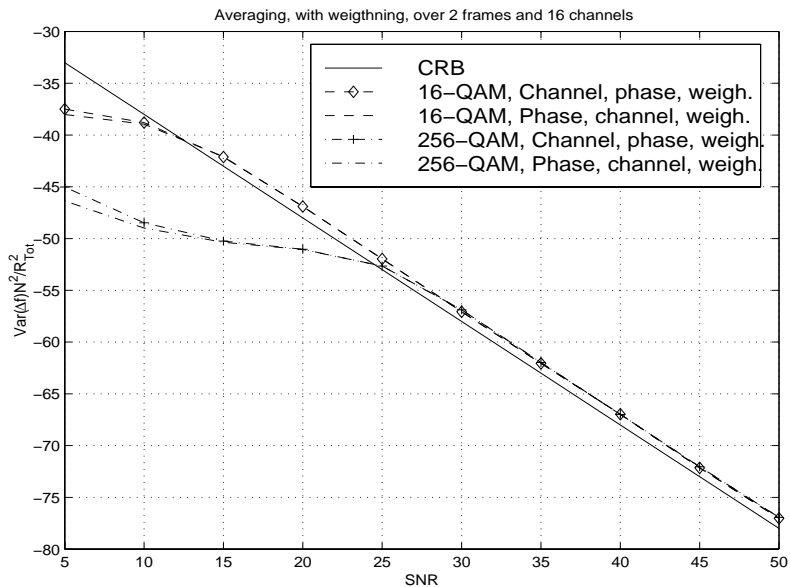
Figure 5.13. *CRB and simulated values for CFO estimate variance (dB) for DD tracking with $N = 16$, $K = 2$ (no time averaging) and chan. weighting for 16-QAM and 256-QAM, with phase extraction before and after channel averaging*

Time and channel averaging

The performance of the estimators are simulated for $K = 24$ frames, $N = 16$ channels and 16-QAM. Non of the estimators use channel weighting, but estimators two, five and six of Table 5.1 are simulated with and without constant amplitude time windowing. estimator four is simulated with neither channel weighting nor time windowing.
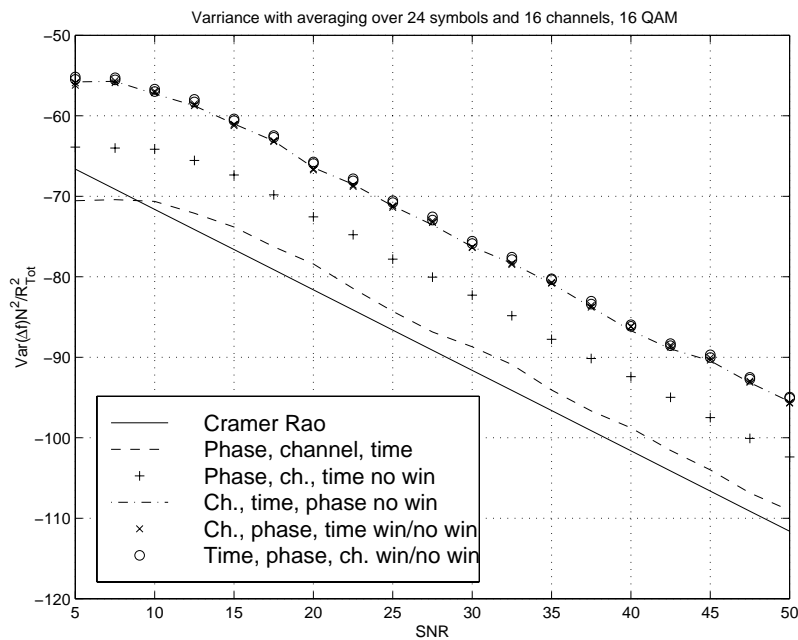
Figure 5.14. *CRB and simulated values for CFO estimate variance (dB) for DD tracking with, $N = 16$, $K = 24$, 16-QAM, and different permutations of phase extraction, time averaging and channel averaging. No channel weighting.*

The results for estimators two and four in Figure 5.14 agrees with the observations in Figure 5.8. In addition, it is observed that estimators five and six have performance equal to estimator four. Considering complexity and performance, estimators five and six will thus not be of interest for non constant amplitude modulation. For the given example, the lower complexity estimator, with averaging before phase extraction, has an estimator variance which is more than 10dB larger than the estimator with time windowing and phase extraction before averaging. For CFO estimation with non constant amplitude modulation, time and channel averaging there will be a trade off between complexity and performance.

5.4.4.3 Variance of frequency estimate with explicit phase difference

Assuming that phase unwrapping is no problem, the "wrapping sensitive" frequency estimators seven and eight in Table 5.2 can be applied.

Variance with channel averaging

The performance of the "wrapping sensitive" estimators for both constant and non constant amplitude modulation are plotted in Figure 5.15, $K = 2$ and $N = 16$.
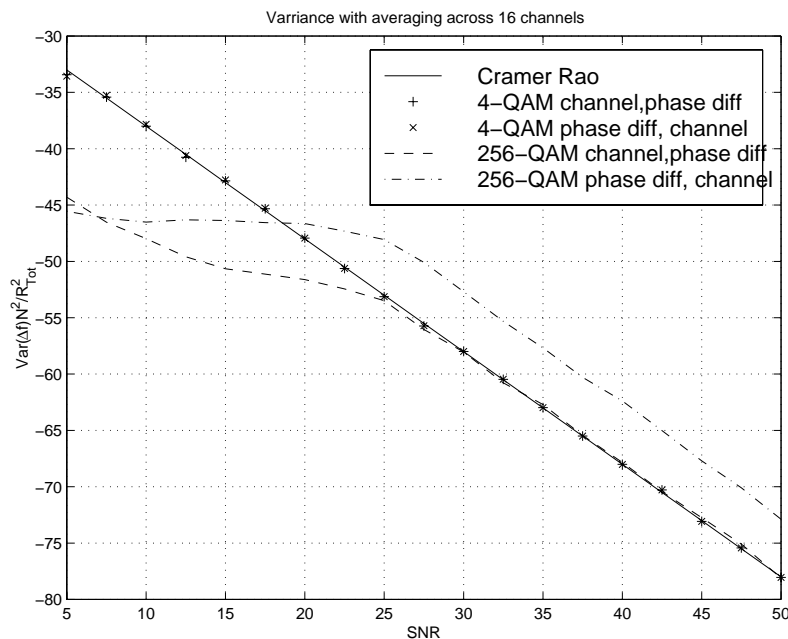
Figure 5.15. *CRB and simulated values for CFO estimate variance (dB) for phase wrapping sensitive DD tracking with, $N = 16$ and $K = 2$.*

Averaging across 16 channels, estimator seven with channel averaging before phase extraction obtains CRB independent of constellation size. Estimator eight, which can be applied to non frequency flat transmission channels as well, suffers from the "constellation loss" $E[1/A^2]$ discussed earlier, where A^2 equals the power of one symbol. Referring to Table 5.2, estimators eight and two without channel weighting are comparable in complexity and performance. Both are applicable for no frequency flat transmission channels and both suffering of a performance loss for non constant amplitude modulation. Comparing estimator seven with estimator four, the complexity is similar and the performance equals CRB, i.e. it is approx. 1 dB better

than estimator four for non constant amplitude modulation. Unlike estimator four, number seven can not be applied with non frequency flat transmission channels. Considering performance, complexity, the phase unwrapping problem and non frequency flat transmission channels, estimator four without channel weighting is a good alternative for CFO estimation without time averaging.

One should keep in mind that the results for non flat transmission channels given in Figure 5.15. are valid for per channel phase and frequency estimation. If the coherence bandwidth is large enough to average over a number of channels before phase extraction, the performance approaches CRB rapidly, Figure 5.4.

Variance with time and channel averaging

Including both time and channel averaging, the performance is plotted in Figure 5.16 with averaging over $K = 24$ frames and $N = 16$ channels.
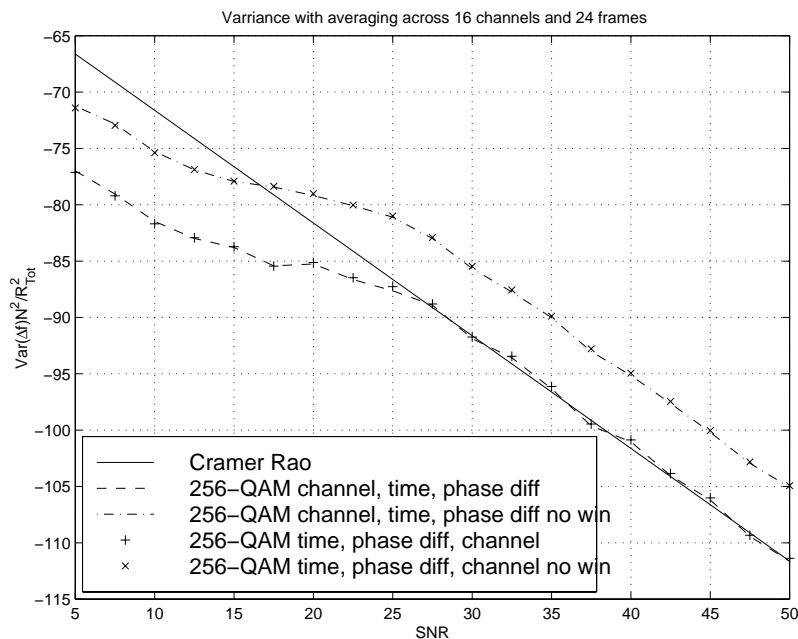
Figure 5.16. *CRB and simulated values for CFO estimate variance (dB) for phase wrapping sensitive DD tracking with, $N = 16$ and $K = 24$.*

Including time averaging and windowing in addition to channel averaging, both estimator seven and eight obtain CRB, independent of constellation size. The phase wrapping sensitive estimators will thus always outperform the phase wrapping insensitive estimators for CFO estimation with non constant amplitude modulation, time and channel averaging. The choice of estimator will thus be a trade off where,

performance, complexity, phase wrapping and time dispersion in the transmission channel must be considered.

5.4.5 Lock-in range of DD frequency tracking

The lock-in range of the carrier frequency tracking algorithms in this chapter will not be discussed, but rather the range of unbiased frequency estimation in a noise less system. The lock-in range will be larger than the unbiased frequency estimation range, but for carrier frequency errors outside the unbiased frequency estimation range the estimated CFO will move slowly towards the true CFO. To speed up synchronization, specialized frequency acquisition algorithms should be applied.

All discussed estimators are unbiased under the assumptions of negligible SER and negligible IBI. With pilot based tracking the transmitted symbols a_{pilots} are known, and the region of unbiased CFO estimation should thus equal $\Delta f = \pm 1/(2T)$. But this would be a violation against the received signal model, Equation 5.15, where IBI is neglected, (Mengali and D'Andrea 97). The true region of unbiased CFO estimation for DA tracking will thus be smaller. A coarse estimate of maximum CFO with unbiased frequency estimation during DD tracking is a requirement of no phase slipping. For 16-QAM with high SNR, the maximum tolerated phase error in front of the decision device is approx. $\pm 0,075\pi$ resulting in an unbiased frequency estimation area of approx. $\Delta f = \pm 0,075/(2T)$.

5.5 Summary

Methods for decision directed (DD) carrier phase tracking and carrier frequency tracking in OFDM have been presented. Their performances have been investigated by comparing estimator variance with Cramer Rao Bound (CRB). The best of the proposed estimators perform close to or equal to CRB. The proposed DD tracking algorithms perform better than DA tracking with a factor close to or equal to the pilot spacing in the DA systems.

All discussed methods are based on removal of the modulation influence of the received signal, by multiplication with the complex conjugated of the receiver estimate of the transmitted symbol. After removing modulation influence, the phase error can be estimated by phase extraction, while the CFO is estimated by dividing the phase change between subsequent frames with the symbol duration.

The proposed phase error estimator performs equal to CRB independent of constellation size and number of symbols used for averaging. CRB decrease with the first

power of the number of channels and frames used for averaging. If no averaging is performed, CRB for non constant amplitude modulation is higher than CRB for constant amplitude modulation. Averaging over a small number of symbols, the difference in CRB for different constellation sizes will be negligible. Compared to pilot based DA phase tracking, the performance of the DD phase tracking is better with a factor equal to the pilot spacing in the DA system. Alternatively, the DA system must average over an increased number of frames to obtain the same performance, decreasing the CFO tolerance of the phase tracking algorithm.

Eight different DD CFO estimators are proposed in this chapter, all of them unbiased for negligible SER. Six are related to the frequency estimator of (Kay 89) and do not need phase unwrapping. These estimators are based on phase extraction after multiplying the signal of consecutive frames. The six estimators differ by the order of phase extraction, channel averaging and frame averaging. The last two estimators are based on per frame phase extraction and explicit phase difference. These two estimators depend on phase unwrapping.

First the six estimators related to the frequency estimator of (Kay 89) are discussed. Comparing performance and complexity, the estimators with phase extraction in the middle and averaging before and after can be excluded. For constant amplitude modulation, two more estimators can be excluded. The two estimators left are the original estimator, number two in Table 5.1, with phase extraction before averaging across channels and frames, and the estimator with averaging across channels and frames before phase extraction, number four in Table 5.1. Estimator two, obtains CRB for constant amplitude modulation, with and without frame and channel averaging. The CRB decreases with the third power of the number of frames used for averaging, as well as with the first power of SNR and number of channels used for averaging. The dependency on number of channels used for averaging makes DD frequency estimation outperform pilot based frequency estimation with a factor equal to the pilot spacing. To reduce the complexity, estimator number four can be used. With only channel averaging the performance of estimator four is identical to the performance of estimator two. If there is both time and channel averaging, estimator four attains CRB asymptotically with increasing SNR, resulting in a performance loss at low and moderate SNR. To obtain CRB, a time windowing function is used during frame averaging. This can be avoided to reduce complexity giving a performance loss proportional to the first power of the number of frames. The variance of the estimators without windowing will thus decrease with the second power of the number of frames.

For non constant amplitude modulation, two Kay related estimators are investigated. One with phase extraction before averaging across frames and channels, and one with averaging across frames and channels before phase extraction. The Kay related

estimators based on multiplication of successive symbols before phase extraction, suffer from a performance loss compared to CRB with non constant amplitude modulation. To maximize performance, symbol dependant channel weighting and time windowing is necessary. But even with optimum weighting and windowing, the performance does not reach CRB. The loss with optimum weighting and windowing increases from 0.8dB using two frames to 1.4dB using six frames. The complexity of the weighting and windowing functions increases rapidly with increasing number of frames and channels. Dropping windowing and weighting to reduce complexity, the performance loss differs for the different CFO estimators. The estimator with phase extraction before averaging and constant amplitude time windowing can be applied even for non constant amplitude modulation. This will result in a constant loss compared to CRB, independent of number of frames and channels applied for averaging. I.e. variance will decrease with the third power of the number of frames used for averaging. The loss increases with increasing constellation size, 256-QAM gives a loss of approx. 5dB. Dropping the windowing function, there is an extra loss dependant on the number of frames used for averaging. The resulting variance decreases with the second power of the number of frames. Using the estimator with averaging before phase extraction, without channel weighting or time windowing, the variance decreases with the first power of the number of frames and is little dependant on constellation size (16-QAM and larger). Averaging over a large number of frames the estimator with phase extraction before averaging is thus superior, but averaging over a small number of frames the estimator with averaging before phase extraction is better.

The two CFO estimators which depend on phase unwrapping perform equal to CRB for constant amplitude modulation. Both estimators also obtain CRB for non constant amplitude modulation using both time and channel averaging. With only channel averaging, the frequency estimator with averaging over all channels before phase extraction, obtains CRB. But for non frequency flat transmission channels this estimator can not be used. With no time averaging, the estimator with phase extraction before channel averaging suffers from a loss equal to $E[1/A^2]$, where A^2 equals the power of one symbol.

Choosing CFO estimator, performance and complexity together with the effects of phase unwrapping and non frequency flat transmission channels must be considered. If only channel averaging is performed, the phase wrapping insensitive estimator four with channel averaging before phase extraction is a good alternative for both constant and non constant amplitude modulation. If both time and channel averaging is performed, there will be a trade off between the factors listed above.

Chapter 6
System degradation due to non ideal carrier tracking and channel time variations

During carrier frequency tracking the synchronization is not perfect. At the output of the tracking module, there will be a stochastic time varying residual CFO with zero mean and variance as described in Chapter 5. This residual CFO will generate Inter Bin Interference (IBI) in an OFDM system. The loss of orthogonality because of CFO, is one of the subjects in discussions about the feasibility of OFDM for different applications. Every system experiencing a CFO will suffer from a system performance degradation. The CFO generated IBI is special for the OFDM systems, and can be viewed as a transformation of signal power into interference power. This signal to interference (i.e. noise) power transformation makes the OFDM systems more vulnerable for CFO than SC systems. In addition, the symbol length is increased in OFDM systems compared to SC systems, making OFDM systems experience phase slipping at a lower CFO than SC systems.

The scope of this chapter is to quantify the system degradation due to IBI, during steady state tracking mode. IBI generated by CFO and IBI generated by Doppler spread are investigated.

The degradation, measured as SNR reduction, will be calculated as a function of CFO on stationary transmission channels. This is done both for rectangular pulse QAM systems and O-QAM systems with different pulse shapes. The influence of SNR and number of subchannels in the system together with the statistical properties of the IBI will also be discussed.

For flat Rayleigh fading transmission channels, degradation quantified by the SER will be calculated as function of CFO and Doppler bandwidth. A CFO is a frequency

shift of the signal, while a fading (i.e. time varying) channel is a frequency dispersion of the signal, also denoted as a Doppler spread of the signal. The fading channel can thus be viewed as a generalization of a CFO. Just like a CFO, a Doppler spread will generate IBI and reduce system performance. On a fading channel without CFO the Doppler spectra will be located around zero frequency. If the CFO is equal to Δf, the Doppler spectrum will be located around Δf. The influence of number of channels in the system and SNR level will be discussed together with statistical properties of the IBI. To isolate the effects of CFO and time varying channels, only non time dispersive, or frequency flat, channels are treated in this work. However during the design of the example system for fading channels, tolerated time dispersion is used as design criterion.

The calculations in this chapter are based on time continuous pulseshaping filtering. The guard channels, Chapter 2.4.3, will thus have no effect and are neglected during the calculations. During the time discrete simulations guard channels are included. Consequences of oscillator phase noise is not specifically treated in this work.

The chapter is organized as follows: Chapter 6.1 contains references to earlier work, degradation due to a CFO on a stationary transmission channel is discussed in Chapter 6.2, while Chapter 6.3 treats the effects of flat fading transmission channels and the effects of CFO on such a channel. Chapter 6.4 is a summary.

This chapter is partly based on (Remvik and Holte 97b) and (Remvik et. al 98).

6.1 Previous work

The earlier contributions to the literature on the consequence carrier errors in OFDM, have been concentrated on the effect of Carrier offset in rectangular pulse systems on stationary transmission channels. Analysis and estimation of CFO for square pulse systems have been treated in (Moose 94) and (Speth et. al 98), while the most extensive work in analysing the effect of CFO in rectangular pulse systems was carried out by (Pollet et. al 95). This last work and (El-Tanany and Wu 97) analyse the effect of phase noise.

6.2 CFO on Stationary AWGN channels

Fixed radio links is one example of systems which can be modelled as stationary Additive White Gaussian Noise (AWGN) channels, typically systems with low SER. In fixed radio links and several other systems, bandwidth is limited at the same time

as co channel interference and co system interference limit transmit power. The system designer must thus optimize the use of both. This chapter will concentrate on bandwidth efficient OFDM systems operating on channels with high SNR and low SER. Both QAM systems with rectangular pulses without guard interval and O-QAM systems with other pulse shapes are discussed.

6.2.1 Received signal

QAM and Square pulses

The OFDM system discussed in this section is the system with rectangular pulses, without guard interval, and a carrier offset as described in Chapter 2. The received symbol including a CFO is given by Equation 3.2 and is repeated here, including a flat AWGN channel:

$$z_{k,m} = \frac{1}{T} \sum_{n=0}^{N-1} \left(a_{k,n} \int_0^T e^{j\frac{2\pi}{T}(n-m+\Delta fT)\tau} d\tau \right) + N_{k,m} \tag{6.1}$$

$N_{k,m}$: Channel noise contribution in channel m, frame k.

A consequence of the carrier offset is the phase rotation, but in the analysis of the CFO created system degradation it is assumed that a perfect phase estimate is available and is used for phase correction. Using this assumption, Equation 6.1 can be rewritten for time $k = 0$, (Pollet et. al 95):

$$z_{0,m} = a_{0,m}|I_0| + \left(\sum_{\substack{n=0 \\ n \neq m}}^{N-1} a_{0,n}I_{m-n} + N_{0,m} \right) e^{-j\arg I_0} \tag{6.2}$$

Where

$$I_p = \frac{1}{T} \int_0^T e^{-j2\pi\frac{p}{T}t} e^{j2\pi\Delta ft} dt \tag{6.3}$$

$a_{0,n}I_{m-n}$: interference from channel n into channel m.

I_0: damping factor of the desired signal.

With symbols transmitted from time $-\infty$ to ∞ there will be no loss of generality by studying time $k = 0$. The factor of $e^{-j \arg I_0}$ in Equation 6.2 is the perfect phase correction discussed earlier.

O-QAM with symmetrical filters

In this section the O-QAM OFDM system described in Chapter 2 with carrier offset is discussed under the assumption of flat AWGN channel. The presentation will be valid for both bandlimited and timelimited pulses. The real and imaginary part of the received symbols was presented in respectively Equation 3.4 and 3.5 for the case of a CFO Δf, these results are repeated here for time $k = 0$ and with the addition of channel noise. With transmission of symbols from $-\infty$ to ∞ there will be no loss in generality by studying the system at time $k = 0$. Studying the system at $k = 0$ will give zero phase error due to the CFO at the sampling instant of the real part.

$$
\begin{aligned}
Re\{z_{0,m}\} = \sum_{n=0}^{N-1} \sum_{l=-\infty}^{\infty} Re\{a_{l,n}\} \int_{-\infty}^{\infty} h(t-lT)h(t) \\
\cdot \cos\left(\left(\frac{2\pi}{T}t + \frac{\pi}{2}\right)(n-m) + 2\pi\Delta f t\right)dt \\
- Im\{a_{l,n}\} \int_{-\infty}^{\infty} h\left(t - lT + \frac{T}{2}\right)h(t) \\
\cdot \sin\left(\left(\frac{2\pi}{T}t + \frac{\pi}{2}\right)(n-m) + 2\pi\Delta f t\right)dt + N_{Rm}
\end{aligned}
\tag{6.4}
$$

The imaginary part, which is transmitted $T/2$ ahead of the real part experiences a phase rotation equal to $e^{-j2\pi\Delta f T/2}$ compared to the real part. This phase difference between real and imaginary part is assumed perfectly compensated. With a substitution of integration variable $\tau = t + T/2$ and the discussed correction of the imaginary part phase angle compared to the real part phase angle, the received imaginary symbol equals:

$$Im\{z_{0,m}\} = \sum_{n=0}^{N-1} \sum_{l=-\infty}^{\infty} Im\{a_{l,n}\} \int_{-\infty}^{\infty} h(\tau - lT)h(\tau) \tag{6.5}$$

$$\cdot \cos\left(\left(\frac{2\pi}{T}\tau + \frac{\pi}{2}\right)(n-m) + 2\pi\Delta f\tau\right)d\tau$$

$$+ Re\{a_{l,n}\} \int_{-\infty}^{\infty} h\left(\tau - (l+1)T + \frac{T}{2}\right)h(\tau)$$

$$\cdot \sin\left(\left(\frac{2\pi}{T}\tau + \frac{\pi}{2}\right)(n-m) + 2\pi\Delta f\tau\right)d\tau + N_{Im}$$

Recognizing the similarity between the shape of the received real part and the shape of the received imaginary part, the complete received complex symbol can be written as

$$z_{0,m} = a_{0,m}\Lambda_{0,0} \tag{6.6}$$

$$+ \sum_{\substack{l=-\infty \\ l \neq 0}}^{\infty} a_{l,m}\Lambda_{l,0} + \sum_{\substack{n=0 \\ n \neq m}}^{N-1} \sum_{l=-\infty}^{\infty} a_{l,n}\Lambda_{l,m-n}$$

$$+ \sum_{n=0}^{N-1} \sum_{l=-\infty}^{\infty} -Im\{a_{l,n}\}\Gamma_{l,m-n} + jRe\{a_{l,n}\}\Gamma_{l+1,m-n} + N_m$$

Where

$$\Lambda_{l,p} = \int_{-\infty}^{\infty} h(t-lT)h(t) \cdot \cos\left(\left(\frac{2\pi}{T}t + \frac{\pi}{2}\right)p + 2\pi\Delta ft\right)dt$$

$$\tag{6.7}$$

$$\Gamma_{l,p} = \int_{-\infty}^{\infty} h\left(t-lT + \frac{T}{2}\right)h(t) \cdot \sin\left(\left(\frac{2\pi}{T}t + \frac{\pi}{2}\right)p + 2\pi\Delta ft\right)dt$$

$\Lambda_{0,0}$: damping factor of the wanted signal.

$\Lambda_{l,\,m-n}$: Interference from real part of channel n, symbol l into real part of channel m, symbol 0, and from imaginary part to imaginary part.

$\Gamma_{l,\,m-n}$: Interference from the imaginary part of channel n, symbol l, into the real part of channel m, symbol 0.

$\Gamma_{l+1,\,m-n}$: Interference from the real part of channel n, symbol l, into the imaginary part of channel m, symbol 0.

N_{Rm}, N_{Im}, N_m: Channel noise in real part, imaginary part and the total complex symbol of channel m.

According to Equation 6.6 it may look like the interference between the real and imaginary part is unsymmetrical, this is not the case. In O-QAM the real and imaginary parts are transmitted with a separation in time of $T/2$, each real part will be transmitted mid way between two imaginary parts and vice versa. Which imaginary part belongs to which real part to produce a complete complex symbol, is only a matter of definition. In this work the definition is that the real part is transmitted after the imaginary part. The interference between the quadratures can be described as:

$\Gamma_{l,\,m-n}$: interference from one quadrature of channel n, into the other quadrature of channel m which is transmitted $(l-1/2)T$ earlier.

Comparison of the systems

With perfect phase correction, the received signal $z_{0,\,m}$ is the transmitted signal $a_{0,\,m}$ multiplied with a damping factor, $|I_0|$ for the QAM system and $\Lambda_{0,\,0}$ for the O-QAM system. In addition to the signal component, there is channel noise and signal generated noise. In the QAM system with square pulses, the signal generated noise is pure ICI originating from the other channels in the same frame, or at the same time, with weight factors for the different channels. In an O-QAM system with pulses of length larger than T there will be both ICI and ISI. The ISI arise both between subsequent frames and between real and imaginary parts of symbols. This ISI behaviour is also known from SC O-QAM systems (Jesupret et. al 91).

6.2.2 SNR at the receiver

The noise observed by the receiver will equal the sum of channel noise and interference. Since a CFO transfer some of the transmitted signal power to ISI and/or ICI, a CFO will reduce the received SNR and increase the symbol error rate of the system. In this chapter the SNR reduction will be quantified according to the same procedure as used by (Pollet et. al 95) for CFO analysis.

In an OFDM system with white Gaussian noise and no other impairments, the SNR at the receiver is given by

$$SNR_{\Delta f = 0} = \frac{E[a^2]}{\sigma_N^2} \tag{6.8}$$

σ_N^2: variance of the white Gaussian noise.

The power of the transmitted signal is normalized, $E[a^2] = 1$. Introducing a CFO of $\Delta f = \Delta F$ will give reduced received signal component power and IBI which will be added to the Gaussian channel noise. The implications of a given level of IBI will depend on its statistical distribution, which is unknown but will be assumed Gaussian with zero mean. The choice of zero mean Gaussian distribution is motivated by the IBI being a weighted sum of zero mean, independent, identically distributed (iid) stochastic variables. The zero mean of the independent members in the sum assures zero mean of the whole sum. The distribution of each member in the sum will depend on the transmitted symbol alphabet, while an unweighted sum of the iid variables approaches a Gaussian distribution as the number of members in the sum grows infinitely, according to the central limit theorem. Assuming Gaussian statistics of the IBI one should keep in mind that both the finite number of members in the sum and the weighting are violations to the use of the central limit theorem.

Under the assumption of zero mean Gaussian IBI, which is uncorrelated with the channel noise, the two noise contributions can be added to one Gaussian noise source. The total noise power equals the sum of the IBI power and the channel noise power, resulting in a SNR equal to:

$$SNR_{\Delta f = \Delta F} = \frac{E_0}{\sigma_N^2 + V_0} \tag{6.9}$$

E_0: power of the received signal component

V_0: power of the signal generated interference, or IBI

Using Equation 6.2 and 6.6, E_0 and V_0 in channel m for a stationary channel equals:

$$E_0 = \begin{cases} |I_0|^2 & QAM \\ \Lambda_{0,0}^2 & OQAM \end{cases} \tag{6.10}$$

$$V_0 = \begin{cases} \displaystyle\sum_{\substack{n=0 \\ n \neq m}}^{N-1} |I_{m-n}|^2 & QAM \\[2em] \displaystyle -\Lambda_{0,0}^2 + \sum_{n=0}^{N-1}\sum_{l=-\infty}^{\infty} (\Lambda_{l,m-n}^2 + \Gamma_{l+1,m-n}^2) & OQAM \end{cases}$$

(6.11)

According to Equation 6.11, V_0 depends on the receiver channel number, m. The SNR will thus not be equal for the different channels in the receiver. But since the largest IBI contribution comes from the closest channels, the only channels with a V_0 differing significantly from the other channels, will be the channels with number close to or equal to 0 and $N-1$. In the calculations in this work, V_0 in all channels are approximated with V_0 for channel number $N/2$.

In the case of O-QAM the largest contributors to the signal generated noise is the interference between the real and the imaginary part at the same channel, and the interference between subsequent symbols at the same channel. In OFDM systems without guard interval a multipath channel will generate ISI and a per channel equalizer will be needed to remove it. The CFO generated ISI can be assumed removed by the same equalizer. Before taking into account the noise enhancement, the power of the signal generated noise with equalizer equals:

$$V_0 = \begin{cases} \displaystyle\sum_{\substack{n=0 \\ m \neq n}}^{N-1} |I_{m-n}|^2 & QAM \\[2em] \displaystyle \sum_{\substack{n=0 \\ n \neq m}}^{N-1}\sum_{l=-\infty}^{\infty} (\Lambda_{l,m-n}^2 + \Gamma_{l,m-n}^2) & OQAM \end{cases}$$

(6.12)

In the SC case $V_0 = 0$, and the only effect of a CFO is a scaling of the signal power for both QAM and O-QAM with equalization. This scaling is given by

$$SNR_{SC} = SNR_{\Delta f = 0} \cdot \begin{cases} |I_0|^2 & QAM \\ \Lambda_{0,0}^2 & OQAM \end{cases} \tag{6.13}$$

A single carrier O-QAM system without equalization suffers from additional signal generated noise, (Jesupret et. al 91).

$$SNR_{SC-OQAM} = \frac{\Lambda_{0,0}^2}{\sigma_N^2 - \Lambda_{0,0}^2 + \sum_{l=-\infty}^{\infty} \Lambda_{l,0}^2 + \Gamma_{l,0}^2} \tag{6.14}$$

The noise enhancement with per channel equalization will inflict on both channel noise and ICI, reducing the SNR. The response to be equalized $h(l)$ is found by setting $n = m$ in Equation 6.6.

$$h(l) = \Lambda_{-l,0} - Im\{ \}\Gamma_{-l,0} + jRe\{ \}\Gamma_{-(l+1),0} \tag{6.15}$$

$Re\{ \}$: Extraction of real part of signal

$Im\{ \}$: Extraction of imaginary part of signal

Rewriting Equation 6.15 as an over sampled system, the noise enhancement Ne can be calculated according to (Lee and Messerschmitt 94) for a zero forcing equalizer. This is included in the results of this chapter. For the CFO area which is investigated for stationary channels the noise enhancement is negligible, but for the CFO area investigated for fading channels the noise enhancement will be of importance.

The SNR degradation D for a given CFO, $\Delta f = \Delta F$, can be measured as the relationship between $SNR_{\Delta f = 0}$ and $SNR_{\Delta f = \Delta F}$

$$D_{\Delta F} = \frac{Ne\left(1 + \frac{V_0}{\sigma_N^2}\right)}{E_0} \tag{6.16}$$

According to Equation 6.16 D is increasing with increasing $1/\sigma_N^2$, i.e. $SNR_{\Delta f = 0}$. Since higher order constellations demand higher SNR for operation than lower order constellations, higher order constellations will suffer from larger degradation for a

given CFO than lower order constellations. $1/\sigma_N^2$ is multiplied with the IBI power V_0, and the problem of increasing degradation with increasing SNR is thus avoided for SC systems using QAM and O-QAM with equalization.

6.2.3 Influence of number of channels N

To be able to compare different systems, total symbol rate, R_{tot}, and power per symbol, $E[a^2]$, are kept constant. The CFO, Δf, is relative to the total symbol rate.

$$R_{tot} = \frac{N_1}{T_1} = \frac{N_2}{T_2} = const \qquad (6.17)$$

$$E[a^2]_1 = E[a^2]_2 \qquad (6.18)$$

$$\frac{\Delta f}{R_{tot}} = \frac{\Delta f T_1}{N_1} = \frac{\Delta f T_2}{N_2} \qquad (6.19)$$

N_1, N_2: Number of channels in system 1 and system 2

T_1, T_2: Symbol duration in system 1 and 2

$E[a^2]_1, E[a^2]_2$: Per channel signal power at the sampler in system 1 and system 2, equals unity in this work

According to the guidelines listed above, two QAM square pulse OFDM systems are compared, the first one with symbol interval T and N channels and the second one with symbol interval $2T$ and $2N$ channels. The interference to a given channel from a channel p channels away is given by Equation 6.3 for the N, T system, for the $2N, 2T$ system the interference equals:

$$I_p = \frac{1}{T}\int_0^T e^{-j2\pi\frac{p}{T}t} e^{j2\pi 2\Delta f t} dt \qquad (6.20)$$

Similarly, doubling the number of channels in an O-QAM OFDM system will give:

$$\Lambda_{l,p} = \int\limits_{-\infty}^{\infty} h(t - lT)h(t) \cdot \cos\left(\left(\frac{2\pi}{T}t + \frac{\pi}{2}\right)p + 2\pi 2\Delta ft\right)dt$$

$$\Gamma_{l,p} = \int\limits_{-\infty}^{\infty} h\left(t - lT + \frac{T}{2}\right)h(t) \cdot \sin\left(\left(\frac{2\pi}{T}t + \frac{\pi}{2}\right)p + 2\pi 2\Delta ft\right)dt$$

(6.21)

With the observation that the largest interference contributions come from the closest channels and assuming N to be sufficiently large, doubling the number of channels in the system equals doubling the CFO. With a tolerated CFO generated SNR degradation $D_{tolerated}$, a multiplication of the number of channels in the system with any factor, divides the tolerated CFO $\Delta F_{tolerated}$ with the same factor. The tolerated CFO is thus constant relative to the subchannel bandwidth.

In Chapter 2 it was shown that the use of O-QAM and optimized pulses will reduce the required number of channels and there by increase the CFO robustness, IF the number of channels is dictated by the spectral requirements. If the number of channels is decided by another criteria like the frequency correlation, as defined by (Steele 92), the different systems will use the same number of channels independent of pulse shaping.

6.2.4 Signal to noise ratio degradation

In this chapter the SNR degradation will be investigated as a function of CFO for given pulses used in OFDM systems. Assuming a system with limited SNR margin in the transmission budget, SNR degradations up to $1\,dB$ will be calculated and plotted. With number of channels influencing the CFO robustness as shown in Chapter 6.2.3, the investigation for O-QAM systems will be limited to the performance of the $4T$ length optimized pulse, which gives the lowest number of channels. The QAM system with rectangular pulse will also be investigated as well as a QAM single carrier system for the purpose of comparison.

To achieve a SER of 10^{-7} for a system with constellation size M, using QAM or OQAM and without other impairments than the additive Gaussian channel noise, a SNR of approx. $10(M-1)$ is necessary (Pollet et. al 95). This means that the SNR is a function of the constellation size, and as discussed in Chapter 6.2.2 the SNR degradation is a function of the SNR. Consequently, with a maximum tolerated degradation, the demands on the accuracy of the estimated carrier frequency in the receiver will increase with increasing constellation size.

Equation 6.16 is evaluated as a function of CFO for different M. $SNR_{\Delta f = 0}$ is chosen to give $SER = 10^{-7}$. In Figure 6.1 degradation D up to $1 dB$ is plotted for $N = 16$ channel OFDM systems, QAM with rectangular pulses and O-QAM with and without per channel equalization.
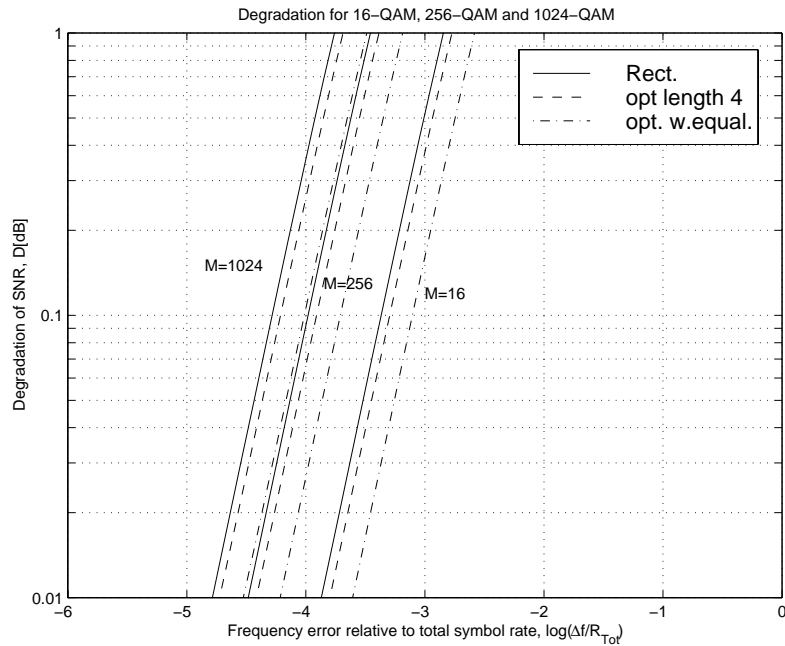
Figure 6.1. *Degradation as function of carrier frequency offset for 16 channel OFDM system with constellation size M.*

QAM shows the poorest performance for all M, while O-QAM without equalization is only slightly better. O-QAM with equalization permits approx. 1.5 times the CFO of the QAM system. Increasing the constellation size M from 16 to 256, the CFO accuracy must be increased approximately by a factor 4 to keep the SNR constant. Similarly, increasing M from 256 to 1024, the carrier frequency accuracy must be increased with a factor 2.

The results of evaluating Equation 6.16 for different number of channels N are shown in Figure 6.2 with a single carrier QAM system for comparison.
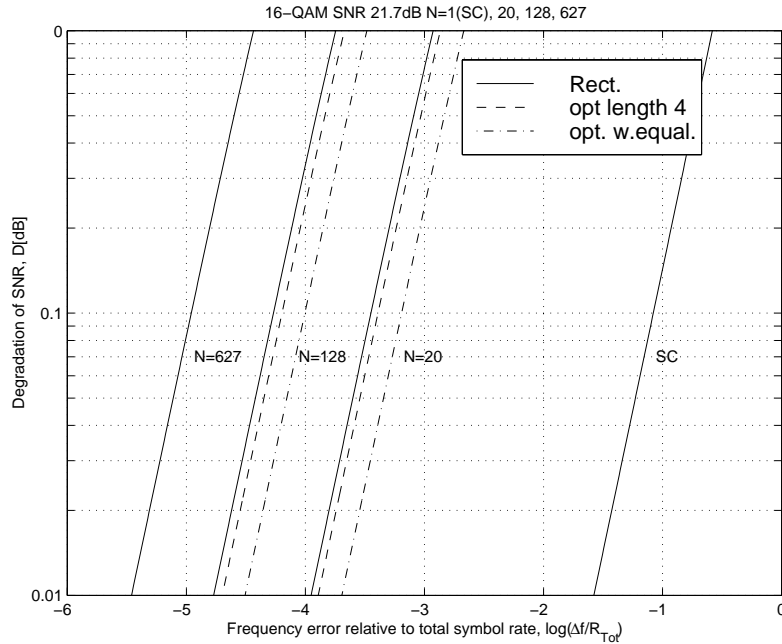
Figure 6.2. *Degradation as function of carrier frequency offset, N channel OFDM system with constellation size 16.*

If the number of channels is decided by the spectral requirements, systems with a different number of channels should be compared for different pulse shapes and modulation techniques.

In Chapter 2.5.1 example systems with $-40dB$ damping at 5% excess bandwidth were given. 627 channels are needed for QAM with rectangular pulses, while 20 channels are sufficient for O-QAM with optimized pulses of length $4T$. These two systems should thus be compared. This reveals a difference in CFO robustness of almost two decades in favour of the O-QAM system. The difference between O-QAM with and without per channel equalization is relatively small (approx. 1.5). Comparing OFDM and SC, the SC system tolerates approx. two decades higher CFO than the $N = 20$ channel OFDM system.

6.2.5 Relationship to tracking performance

The SNR degradation D as function of normalized CFO, $\Delta f / R_{tot}$, is calculated above for stationary transmission channels. A maximum tolerated SNR degradation $D_{tolerated}$ gives a related maximum tolerated CFO, $\Delta F_{tolerated}$. But looking at the carrier frequency tracking algorithms described in Chapter 5, the output of the tracking algorithms give a stochastic residual CFO[1]. It is the residual CFO which is observed by the receiver and generates SNR degradation. The residual CFO is modelled as zero mean Gaussian with a given variance, it will thus always be a finite probability to exceed $\Delta F_{tolerated}$.

The design criterion for a system is thus the probability to exceed a tolerated SNR degradation $D_{tolerated}$.

The probability for the degradation D to exceed $D_{tolerated}$ equals the probability for the residual CFO to exceed $\Delta F_{tolerated}$, given by:

$$p_{D > D_{tolerated}} = p_{|\Delta f| > \Delta F_{tolerated}} = 2Q\left[\frac{\Delta F_{tolerated}}{\sqrt{Var(\hat{\Delta f})}}\right] \tag{6.22}$$

$$Q[x] = \frac{1}{\sqrt{2\pi}}\int_{x}^{\infty} e^{-\alpha^2/2} d\alpha \tag{6.23}$$

$\Delta F_{tolerated}$: CFO giving a SNR degradation equal to the tolerated SNR degradation

$Q[\ ]$: Q-function, integral of the Gaussian density, (Lee and Messerschmitt 94).

$Var(\hat{\Delta f})$: Variance of the chosen carrier frequency tracking algorithm

Examples

The variance of the DD tracking algorithms proposed in Chapter 5.4, normalized with total symbol rate, can be written as:

$$\frac{Var(\hat{\Delta f})}{R_{tot}^2} = \frac{6\Upsilon}{(2\pi)^2 L^3 (SNR) K(K^2 - 1)} \tag{6.24}$$

---

1. The residual CFO is constant over each block used for tracking averaging

$\Upsilon = Var(\Delta \hat{f})/CRB$: Performance loss of the chosen tracking algorithm relative to the optimal CRB, Chapter 5.4

The SNR in Equation 6.24 is the SNR in the frames used for CFO estimation $SNR = SNR_{\Delta f = 0}[dB]-D[dB]$. This SNR will be stochastic since the SNR degradation D depends on the stochastic CFO. To simplify, for a maximum tolerated degradation $D_{tolerated}$, the SNR is pessimistically approximated with:

$$SNR[dB] \approx SNR_{\Delta f = 0}[dB]-D_{tolerated}[dB] \qquad (6.25)$$

Inserting Equation 6.24 and 6.25 into Equation 6.22, the probability to exceed a degradation $D_{tolerated}$ can be calculated for the proposed algorithms.

Example 1: The probabilities to exceed $D_{tolerated}$ for some estimators are calculated and shown in Table 6.2 with:

- $D_{tolerated}[dB] = 1dB$

- 16-QAM, rectangular pulseshaping filters

- $SNR_{\Delta f = 0} = 21.7dB$ to obtain $SER = 10^{-7}$ for no CFO

- Tolerated CFO, $\Delta F_{tolerated}$, are found in Figure 6.1, using $D = 1dB$. The results are scaled according to number of channels.

- All estimators use uniform windowing and weighting.

- Table 6.1 contains Υ , loss relative to CRB for the proposed carrier frequency tracking algorithms (Chapter 5.4.2), estimator numbers referring to Table 5.1

Case	Freq. est. Table 5.1	Frames K	Distance to CRB
1	7	2	$\Upsilon = 0dB$
2	4	2	$\Upsilon = 1,2dB$
3	2,8	2	$\Upsilon = 2,8dB$
4	2,8	3	$\Upsilon = 2,8dB$

Table 6.1. *Loss relative to CRB for the investigated estimators 16-QAM*

- The probability to exceed the tolerated CFO $\Delta F_{tolerated}$, and thus the tolerated degradation $D_{tolerated}$, becomes:

N	Tolerated CFO, $\Delta F_{tolerated}$	Case 1 Table 6.1	Case 2 Table 6.1	Case 3 Table 6.1	Case 4 Table 6.1
16	$1,4 \cdot 10^{-3}$	$9,8 \cdot 10^{-10}$	$1,0 \cdot 10^{-7}$	$9,5 \cdot 10^{-6}$	$< 10^{-10}$
20	$1,1 \cdot 10^{-3}$	$< 10^{-10}$	$2,6 \cdot 10^{-9}$	$7,4 \cdot 10^{-7}$	$< 10^{-10}$
128	$1,8 \cdot 10^{-4}$	$< 10^{-10}$	$< 10^{-10}$	$< 10^{-10}$	$< 10^{-10}$
627	$4,0 \cdot 10^{-5}$	$< 10^{-10}$	$< 10^{-10}$	$< 10^{-10}$	$< 10^{-10}$

Table 6.2. *Probability to exceed tolerated CFO $\Delta F_{tolerated}$ for 16-QAM*

For the given examples in Table 6.2, time averaging is not necessary to keep the probability of exceeding the tolerated CFO below the SER for $N \geq 16$ channels.

Example 2: Increasing the constellation size, the results are found in Table 6.4.

- $D_{tolerated}[dB] = 1dB$
- 256-QAM, rectangular pulseshaping filters
- $SNR_{\Delta f = 0} = 34.1dB$ to obtain $SER = 10^{-7}$ for no CFO
- Tolerated CFO, $\Delta F_{tolerated}$, are found in Figure 6.1, using $D = 1dB$. The results are scaled according to number of channels.
- All estimators use uniform windowing and weighting.
- Table 6.3 contains Υ, loss relative to CRB for the proposed carrier frequency tracking algorithms (Chapter 5.4.2), estimators referring to Table 5.1.

Case	Freq. est. Table 5.1	Frames K	Distance to CRB
5	7	2	$\Upsilon = 0dB$
6	4	2	$\Upsilon = 1,4dB$

Table 6.3. *Loss relative to CRB for the investigated estimators, 256-QAM*

Case	Freq. est. Table 5.1	Frames K	Distance to CRB
7	2,8	2	$\Upsilon = 5,4\,dB$
8	2,8	3	$\Upsilon = 5,4\,dB$

Table 6.3. *Loss relative to CRB for the investigated estimators, 256-QAM*

- The probability to exceed the tolerated CFO $\Delta F_{tolerated}$, and thus the tolerated degradation $D_{tolerated}$, becomes:

N	Tolerated CFO, $\Delta F_{tolerated}$	Case 5 Table 6.3	Case 6 Table 6.3	Case 7 Table 6.3	Case 8 Table 6.3
16	$3,5 \cdot 10^{-4}$	$1,1 \cdot 10^{-10}$	$4,1 \cdot 10^{-8}$	$5,4 \cdot 10^{-4}$	$< 10^{-10}$
20	$2,8 \cdot 10^{-4}$	$< 10^{-10}$	$8,5 \cdot 10^{-10}$	$1,1 \cdot 10^{-5}$	$< 10^{-10}$
128	$4,4 \cdot 10^{-5}$	$< 10^{-10}$	$< 10^{-10}$	$< 10^{-10}$	$< 10^{-10}$
627	$9,1 \cdot 10^{-6}$	$< 10^{-10}$	$< 10^{-10}$	$< 10^{-10}$	$< 10^{-10}$

Table 6.4. *Probability to exceed tolerated CFO ΔF for 256-QAM*

Algorithm number two and eight need time averaging for small number of channels, while algorithm four and seven does not need time averaging.

6.2.6 Simulations

The results in Chapter 6.2.4 were calculated under the assumption of Gaussian behaviour of the IBI. To achieve a confirmation of the assumption, simulations of SER as function of CFO are compared with calculations of SER as function of CFO based on the Gaussian assumption. This is carried out for both a rectangular pulse QAM system and an O-QAM system with equalization.

Simulated $SER(\Delta f)$ is found for $SNR_{\Delta f = 0} = 10(M-1)$ ensuring $SER(0) = 10^{-7}$ (Pollet et. al 95). This is done by Monte Carlo simulations with a confidence of 90%, (Jeruchim 84). The simulated results are compared with calculated $SER(\Delta f)$. According to (Lee and Messerschmitt 94) a system with constellation size 16 has a SER approx. equal to:

$$SER = 3Q\left(\frac{d\sqrt{SNR}}{2}\right) \tag{6.26}$$

d : Distance between points in the constellation

Inserting the SNR as function of CFO and $d = 0.63$ for unity power with 16 QAM and 16 O-QAM constellations the SER equals:

$$SER(\Delta f) = 3Q\left(\frac{0,63\sqrt{SNR_{\Delta f=0} - D(\Delta f)}}{2}\right) \tag{6.27}$$

$D(\Delta f)$ given by Equation 6.16.

The results are plotted in Figure 6.3.
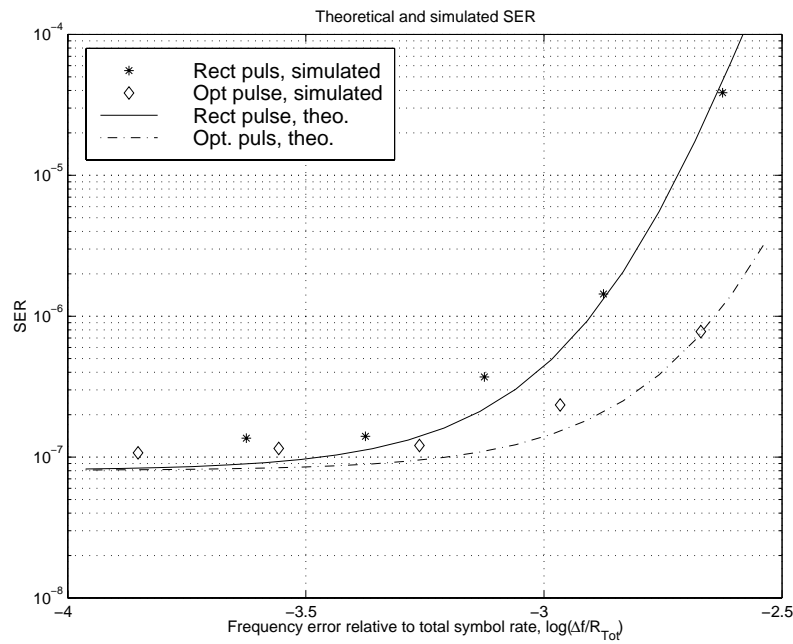
Figure 6.3. *Simulated and calculated SER as function of Δf for 16 channel OFDM systems, with constellation size 16 and $SNR_{\Delta f=0}$ 21.7 dB.*

The agreement of calculations and simulations indicates that signal generated noise caused by a CFO can be approximated as Gaussian.

6.3 IBI on flat fading AWGN channels

Fading or time varying channels are typical for multipath radio links where transmitter or receiver are in motion. The most common example is the mobile radio channel. The typical average SNR in mobile radio channels is low compared to the typical SNR in stationary radio links. In mobile radio channels the time variations make the signal frequently fade down and give negative SNR. Compared to stationary channel systems, in mobile channel systems there is more emphasis on combating multipath and fading and less on combating neighbour-channel interference. This gives less stringent frequency masks, allowing a small number of channels. At the same time there is a wish of keeping the time dispersion $\ll T$ to make each subchannel to behave close to a non time dispersive system. For channels with long delay spread, a large number of subchannels must be used. A typical mobile OFDM system has low SNR, lower order modulation and number of channels decided by the delay spread of the channel.

The scope of Chapter 6.3 is to analyse the impact of Doppler spread and CFO on fading channels. Due to mathematical convenience the calculations are limited to non time dispersive or flat fading channels, Chapter 3.8. Both with and without time dispersion on the channel, the consequences of Doppler spread and CFO will be introduction of IBI. The results presented in this work will thus be of interest for time dispersive channels as well. Investigating the consequences of Doppler spread, the CFO is set to zero, while investigating the consequences of a CFO the fading will be slow enough to view the channel as constant during one OFDM frame, i.e. Doppler spread $\ll 1/T$.

6.3.1 Received signal

QAM and Square pulses

The rectangular pulse OFDM system discussed in this section is the same rectangular pulse system that was discussed in Chapter 6.2.1 with the flat Rayleigh fading channel described in Chapter 2.6.3. Due to the non time dispersive transmission channel, guard interval is not included. A guard interval would in addition complicate the comparison with other systems since spectral efficiency and transmitted power would have been changed.

The description of the received signal for the stationary channel case, Equation 6.2 is still valid and repeated here.

$$z_{0,m} = a_{0,m}|I_0| + \left(\sum_{\substack{n=0 \\ n \neq m}}^{N-1} a_{0,n}I_{m-n} + N_{0,m} \right) e^{-j\arg I_0} \tag{6.28}$$

The expression for the interference weights is modified, Equation 6.29. This includes phase correction for the fading channel.

$$I_p = \frac{1}{T} \int_0^T c(t) e^{-j2\pi\frac{p}{T}t} e^{j2\pi\Delta f t} dt \tag{6.29}$$

In the OFDM system using M-QAM and rectangular pulses, the fading or Doppler generated IBI is just like the CFO generated IBI a pure ICI. One should note that $c(t)$ is a stochastic function of time, resulting in the interference weights given by Equation 6.29 to be stochastic and time dependent. This is in contrast to the CFO generated deterministic and non time dependent interference weights for the stationary channel, Equation 6.3.

O-QAM with symmetrical filters

The system discussed in this section is identical to the O-QAM system discussed in Chapter 6.2.1 with exception of the flat stationary channel, which has been replaced with the flat Rayleigh fading channel.

The description of the received signal, Equation 6.6, is still valid under the assumption of perfect phase correction.

$$z_{0,m} = a_{0,m}\Lambda_{0,0} + \sum_{\substack{n=0 \\ n \neq m \vee l \neq 0}}^{N-1} \sum_{l=-\infty}^{\infty} a_{l,n}\Lambda_{l,m-n} \tag{6.30}$$

$$+ \sum_{n=0}^{N-1} \sum_{l=-\infty}^{\infty} -Im\{a_{l,n}\}\Gamma_{l,m-n} + jRe\{a_{l,n}\}\Gamma_{l+1,m-n} + N_m$$

The interference weights are modified to:

$$\Lambda_{l,p} = \int_{-\infty}^{\infty} h(t-lT)h(t)Re\left\{c'(t)e^{j\left(\left(\frac{2\pi}{T}t+\frac{\pi}{2}\right)p+2\pi\Delta ft\right)}\right\}dt$$

$$\Gamma_{l,p} = \int_{-\infty}^{\infty} h\left(t-lT+\frac{T}{2}\right)h(t)Im\left\{c'(t)e^{j\left(\left(\frac{2\pi}{T}t+\frac{\pi}{2}\right)p+2\pi\Delta ft\right)}\right\}dt$$

(6.31)

Where:

$$c'(t) = c(t)e^{-j\arg(c(t))}$$

(6.32)

t' : Sampling instant

Similar to CFO generated IBI on a stationary channel, Doppler generated IBI will be a combination of ISI and ICI. The Doppler generated O-QAM interference weights, Equation 6.31, are stochastic and time dependent, while the stationary channel CFO generated interference weights are deterministic and non time dependent, Equation 6.7. The weights of the real and imaginary parts will differ since the real and imaginary part are transmitted at different points of time, but in a statistical sense the observation made in Chapter 6.2.1 about symmetry in the interference is still valid.

CFO on flat fading channels

If there exists a CFO in addition to the fading channel, the interference weights will still be stochastic. But if the fading is very slow, i.e. small Doppler band width, and the CFO is large enough to dominate the interference, the interference weights will become close to the deterministic weights in the stationary channel. This is easily realized by examining Equation 6.29 and 6.31. For slow fading $c(t)$ can be viewed as constant in the integration interval and the stationary channel scenario is recreated.

6.3.2 SNR at the receiver

A fading channel alone or in combination with CFO, will transform transmitted signal power to noise power in the receiver. This alters the received SNR.

Assuming a fading channel with average amplification equal to one, Doppler bandwidth $\ll 1/T$, AWGN, no CFO and unity transmitted power, the received SNR equals:

$$SNR_{IBI = 0} = \frac{1}{\sigma_N^2} \qquad \textbf{(6.33)}$$

If there exists a CFO or a Doppler bandwidth of significance compared to $1/T$, IBI will be created and the received signal power will decrease. The CFO created IBI on stationary channels was assumed additive white Gaussian with zero mean. This was motivated in Chapter 6.2.2 while simulations in Chapter 6.2.6 indicated the assumption to be correct. The same motivation can be used for both Doppler and CFO generated IBI on fading channels, and they will be assumed white zero mean additive Gaussian and uncorrelated with the channel noise.

The white Gaussian channel noise is independent of the transmitted signal and channel fading. The IBI on the other hand is generated from the transmitted signal, and with a fading channel, the level of the signal component and the level of the IBI must be checked for coupling. The normalized covariance between the instant signal power and the instant IBI power can be calculated from Equation 6.28 and 6.30.

$$\frac{K(|\alpha a|^2, |IBI|^2)}{E[|\alpha a|^2] E[|IBI|^2]} = \frac{E[(|\alpha a|^2 - E[|\alpha a|^2])(|IBI|^2 - E[|IBI|^2])]}{E[|\alpha a|^2] E[|IBI|^2]} \qquad \textbf{(6.34)}$$

$\alpha = I_0$ for QAM with rectangular pulses.

$\alpha = \Lambda_{0,0}$ for O-QAM.

The calculations of the covariance are straight forward but quite tedious, the details can be found in Appendix B and only the results are given here. CFO generated IBI on fading channels and doppler spread generated IBI will be treated separately.

Doppler generated IBI

To examine the doppler generated IBI the CFO is set to zero resulting in

$$\frac{K(|\alpha a|^2, |IBI|^2)_{Fading}}{E[|\alpha a|^2] E[|IBI|^2]} \approx 0 \qquad \textbf{(6.35)}$$

With uncorrelated IBI power and signal power, the IBI is assumed to be independent of the channel fading level and is assumed to perform similar to the white additive Gaussian channel noise. The IBI power and the channel noise power can be added giving a resulting system similar to a flat fading channel with AWGN and no other impairments, SNR given by Equation 6.9.

CFO generated IBI

In the case of CFO created IBI and Doppler bandwidth $\ll 1/T$, the normalized covariance is close to unity:

$$\frac{K(|\alpha a|^2, |IBI|^2)_{CFO}}{E[|\alpha a|^2]E[|IBI|^2]} = 1 \tag{6.36}$$

This gives an IBI power following the fluctuation of the signal. This demands separate treatment of the IBI following the signal fluctuations, and the channel noise which is independent of the signal fluctuations. In the case of a small CFO, the channel noise will be dominating, and we will have a scenario with a fading signal and a non fading (channel) noise, which equals the ordinary fading channel with:

$$SNR \approx \frac{1}{\sigma^2} \tag{6.37}$$

When the CFO is large, the IBI will dominate over the channel noise, which is a scenario with signal and (IBI) noise fading strongly correlated. This can be regarded as a stationary channel system with

$$SNR \approx \frac{E_0}{V_0} \tag{6.38}$$

Between these two extremes the noise will be a sum of IBI and channel noise.

6.3.3 Influence of the number of channels N

The considerations mentioned in Chapter 6.2.3 when comparing different systems, are still valid: constant total rate, constant total power and CFO relative to total symbol rate. Similarly, the Doppler bandwidth of the fading must be relative to the total symbol rate. Looking at mobile radio channels it has been advocated earlier in this thesis for using the same number of channels independent of pulse shaping. So comparison of different pulse shapes should be done with the same number of channels.

Despite these considerations, it is of interest to analyse the effect of changing the number of channels in an OFDM system with a flat fading AWGN channel. Following the procedure of Chapter 6.2.3, the interference into one channel from a channel p channels away in a rectangular pulse system with $2N$ channels and symbol duration $2T$ equals, with substitution of the integration variable:

$$I_p = \frac{1}{T}\int\limits_0^T c(2t)e^{-j2\pi\frac{p}{T}\tau}e^{j2\pi 2\Delta f\tau}d\tau \tag{6.39}$$

Doubling the number of channels equals doubling the CFO and the doppler spread. The last based on the observation that moving from $c(t)$ to $c(2t)$ equals doubling the mobile speed, which doubles the doppler. Making the same considerations about total interference as in the stationary channel case, it can be stated that:

Systems with a sufficiently high number of channels N and a given tolerated IBI, a multiplication of the number of channels in the system with any factor, divides the tolerated CFO Δf and tolerated mobile speed v with the same factor. This keeps tolerated CFO Δf and tolerated mobile speed v constant relative to the subchannel bandwidth.

6.3.4 Design of the example system

An example system is designed according to the procedure in Chapter 2.5.2. With bandwidth $B_W = 50kHz$, delay spread $\varsigma(t) = 50\mu s$, which is very conservative, and $N = 64$ channels, the frequency correlation across the main lobe for each subchannel equals 0.8. The Carrier frequency is chosen to be 1800 MHz.

The transmission conditions on the mobile radio channel are far more challenging than for the stationary radio channel, lower SNR with smaller constellations must be accepted. In this work 4-OQAM and 4-QAM are considered for use in mobile channels. The motivation for using the $4T$ pulse with O-QAM at the stationary channel was the low sidelobe level, which gave a low number of channels. Since the sidelobe level does not decide the number of channels in the mobile case, the shorter $2T$ pulse should be preferred considering complexity in transmitter and receiver filterbanks. If per channel equalization is implemented, further complexity reductions can be achieved with the $2T$ pulse compared to the $4T$ pulse. The $2T$ and the $4T$ pulses should however be investigated for CFO and Doppler spread robustness differences.

A coarse estimate of maximum multipath delay, based on an uniform delay profile, equals 4/3 of the delay spread. Adding a guard interval of $67\mu s$ to the proposed system, the bandwidth loss would equal approx. 5%. Guard interval is not included in the rest of this chapter.

6.3.5 Symbol error rate

With a stationary channel, the system degradation as function of CFO was measured by the reduction in SNR, Chapter 6.2.2. According to the result in Equation 6.35, this can also be done for Doppler generated degradation on a flat fading channel. Equation 6.29 and 6.31 are inserted in Equation 6.10 and 6.11 and finely these results are inserted in Equation 6.16. CFO generated degradation on the other hand can not be treated in the same manner. With different properties for the IBI and the channel noise it would not make sense to add the power of the two to evaluate a SNR degradation. Instead the SER is calculated as a function of Doppler spread and CFO.

Calculated and simulated results are shown below. All the simulations in this chapter include perfect phase correction, sampled signal component has zero phase error.

Doppler spread generated degradation

To isolate the effect of the doppler spread, the CFO is set to zero during the analysis. With carrier frequency $f_c = 1800MHz$, a Doppler bandwidth of the fading in the range of $B_D \in \langle 10^{-4}, 10^{-2} \rangle BW$ equals a range of speed of $v \in \langle 3, 300 \rangle km/h$ for the mobile. Theoretical results and simulations of SER as function of Doppler bandwidth are plotted in the same figure for comparison, with $SNR_{IBI=0} = 13dB$ and $SNR_{IBI=0} = 20dB$, Figure 6.4.
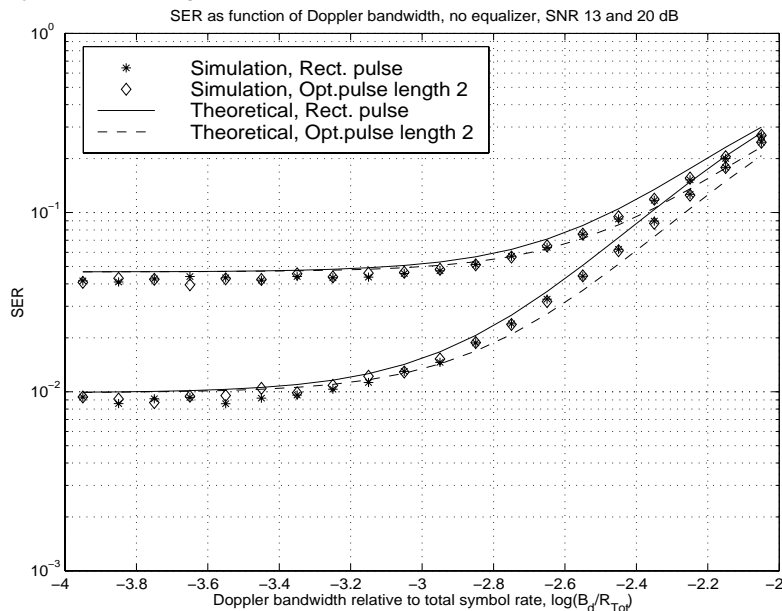
Figure 6.4. *Calculated and simulated SER as function of Doppler bandwidth B_d for 64 channel OFDM systems, constellation size 4 and pulse length $2T$ for O-QAM. SNR 13dB, upper, and 20dB, lower.*

Replacing the $2T$ pulse shape with the $4T$ pulse shape, gives a performance which is slightly worse, i.e. the $2T$ is a little more robust to Doppler spread than the $4T$ pulse.
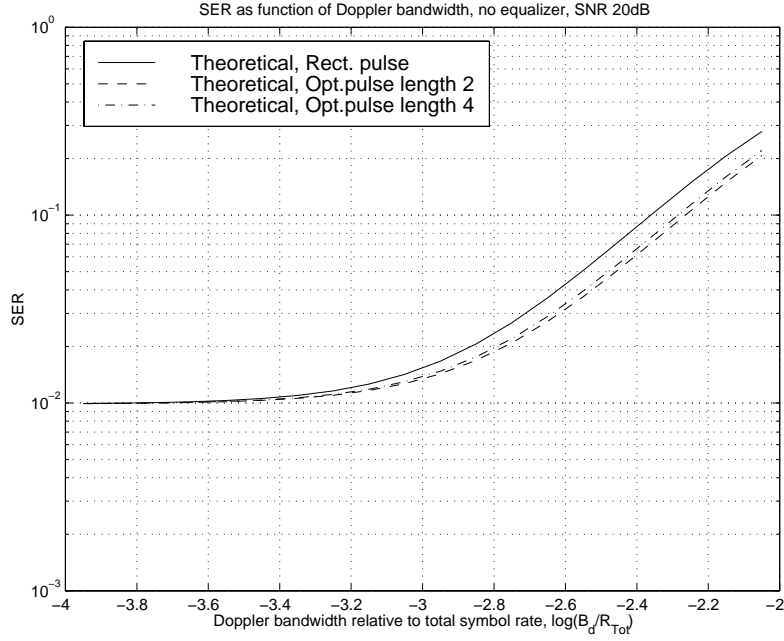
Figure 6.5. *Calculated SER as function of Doppler bandwidth B_d for 64 channel OFDM systems, constellation size 4 and pulse length $2T$ and $4T$ for O-QAM. SNR 20dB.*

The calculated values are based on the SER formulas for flat Rayleigh fading channels found in (Proakis 95), with $SNR = SNR(B_D)$ given by Equation 6.9

$$p_{eq} = \frac{1}{2}\left[1 - \sqrt{\frac{SNR/2}{1 + SNR/2}}\right] \qquad (6.40)$$

$$SER = 2p_{eq} - p_{eq}^2 \qquad (6.41)$$

p_{eq}: probability of error in one quadrature channel

The match between simulations and calculations indicates that the assumption about no fading $IBI_{Doppler}$ with properties similar to AWGN is appropriate. The degradation caused by $IBI_{Doppler}$ is visible from $B_D = 10^{-3}$ (30km/h) both for $SNR_{IBI=0} = 20dB$ and $13dB$, with a doubled SER at $B_D = 10^{-2,82}$ (45km/h) and

$B_D = 10^{-2,48}$ (100km/h) for SNR equal to respectively 20 and 13 dB. According to the calculations, the O-QAM system is slightly more robust to Doppler spread than the QAM system, but the simulations show equal robustness for the two systems.

CFO generated degradation

To isolate the effect of the CFO generated IBI for flat fading channels, the Doppler bandwidth B_D is set close to zero. The CFO is in the range of $\Delta f \in \langle 10^{-4}, 10^{-2} \rangle BW$, comparable with the tolerated CFO in the GSM system.

In Chapter 6.3.2 the total SNR was divided in two scenarios according to the amount of CFO. For small CFO the channel noise is dominating and the IBI is neglected. The system experiences AWGN and a fading signal component, and it can be viewed as a standard flat fading case. The $SER(\sigma^2)$ for this case is given by Equation 6.40 and 6.41, with $SNR = 1/\sigma^2$ and is thus only dependent on $SNR_{IBI=0}$. The independency of the CFO is shown by the horizontal line in Figure 6.6 for the case of $SNR_{IBI=0} = 20dB$.
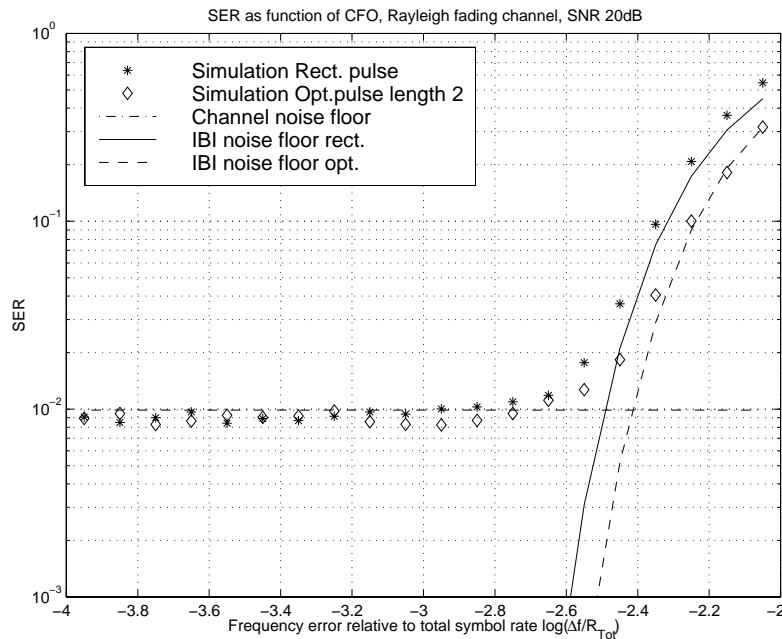
Figure 6.6. *Calculated and simulated SER as function of CFO for 64 channel OFDM systems with constellation size 4, SNR 20dB and slow Rayleigh fading. No equalization for O-QAM*

For high CFO the IBI is dominating and the channel noise is neglected. With fading signal and fading IBI, where the fading of the two components are correlated, the SNR will be constant. This is similar to a stationary channel and AWGN, with $SNR(\Delta f)$ given by Equation 6.38. The resulting $SER(IBI)$ is given by inserting Equation 6.42 into Equation 6.41.

$$p_{eq} = Q(\sqrt{SNR(\Delta f)})$$ **(6.42)**

For high CFO, $SNR(\Delta f)$ is independent of $SNR_{IBI = 0}$, but differs between QAM and O-QAM, explaining the difference in SER behaviour. $SER(IBI)$ is plotted as the two steep lines to the right in Figure 6.6. The line to the left representing the QAM system and the line to the right representing OQAM without equalization. Replacing the $2T$ pulse with the $4T$ pulse would give slightly worse results.
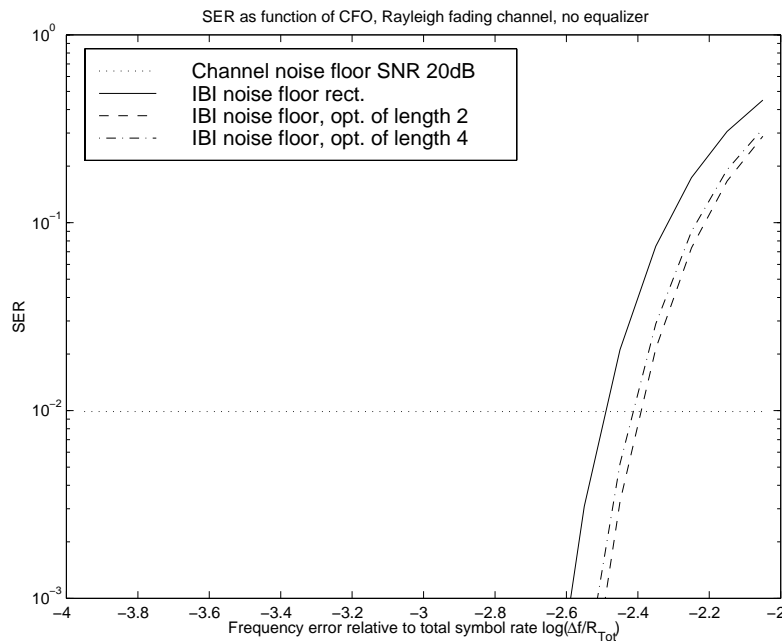
Figure 6.7. *Calculated SER as function of CFO for 64 channel OFDM systems with constellation size 4, SNR 20dB and slow Rayleigh fading. No equalization for O-QAM with pulses of length $2T$ and $4T$*

A change of channel noise power will only inflict on the horizontal $SER(\sigma^2)$ valid for low CFO. $SER(IBI)$, valid at high CFO will not be altered, but changing σ^2 will change the insertion points between $SER(\sigma^2)$ and $SER(IBI)$. Decreased

$SNR_{IBI\,=\,0} \,=\, 1/\sigma^2$ will move the insertion point to a higher CFO, but because of the steep angle of $SER(IBI)$, a large $SNR_{IBI\,=\,0}$ change will only give a small change to the CFO value at the insertion point. Results for $SNR_{IBI\,=\,0} \,=\, 13dB$ are shown below.
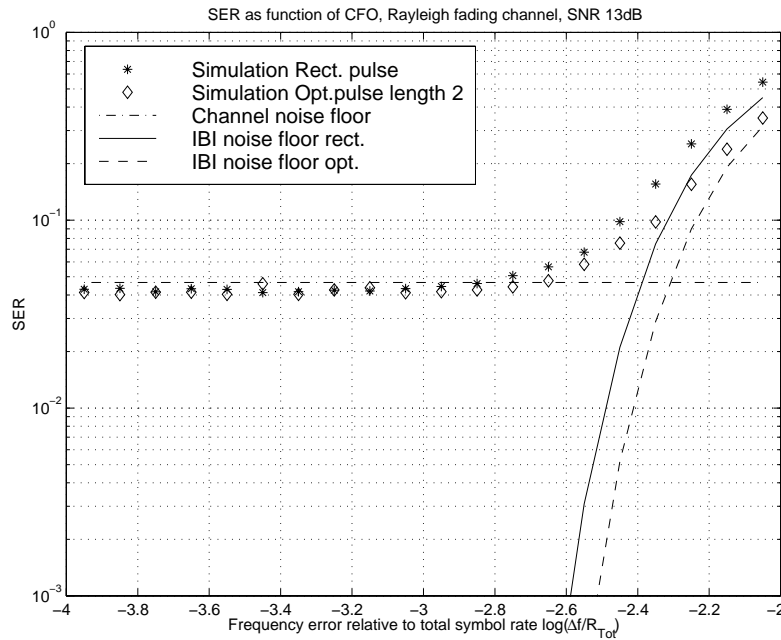
Figure 6.8. *Calculated and simulated SER as function of CFO for 64 channel OFDM systems with constellation size 4 and SNR 13dB. No equalization for O-QAM*

In the case of stationary channels and small CFO, the CFO robustness was increased for O-QAM systems by using a per channel zero forcing equalizer. The CFO range studied for a fading channel is several decades higher, and as shown in Figure 6.9 the performance gain with per channel equalization is small for the mobile scenario.

The reason for the noise floor to bend up for the case of per channel equalization is due to noise enhancement caused by the zero forcing equalizer.

The match between calculations and simulations are good for all the simulations, except for a transition period when both channel noise and IBI is significant. The match indicates that the assumption of noise behaviour made in Chapter 6.3.2 is valid. This gives a close to constant SER decided by the channel noise for low CFO, increasing the CFO a breakpoint is reached of approximately $\Delta f \,=\, 2.5 \; 10^{-3} BW$
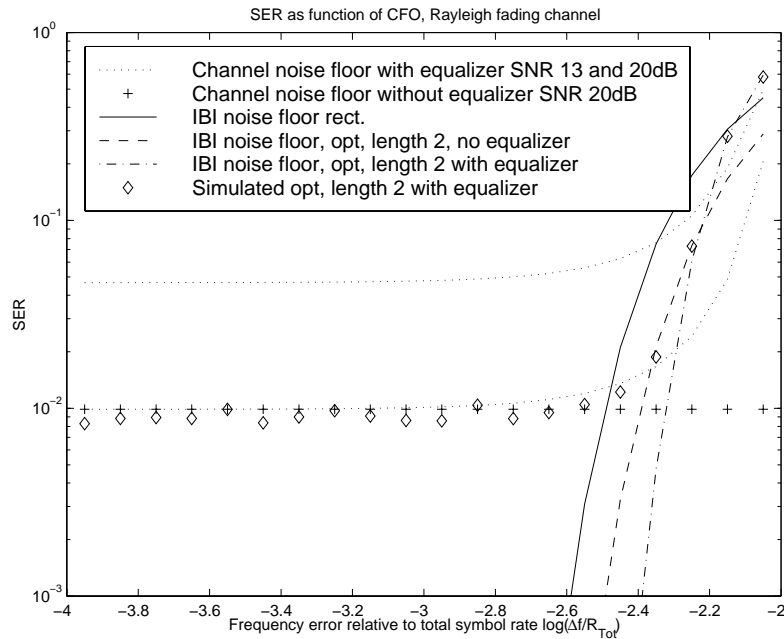
Figure 6.9. *Calculated and simulated SER as function of CFO with and without equalization for 64 channel OFDM systems with constellation size 4. Simulated SER for O-QAM with equalization.*

after which the SER increase rapidly. The CFO robustness for QAM with rectangular pulses and O-QAM with optimized pulses of length $2T$ and no equalizer are close to equal, with a factor of 1.2 in favour of the OQAM system.

6.3.6 Phase slipping due to CFO

The example system has $N = 64$ subchannels, a frequency error of $\Delta f = 2.5 \ 10^{-3} BW$ equals approx. $0.16/T$. The assumption about zero phase error for the signal component is not realistic with a CFO. In fact with a CFO $\Delta f = 0.16/T$, BPSK, perfect feedback phase correction (one frame delay on the phase estimate) and slowly fading channel, the noise resistance will be reduced with approx. 50% due to phase error of $0.16 \cdot 2\pi$. Using 4-QAM the system will not work at all due to phase slipping since $\Delta f > 0.125/T$. Using 4-QAM on flat fading channels, the CFO robustness is thus not decided by the IBI, but rather by the tolerated phase error at the sampling instant. Compared to SC systems the CFO robustness of OFDM systems is reduced with a factor of approx. N due to increased symbol length giving increased CFO generated phase error.

6.3.7 Generalization of results

The example system was designed for rural macro cellular environment, tolerating a large amount of time dispersion. For micro cellular systems the delay spread will be reduced to a figure in the order of 5% of the delay spread in the macro cellular system. Assuming the number of subchannels N to be sufficiently high, this reduces the coherence bandwidth and the number of channels with the same factor, increasing the mobile speed for visible degradation to 600 km/h. While doppler spread generated degradation is visible for moderate velocities in the example macro cellular system, it will only be visible at very high velocities in micro cellular systems. Despite that delay profiles up to $100\mu s$ have been measured in hilly terrain, the example system is conservative for macro cellular systems. Reducing the delay spread from $50\mu s$ to $15\mu s$, which equals the maximum delay handled by the GSM, the mobile speed for visible degradation is increased to 100 km/h. Considering CFO robustness, the tolerated CFO is increased with a factor of 3.3 for the $15\mu s$ system and a factor of 20 for the micro cellular system as a result of decreased number of channels, i.e. decreased symbol length.

Increasing the system bandwidth/capacity while keeping the frequency correlation in each subchannel constant, i.e. constant subchannel bandwidth, the doppler sensitivity will stay constant measured in tolerated velocity. The CFO sensitivity compared to total symbol rate will decrease with the same factor as the capacity was increased, keeping the CFO robustness constant relative to the channel spacing, i.e. constant measured in Hz.

6.4 Summary

OFDM systems loose their orthogonality when experiencing a CFO or a Doppler spread, i.e. fading channel. Some of the signal power will be transformed into inter bin interference (IBI), reducing the SNR at the receiver. For OFDM with QAM and rectangular pulses of length one symbol interval, the IBI will be pure inter channel interference (ICI). For systems using O-QAM and pulse lengths of more than one symbol interval, the IBI will be a combination of inter symbol interference (ISI) and ICI.

If the total system bandwidth is kept constant, the number of channels influence on the sensitivity for CFO and doppler spread. If a given degradation is tolerated in the system, the tolerated CFO and doppler bandwidth, i.e. speed of the mobile, will be a function proportional to $1/N$, where N is the number of channels in the system. In the same manner, systems operating at high SNR will be more sensitive to CFO and Doppler spread than systems operating at low SNR.

The effect of IBI generated by CFO at stationary channels and IBI generated by Doppler spread at fading channels is similar to the effect of AWGN. This IBI can be viewed as an increase of the AWGN on the channel. The IBI generated by CFO on fading channels behaves differently from the channel noise, and the two noise contributions must thus be treated separately. The IBI is ignored for low CFO, and the system performs like a standard flat fading system with SNR equal to signal to channel noise power ratio. For high CFO the channel noise is ignored. Because the signal fade level and IBI power are highly correlated, this can be viewed as a stationary channel with SNR equal to the signal to IBI power ratio.

The robustness against CFO for different pulse shapes has been analysed on stationary channels. An N channel OFDM system using optimized pulses in combination with O-QAM, has shown to be as good as or better than an N channel OFDM system using square pulses and QAM. The performance is only slightly better for the O-QAM system when no per channel equalization is used. While introducing a per channel equalization increases the tolerated CFO with a factor of approx. 1.8 compared to the QAM system. In systems where spectral efficiency is an important issue, the QAM system must use a large number of channels because of the high spectral side lobe level of the square pulses, while the O-QAM system with optimized pulses only need a fraction of that number of channels to achieve the same out of band damping. Because the system performance degradation is a function of the number of channels, the O-QAM system with fewer channels will tolerate a larger carrier frequency deviation than the QAM system. In a typical case with 5% excess bandwidth for sidelobe level -40 dB, the difference in tolerated CFO is almost two decades.

For flat fading channels both the consequence of CFO and doppler bandwidth are examined under the assumption of zero phase error at the sampling instant. On mobile channels it is not likely that spectral requirements will dictate the number of channels in the system, but rather the delay spread of the channel, resulting in the same number of channels independent of pulse shaping strategy. This gives close to equal tolerated CFO and Doppler spread independent of pulse shaping strategy. In an example macro cellular system at $1800 MHz$, degradation due to Doppler spread is visible from approx. 30km/h. For a micro cellular system with increased subchannel spacing and identical modulation and SNR, degradation will be visible from 600 km/h . The example macro cellular system SER is unchanged (no IBI degradation) with increasing CFO until it reaches a threshold at $2,5 \cdot 10^{-3} R_{tot}$ or $0.16/T$, after which it increases rapidly. Removing the assumption about zero phase error at the sampling instant, $\Delta f > 0.125/T$ give phase slipping with 4-QAM. On flat fading channels, the CFO robustness is thus not decided by the IBI, but rather by the tolerated phase error which is a function of CFO and symbol length.

Chapter 7
Conclusion

This work has presented research on the topic of carrier synchronization in OFDM. The main focus has been carrier acquisition and tracking without the use of pilots on stationary transmission channels using higher order modulation. Further, consequences of residual carrier frequency offset (CFO) during carrier tracking has been investigated for stationary channels and flat fading channels. Consequences of the doppler spread on flat fading channels have been investigated as well.

The OFDM carrier acquisition and tracking algorithms have been developed for use with M-QAM and rectangular pulses, but the algorithms can be modified for use with other modulation schemes and pulse shapes. The algorithms do not depend on pilots or other redundant signalling, maintaining spectral efficiency. The consequences of carrier frequency tracking error and doppler spread have been investigated for QAM with rectangular pulses and O-QAM with pulses optimized for minimum out of band power.

Acquisition

Critically sampled LMS carrier frequency acquisition algorithms have been developed for OFDM systems, using a single filterbank in the receiver to maintain minimum complexity. Error functions for the LMS carrier frequency acquisition algorithm has been developed by identifying similarities between OFDM carrier acquisition and single carrier (SC) timing, where as other error functions have been developed by identifying similarities with SC blind equalization. The carrier acquisition algorithms in this work are developed by viewing each OFDM frame as one sequence, but the carrier estimate in the LMS algorithm is updated only once per frame.

The performances of the developed algorithms have been compared to each other and to the performance of the ML OFDM carrier frequency acquisition algorithm of (Daffra and Chouly 93). The Daffara algorithm assumes a critically sampled OFDM system, but applies a double set of filterbanks in the receiver. Adopting acquisition time for a given steady state variance as a performance measure, the developed algorithm with the best performance is based on the second order blind equalization algorithm of (Godard 80). The performance of the Daffara algorithm is heavily dependent on the SNR and little dependent on the number of subchannels in the OFDM system. For the second order Godard based algorithm it is opposite. For moderate SNR and low number of subchannels in the OFDM system, the Daffara algorithm performs better than the second order Godard algorithm, while for a high number of channels and low SNR the second order Godard algorithm performs better than the Daffara algorithm. Increasing the CFO to several subchannel bandwidths (channel number offset), the acquisition time of the Daffara algorithm increase, while the second order Godard based algorithm is little influenced. The Daffara algorithm is also sensitive to time dispersive transmission channels. If the transmission channel introduces zeros close to the edges of the total OFDM signal spectra, the acquisition time of the Daffara algorithm will increase rapidly. The second order Godard algorithm is little influenced by time dispersive transmission channels.

Compared to the Daffara carrier frequency acquisition algorithm, the second order Godard based algorithm developed in this work is more robust against low SNR, high CFO and time dispersive transmission channels. The second order Godard based algorithm also give lower receiver complexity.

Tracking

Methods for decision directed (DD) carrier phase tracking and carrier frequency tracking in OFDM have been presented for use with M-QAM. The methods are based on feedback solutions. When averaging the carrier estimate over several received symbols, non-overlapping windows are used in the time direction (the weights put on each symbol is NOT an uniformly decaying function of the symbol age). This is in opposition to the well known method of SC tracking with first order phase locked loops (PLL), which equals decaying weights for older symbols and overlapping windows. Another difference compared to SC systems is the need for separate carrier phase and frequency tracking in OFDM. All discussed methods are based on removal of the modulation influence by use of the receiver estimate of the transmitted symbol. Phase error is estimated by phase extraction, while the CFO is estimated from the phase change between subsequent frames.

The performance has been investigated by comparing estimator variance with Cramer Rao Bound (CRB). The best of the proposed estimators perform close to or

equal to CRB. The proposed DD tracking algorithms perform better than DA tracking with a factor close (or equal) to the pilot spacing in the DA systems.

The proposed phase error estimator performs equal to CRB, with the exception of when averaging over a small number of symbols while using higher order modulation. This gives a moderate loss.

Six different versions of a carrier frequency tracking algorithm have been developed based on the frequency estimator of (Kay 89). Considering complexity and performance, four of them are excluded. These six estimators does not need phase unwrapping. With constant amplitude modulation they obtain CRB independent of number of frames and channels used for averaging. With higher order modulation one of the estimators has a constant, moderate loss relative to CRB, while the other estimator has a loss relative to CRB which is proportional to the second power of the number of frames used for averaging.

In addition, two carrier frequency estimators based on per frame phase extraction and explicit phase difference have been developed. These two estimators depend on phase unwrapping. Of the two estimators, one obtains CRB in all situations, while the other has a moderate loss compared to CRB for higher order modulation and no frame averaging.

For the examples in Chapter 6, averaging over only a few frames was necessary to obtain adequate carrier estimation accuracy.

Compared to pilot based methods, several of the presented DD carrier tracking methods give better tracking performance and a system with higher bandwidth efficiency.

Performance loss due to imperfect carrier tracking and fading channels

Degradation due to Inter Bin Interference (IBI) generated by CFO and flat Rayleigh fading transmission channels have been calculated and simulated.

OFDM systems loose their orthogonality when experiencing a CFO or a Doppler spread, i.e. fading channel. Some of the signal power will be transformed into IBI, reducing the SNR at the receiver. For OFDM with QAM and rectangular pulses of length one symbol interval, the IBI will be pure inter channel interference (ICI). For systems using O-QAM and pulse lengths of more than one symbol interval, the IBI will be a combination of inter symbol interference (ISI) and ICI.

The IBI generated by CFO at stationary channels and doppler spread at fading channels are found to behave similar to the channel noise. This IBI can be viewed as an increase of the AWGN on the channel. On the other hand, if the IBI is generated by CFO on a fading channel, signal fade level and IBI power are highly correlated. The IBI can be ignored for low CFO, and the system performs like a standard flat fading system with SNR equal to signal to channel noise power ratio. For high CFO the channel noise is ignored and the system can be viewed as a stationary channel with SNR equal to the signal to IBI power ratio. Systems operating at high SNR will be more sensitive to CFO and Doppler spread than systems operating at low SNR. In the same manner, sensitivity to CFO and doppler spread is proportional to the number of subchannels in the system.

On stationary transmission channel where spectral efficiency is an important issue, QAM systems with square pulses must use a higher number of subchannels than O-QAM system with optimized pulses, due to the difference in spectral side lobe level. The O-QAM system with fewer subchannels will thus tolerate a larger carrier frequency deviation than the QAM system with square pulses. An typical example is shown, with 5% excess bandwidth for sidelobe level $-40dB$ the difference in tolerated CFO between the two systems is almost two decades.

For flat fading transmission channels both consequences of CFO and fading doppler bandwidth are examined, under the assumption of zero phase error at the sampling instant. In a mobile communications environment, the number of subchannels will be equal, independent of modulation and pulse shaping strategy. This results in almost equal tolerated CFO and Doppler spread for the discussed QAM and O-QAM systems. Increment in symbol error rate (SER) is used as degradation measure. In an example macro cellular system at $1800MHz$, degradation due to Doppler spread is visible from approx. $30km/h$. For a micro cellular system with increased subchannel spacing and identical modulation and SNR, degradation will be visible from $600km/h$. The example macro cellular system SER is unchanged (not influenced by IBI) with increasing CFO until it reaches a threshold at $2,5 \cdot 10^{-3}R_{tot}$ (or referring to the subchannel spacing, $0.16/T$), after which the BER increases rapidly. Removing the zero phase error assumption, 4-QAM can not operate with a CFO of $0.16/T$ due to phase slipping. The tolerated CFO is thus not decided by the IBI but rather the phase error/slipping, which is a function of symbol length.

7.1 Future work

This work has discussed carrier tracking and carrier frequency acquisition without the use of pilots, guard interval or repeated signals. To complete the work on pilot less carrier synchronization in OFDM, methods for Non Data Aided (NDA) carrier phase acquisition should be investigated. Possible approaches are indicated earlier in this work. Similar, the transition between acquisition an tracking should be investigated, including how to detect sufficient carrier synchronization for the tracking algorithms to operate.

Spectral efficient methods for frame acquisition is another research topic. Several methods for frame acquisition in OFDM is proposed, but all methods assume the use of either pilots, guard intervals or repeated signals. All these methods will thus reduce system capacity. NDA alternatives might be developed both by a time approach where subsequent frames are investigated and by a frequency approach where neighbouring subchannels are investigated. Methods for spectral efficient frame tracking are referred to earlier in this work.

The methods developed for carrier synchronization assumes perfect frame synchronization, even though some carrier acquisition algorithms in this work have been tested with frame synchronization error. Similar, many frame synchronization algorithms assume perfect carrier synchronization. With simultaneous frame and carrier errors in addition to a multipath transmission channel, care must be taken to ensure that the synchronization algorithms and the equalizer converges. The same problems are known from SC systems. To overcome these difficulties, methods for joint synchronization, equalization and detection in SC systems have been proposed. Some of these theories can be adapted to joint frame and carrier acquisition in OFDM, even including equalization and detection. This will give a challenging, rather complex, multi dimensional problem.

Appendix A
Weighting factors and variance for frequency estimation over two frames

As discussed in Chapter 5.4.2, during calculations of the carrier frequency offset estimate, averaging over several independent OFDM subchannels will increase the estimate performance, i.e. reduce estimate variance. With non constant amplitude modulation each term in the averaged CFO estimator has symbol dependant SNR. To obtain maximum performance, symbol dependant weights should be applied for each term. In this appendix the optimum weights are calculated for two different estimators, together with the estimator variance with and without use of the weights. Only the case of estimators based on $K = 2$ frames is investigated.

With $K = 2$ frames there is no time windowing, only channel weighting. Without loss of generality, the case of $k = 1$ is investigated, i.e. frequency estimate based on frame number 1 and 2. The estimators of Equation 5.24 and 5.25 can be rewritten as:

$$\Delta \hat{f_2} = \frac{1}{2\pi TN} \sum_{m=0}^{N-1} u(m) \angle (z_{2,m} z^*_{1,m} \hat{a}^*_{2,m} \hat{a}_{1,m}) \qquad \text{(A.1)}$$

$$\Delta \hat{f_2} = \frac{1}{2\pi T} \angle \sum_{m=0}^{N-1} u(m) (z_{2,m} z^*_{1,m} \hat{a}^*_{2,m} \hat{a}_{1,m}) \qquad \text{(A.2)}$$

$u(m)$: Weight due to channel weighting, channel m

The received signal $z_{k,m}$ can be rewritten as:

$$z_{k,m} = a_{k,m}e^{j(2\pi\Delta fkT+\theta)} + n_{k,m} \tag{A.3}$$

Giving:

$$\angle p_{1,m} = \angle z_{2,m}z^*_{1,m}a^*_{2,m}a_{1,m} = 2\pi\Delta fT + n \tag{A.4}$$

n : Noise

Still without loss of generality, CFO Δf is set to zero:

$$p_{1,m} = z_{2,m}z^*_{1,m}a^*_{2,m}a_{1,m} = |a_{1,m}|^2|a_{2,m}|^2$$
$$+ |a_{1,m}|^2 a^*_{2,m}n_{2,m}$$
$$+ a_{1,m}|a_{2,m}|^2 n^*_{1,m}$$
$$+ a_{1,m}a^*_{2,m}n^*_{1,m}n_{2,m} \tag{A.5}$$

The following approximations are made under the assumption of sufficient SNR:

$$\left|a_{1,m}a^*_{2,m}n^*_{1,m}n_{2,m}\right| \ll \left||a_{1,m}|^2 a^*_{2,m}n_{2,m} + a_{1,m}|a_{2,m}|^2 n^*_{1,m}\right| \tag{A.6}$$

$$\angle p_{1,m} \approx ni_{1,m}/(|a_{1,m}|^2|a_{2,m}|^2) \tag{A.7}$$

Where:

$$ni_{1,m} = Im\{|a_{1,m}|^2 a^*_{2,m}n_{2,m} + a_{1,m}|a_{2,m}|^2 n^*_{1,m}\} \tag{A.8}$$

Channel averaging before phase extraction

The frequency estimator with averaging across subchannels before phase extraction is given by Equation A.2. For uniform channel weighting $u(m) = 1$ the variance of the frequency estimate equals:

$$Var(\Delta \hat{f}_{Ch, phase}) = \left(\frac{1}{2\pi T}\right)^2 E_a \left[E_{ni} \left[\left| \frac{\sum_{m=0}^{N-1} ni_{1,m}}{\sum_{m=0}^{N-1} |a_{1,m}|^2 |a_{2,m}|^2} \right|^2 \right] \right] \qquad \text{(A.9)}$$

E_{ni} : Expectation with respect to noise

E_a : Expectation with respect to symbols

$$Var(\Delta \hat{f}_{Ch, phase}) = \left(\frac{1}{2\pi T}\right)^2 \frac{\sigma^2}{2} E_a \left[\frac{\sum_{m=0}^{N-1} |a_{1,m}|^2 |a_{2,m}|^2 (|a_{1,m}|^2 + |a_{2,m}|^2)}{\left(\sum_{m=0}^{N-1} |a_{1,m}|^2 |a_{2,m}|^2\right)^2} \right] \qquad \text{(A.10)}$$

Assuming N to be sufficiently large and normalized power $E_a[|a|^2] = 1$:

$$Var(\Delta \hat{f}_{Ch, phase}) \approx \left(\frac{1}{2\pi T}\right)^2 \frac{\sigma^2}{N} E_a[|a|^4] \qquad \text{(A.11)}$$

To increase the estimator performance, symbol dependent weighting should be applied to each channel. Minimum variance is given by weights equal to:

$$u'(m) = \frac{E_{ni}[p_{1,m}]}{E_{ni}[|ni_{1,m}|^2]} = \frac{2/\sigma^2}{|a_{1,m}|^2 + |a_{2,m}|^2} \qquad \text{(A.12)}$$

The common factor $2/\sigma^2$ can be removed:

$$u(m) = \frac{1}{|a_{1,m}|^2 + |a_{2,m}|^2} \qquad \text{(A.13)}$$

Including weighting the frequency estimator variance equals:

$$Var(\Delta\hat{f}_{Ch,phase}) = \left(\frac{1}{2\pi T}\right)^2\frac{\sigma^2}{2}E_a\left[\frac{\displaystyle\sum_{m=0}^{N-1}\frac{|a_{1,m}|^2|a_{2,m}|^2}{|a_{1,m}|^2+|a_{2,m}|^2}}{\left(\displaystyle\sum_{m=0}^{N-1}\frac{|a_{1,m}|^2|a_{2,m}|^2}{|a_{1,m}|^2+|a_{2,m}|^2}\right)^2}\right] \qquad \textbf{(A.14)}$$

$$= \left(\frac{1}{2\pi T}\right)^2\frac{\sigma^2}{2}E_a\left[\frac{1}{\displaystyle\sum_{m=0}^{N-1}\frac{|a_{1,m}|^2|a_{2,m}|^2}{|a_{1,m}|^2+|a_{2,m}|^2}}\right]$$

$$\approx \left(\frac{1}{2\pi T}\right)^2\frac{\sigma^2}{N}\frac{1}{2E_a\left[\frac{|a_1|^2|a_2|^2}{|a_1|^2+|a_2|^2}\right]}$$

Channel averaging after phase extraction

The frequency estimator with phase extraction before averaging across subchannels is given by Equation A.1. For uniform channel weighting $u(m) = 1$ the variance of the frequency estimate equals:

$$Var(\Delta\hat{f}_{Phase,Ch}) = \left(\frac{1}{2\pi TN}\right)^2 E_a\left[E_{ni}\left[\left|\sum_{m=0}^{N-1}\frac{ni_{1,m}}{|a_{1,m}|^2|a_{2,m}|^2}\right|^2\right]\right] \qquad \textbf{(A.15)}$$

$$= \left(\frac{1}{2\pi T}\right)^2\frac{\sigma^2}{N}E_a\left[\frac{1}{|a|^2}\right]$$

Equation A.15 is valid independent of the size of N. The optimum weighting factor to minimize estimator variance equals:

$$u'(m) \ = \ \cfrac{1}{E_{ni}\left[\left|\cfrac{ni_{1,\,m}}{|a_{1,\,m}|^2|a_{2,\,m}|^2}\right|^2\right]} \ = \ \frac{2|a_{1,\,m}|^2|a_{2,\,m}|^2/\sigma^2}{|a_{1,\,m}|^2 + |a_{2,\,m}|^2} \tag{A.16}$$

With removal of the common factor $2/\sigma^2$ and scaling to keep the estimator unbiased, the channel weights equal:

$$u(m) \ = \ \cfrac{\cfrac{|a_{1,\,m}|^2|a_{2,\,m}|^2}{|a_{1,\,m}|^2 + |a_{2,\,m}|^2}}{\cfrac{1}{N}\displaystyle\sum_{n=0}^{N-1}\cfrac{|a_{1,\,n}|^2|a_{2,\,n}|^2}{|a_{1,\,n}|^2 + |a_{2,\,n}|^2}} \tag{A.17}$$

Variance with weighting equals:

$$Var(\Delta \hat{f}_{Phase,\,Ch}) \ = \ \left(\frac{1}{2\pi TN}\right)^2 E_a\left[E_{ni}\left[\left|\sum_{m=0}^{N-1}\frac{u(m)ni_{1,\,m}}{|a_{1,\,m}|^2|a_{2,\,m}|^2}\right|^2\right]\right] \tag{A.18}$$

$$= \ \left(\frac{1}{2\pi TN}\right)^2\frac{N^2\sigma^2}{2}E_a\left[\cfrac{\displaystyle\sum_{m=0}^{N-1}\cfrac{|a_{1,\,m}|^2|a_{2,\,m}|^2}{|a_{1,\,m}|^2 + |a_{2,\,m}|^2}}{\left(\displaystyle\sum_{n=0}^{N-1}\cfrac{|a_{1,\,n}|^2|a_{2,\,n}|^2}{|a_{1,\,n}|^2 + |a_{2,\,n}|^2}\right)^2}\right]$$

Assuming N to be sufficiently large:

$$Var(\Delta \hat{f}_{Phase,\,Ch}) \ \approx \ \left(\frac{1}{2\pi T}\right)^2\frac{\sigma^2}{N}\cfrac{1}{2E_a\left[\cfrac{|a_1|^2|a_2|^2}{|a_1|^2 + |a_2|^2}\right]} \tag{A.19}$$

Appendix B
IBI power and signal power covariance

As discussed in Chapter 6.3, a time varying transmission channel and/or a CFO generates IBI in an OFDM system. The time varying transmission channel investigated in this work is the frequency flat fading channel $c(t)$ described in Chapter 2.6.2. In this appendix the coupling or covariance between the instant signal power $|\alpha a|^2$ and the instant IBI power $|IBI|^2$ is investigated.

$$\frac{K(|\alpha a|^2, |IBI|^2)}{E[|\alpha a|^2]E[|IBI|^2]} = \frac{E[(|\alpha a|^2 - E[|\alpha a|^2])(|IBI|^2 - E[|IBI|^2])]}{E[|\alpha a|^2]E[|IBI|^2]} \tag{B.1}$$

Without loss of generality frame $k = 0$ is investigated. The number of channels N is assumed to be sufficiently large to neglect special effects due to channel 0 and $N-1$.

For OFDM using QAM and square pulses without guard interval, the signal component and IBI in channel m, frame k at the receiver is found by rewriting Equation 6.28:

$$(\alpha a_{0,m})_{QAM} = a_{0,m}|I_0| \tag{B.2}$$

$$(IBI_{0,m})_{QAM} = \left(\sum_{\substack{n=0 \\ n \neq m}}^{N-1} a_{0,n}I_{m-n} \right) e^{-j\arg I_0} \tag{B.3}$$

Where:

$$I_p = \frac{1}{T}\int_0^T c(t)e^{-j2\pi\frac{p}{T}t}e^{j2\pi\Delta ft}dt \tag{B.4}$$

Using O-QAM with symmetrical pulse shaping filters, Equation 6.30 can be rewritten as:

$$(\alpha a_{0,m})_{O\text{-}QAM} = a_{0,m}\Lambda_{0,0} \tag{B.5}$$

$$(IBI_{0,m})_{O\text{-}QAM} = \sum_{\substack{n=0 \\ n\neq m \vee l\neq 0}}^{N-1}\sum_{l=-\infty}^{\infty} a_{l,n}\Lambda_{l,m-n} \tag{B.6}$$

$$+ \sum_{n=0}^{N-1}\sum_{l=-\infty}^{\infty} -Im\{a_{l,n}\}\Gamma_{l,m-n} + jRe\{a_{l,n}\}\Gamma_{l+1,m-n}$$

Where:

$$\Lambda_{l,p} = \int_{-\infty}^{\infty} h(t-lT)h(t)Re\left\{c'(t)e^{j\left(\left(\frac{2\pi}{T}t+\frac{\pi}{2}\right)p+2\pi\Delta ft\right)}\right\}dt$$

$$\Gamma_{l,p} = \int_{-\infty}^{\infty} h\left(t-lT+\frac{T}{2}\right)h(t)Im\left\{c'(t)e^{j\left(\left(\frac{2\pi}{T}t+\frac{\pi}{2}\right)p+2\pi\Delta ft\right)}\right\}dt \tag{B.7}$$

$$c'(t) = c(t)e^{-j\arg(c(t'))} \tag{B.8}$$

t' : Sampling instant

It is assumed unity transmitted power and unity amplification by the fading transmission channel:

$$E[|a|^2] = 1 \tag{B.9}$$

$$E[|c(t)|^2] = 1 \tag{B.10}$$

B.1 CFO generated IBI

QAM and rectangular pulses

In the case of Doppler bandwidth $\ll 1/T$, the fading channel can be approximated as constant over one frame, for simplicity denoted c_k. The IBI is thus CFO created. First OFDM using QAM and rectangular pulses is investigated (frame $k = 0$):

$$K(|\alpha a|^2, |IBI|^2)_{CFO} = \tag{B.11}$$

$$E\left[(|a_{0,m}I_0|^2 - E[|a_{0,m}I_0|^2])\left(\left|\sum_{\substack{n=0 \\ n \neq m}}^{N-1} a_{0,n}I_{m-n}\right|^2 - E\left[\left|\sum_{\substack{n=0 \\ n \neq m}}^{N-1} a_{0,n}I_{m-n}\right|^2\right]\right)\right]$$

Equation B.1 can be rewritten as:

$$K(|\alpha a|^2, |IBI|^2)_{CFO} = \tag{B.12}$$

$$E\left[|a_{0,m}I_0|^2\left|\sum_{\substack{n=0 \\ n \neq m}}^{N-1} a_{0,n}I_{m-n}\right|^2\right] - E[|a_{0,m}I_0|^2]E\left[\left|\sum_{\substack{n=0 \\ n \neq m}}^{N-1} a_{0,n}I_{m-n}\right|^2\right]$$

Defining:

$$I_p = c_k I_p' \tag{B.13}$$

$$I_p' = \frac{1}{T}\int_0^T e^{-j2\pi\frac{p}{T}t}e^{j2\pi\Delta ft}dt \tag{B.14}$$

Inserting Equation B.3 into B.2:

$$K(|\alpha a|^2, |IBI|^2)_{CFO} = |I_0'|^2 \sum_{\substack{n = 0 \\ n \neq m}}^{N-1} |I_{m-n}'|^2 E[|c_0|^4] - |I_0'|^2 \sum_{\substack{n = 0 \\ n \neq m}}^{N-1} |I_{m-n}'|^2 E[|c_0|^2]^2 \quad \text{(B.15)}$$

Recognizing $c(t)$ as a filtered zero mean complex Gaussian signal, the expectation of the fourth power equals (Nikias and Petropulu 93):

$$E[|c_0|^4] = 2E[|c_0|^2]^2 \quad \text{(B.16)}$$

Combining Equation B.10, B.5 and B.6:

$$K(|\alpha a|^2, |IBI|^2)_{CFO} = |I_0'|^2 \sum_{\substack{n = 0 \\ n \neq m}}^{N-1} |I_{m-n}'|^2 \quad \text{(B.17)}$$

At the same time:

$$E[|\alpha a|^2]E[|IBI|^2] = |I_0'|^2 \sum_{\substack{n = 0 \\ n \neq m}}^{N-1} |I_{m-n}'|^2 \quad \text{(B.18)}$$

Resulting in:

$$\frac{K(|\alpha a|^2, |IBI|^2)_{CFO}}{E[|\alpha a|^2]E[|IBI|^2]} = 1 \quad \text{(B.19)}$$

O-QAM with symmetrical pulseshaping filters

For O-QAM with symmetrical pulseshaping filters, the covariance equals (frame $k = 0$):

$$
\begin{aligned}
K(|\alpha a|^2, |IBI|^2)_{CFO} = {} & E[(|a_{0,m}\Lambda_{0,0}|^2 - E[|a_{0,m}\Lambda_{0,0}|^2]) \\
& \cdot (|(IBI_{0,m})_{O\text{-}QAM}|^2 - E[|(IBI_{0,m})_{O\text{-}QAM}|^2])]
\end{aligned}
\quad \text{(B.20)}
$$

Giving:

$$K(|\alpha a|^2, |IBI|^2)_{CFO} = E[|a_{0,m}\Lambda_{0,0}|^2|(IBI_{0,m})_{O\text{-}QAM}|^2]$$
$$- E[|a_{0,m}\Lambda_{0,0}|^2]E[|(IBI_{0,m})_{O\text{-}QAM}|^2] \tag{B.21}$$

With $c(t)$ approximated as constant over the observation interval and phase correction as defined in Equation B.8 the following definition is valid:

$$\Lambda_{l,p} = |c(t)|\Lambda_{l,p}' = |c(t)| \int_{-\infty}^{\infty} h(t-lT)h(t)Re\left\{ e^{j\left(\left(\frac{2\pi}{T}t+\frac{\pi}{2}\right)p + 2\pi\Delta ft\right)} \right\}dt$$

$$\Gamma_{l,p} = |c(t)|\Gamma_{l,p}' = |c(t)| \int_{-\infty}^{\infty} h\left(t-lT+\frac{T}{2}\right)h(t)Im\left\{ e^{j\left(\left(\frac{2\pi}{T}t+\frac{\pi}{2}\right)p + 2\pi\Delta ft\right)} \right\}dt \tag{B.22}$$

Applying Equation B.12:

$$E[|a_{0,m}\Lambda_{0,0}|^2] = \Lambda_{0,0}'^2 \tag{B.23}$$

$$E[|(IBI_{0,m})_{O\text{-}QAM}|^2] = \sum_{\substack{n=0 \\ n \neq m \vee l \neq 0}}^{N-1} \sum_{l=-\infty}^{\infty} \Lambda_{l,m-n}'^2 + \sum_{n=0}^{N-1} \sum_{l=-\infty}^{\infty} \Gamma_{l,m-n}'^2 \tag{B.24}$$

$$E[|a_{0,m}\Lambda_{0,0}|^2|(IBI_{0,m})_{O\text{-}QAM}|^2] = E[|c(t)|^4]\Lambda_{0,0}'^2\left(\sum_{\substack{n=0 \\ n \neq m \vee l \neq 0}}^{N-1} \sum_{l=-\infty}^{\infty} \Lambda_{l,m-n}'^2 \right. \tag{B.25}$$

$$\left. + E\left[|a_{0,m}|^2 \sum_{n=0}^{N-1} \sum_{l=-\infty}^{\infty} Im\{a_{l,n}\}^2\Gamma_{l,m-n}'^2 + Re\{a_{l,n}\}^2\Gamma_{l+1,m-n}'^2 \right] \right)$$

In the last double sum of Equation B.15, term $n = m$ $l = 0$ includes $E[|a_{0,m}|^2Im\{a_{0,m}\}^2]$ and $E[|a_{0,m}|^2Re\{a_{0,m}\}^2]$. Assuming this term not to be dominating in the total sum the following approximations is used:

$$E[|a_{0,m}|^2Im\{a_{0,m}\}^2] \approx E[|a_{0,m}|^2]E[Im\{a_{0,m}\}^2] \tag{B.26}$$

$$E[|a_{0,m}|^2Re\{a_{0,m}\}^2] \approx E[|a_{0,m}|^2]E[Re\{a_{0,m}\}^2] \tag{B.27}$$

For 4-QAM the approximations in Equation B.16 and B.17 is fulfilled with equality, while for larger constellation sizes there will be an error increasing with increasing constellation size (an error approx. equal to a factor 1.4 for 256-QAM). Equation B.15 can be rewritten as:

$$E[|a_{0,m}\Lambda_{0,0}|^2|(IBI_{0,m})_{O\text{-}QAM}|^2] \approx \tag{B.28}$$

$$E[|c(t)|^4]\Lambda_{0,0}'^2\left(\sum_{\substack{n=0\\n\neq m\vee l\neq 0}}^{N-1}\sum_{l=-\infty}^{\infty}\Lambda_{l,m-n}'^2 + \sum_{n=0}^{N-1}\sum_{l=-\infty}^{\infty}\Gamma_{l,m-n}'^2\right)$$

Applying Equation B.6 and inserting Equation B.13, B.14 and B.18 into Equation B.11:

$$K(|\alpha a|^2, |IBI|^2)_{CFO} \approx E[|a_{0,m}\Lambda_{0,0}|^2]E[|(IBI_{0,m})_{O\text{-}QAM}|^2] \tag{B.29}$$

Resulting in:

$$\frac{K(|\alpha a|^2, |IBI|^2)_{CFO}}{E[|\alpha a|^2]E[|IBI|^2]} \approx 1 \tag{B.30}$$

B.2 Fading generated IBI

QAM and rectangular pulses

In the case of zero CFO and transmission channel variations large enough to be observable within each frame, the IBI is Doppler spread generated. First investigating OFDM using QAM and rectangular pulses (frame $k = 0$):

$$K(|\alpha a|^2, |IBI|^2)_{Fading} = \qquad\qquad\qquad\qquad\qquad\text{(B.31)}$$

$$E\left[|a_{0,m}I_0|^2\left|\sum_{\substack{n=0\\n\neq m}}^{N-1}a_{0,n}I_{m-n}\right|^2\right] - E[|a_{0,m}I_0|^2]E\left[\left|\sum_{\substack{n=0\\n\neq m}}^{N-1}a_{0,n}I_{m-n}\right|^2\right]$$

Where mean signal power equals:

$$E[|a_{0,m}I_0|^2] = E\left[\left|\int_0^T c(t)dt\right|^2\right] = \int_0^T\int_0^T E[c(t_1)c^*(t_2)]dt_1dt_2 \qquad\text{(B.32)}$$

Repeating the model of $c(t)$, Chapter 2.6.3:.
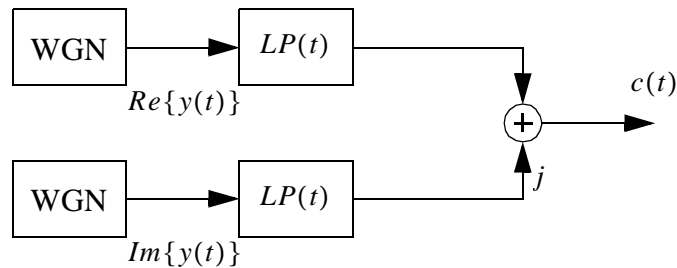
Figure 7.1. *Rayleigh fading model*

WGN: White Gaussian noise

$LP(t)$: Impulse response of Butterwort low pass filter

$y(t)$: Complex white Gaussian noise

$$E[|a_{0,m}I_0|^2] = \int_0^T\int_0^T\int_{-\infty}^{\infty}\int_{-\infty}^{\infty} LP(t_3)LP(t_4)R_y(t_2-t_1-t_3+t_4)dt_1dt_2dt_3dt_4 \qquad\text{(B.33)}$$

$R_y(t)$: Auto correlation function of $y(t)$

For $y(t)$ white:

$$E[|a_{0,m}I_0|^2] = \int_0^T\int_0^T\int_{-\infty}^{\infty} LP(t_2 - t_1 + t_4)LP(t_4)dt_1 dt_2 dt_4 \tag{B.34}$$

Mean IBI power equals:

$$E\left[\left|\sum_{\substack{n=0 \\ n \neq m}}^{N-1} a_{0,n}I_{m-n}\right|^2\right] = \sum_{\substack{n=0 \\ n \neq m}}^{N-1}\int_0^T\int_0^T E[c(t_1)c^*(t_2)]e^{-j2\pi\frac{m-n}{T}(t_1-t_2)}dt_1 dt_2 \tag{B.35}$$

Expanding $c(t)$ and rewriting:

$$E\left[\left|\sum_{\substack{n=0 \\ n \neq m}}^{N-1} a_{0,n}I_{m-n}\right|^2\right] = \sum_{\substack{n=0 \\ n \neq m}}^{N-1}\int_0^T\int_0^T\int_{-\infty}^{\infty} LP(t_2 - t_1 + t_4)LP(t_4)e^{-j2\pi\frac{m-n}{T}(t_1-t_2)}dt_1 dt_2 dt_4 \tag{B.36}$$

The cross term between signal and IBI:

$$E\left[|a_{0,m}I_0|^2\left|\sum_{\substack{n=0 \\ n \neq m}}^{N-1} a_{0,n}I_{m-n}\right|^2\right] = \tag{B.37}$$

$$\sum_{\substack{n=0 \\ n \neq m}}^{N-1}\int_0^T\int_0^T\int_0^T\int_0^T E[c(t_1)c^*(t_2)c(t_3)c^*(t_4)]e^{-j2\pi\frac{m-n}{T}(t_3-t_4)}dt_1 dt_2 dt_3 dt_4$$

Recognizing $c(t)$ as an filtered zero mean complex Gaussian signal, (Nikias and Petropulu 93):

$$E[c(t_1)c^*(t_2)c(t_3)c^*(t_4)] = \tag{B.38}$$
$$E[c(t_1)c^*(t_2)]E[c(t_3)c^*(t_4)] + E[c(t_1)c^*(t_4)]E[c^*(t_2)c(t_3)]$$

Resulting in:

$$E\left[\left|a_{0,m}I_0\right|^2\left|\sum_{\substack{n=0\\n\neq m}}^{N-1}a_{0,n}I_{m-n}\right|^2\right] = E[\left|a_{0,m}I_0\right|^2]E\left[\left|\sum_{\substack{n=0\\n\neq m}}^{N-1}a_{0,n}I_{m-n}\right|^2\right] \tag{B.39}$$

$$+ \sum_{\substack{n=0\\n\neq m}}^{N-1}\int_0^T\int_0^T\int_0^T\int_0^T E[c(t_1)c^*(t_4)]E[c^*(t_2)c(t_3)]e^{-j2\pi\frac{m-n}{T}(t_3-t_4)}dt_1dt_2dt_3dt_4$$

Combining Equation B.1 and B.9:

$$K(\left|\alpha a\right|^2, \left|IBI\right|^2)_{Fading} = \left(\sum_{\substack{n=0\\n\neq m}}^{N-1}\int_0^T\int_0^T E[c(t_1)c^*(t_4)]e^{j2\pi\frac{m-n}{T}t_4}dt_1dt_4\right) \tag{B.40}$$

$$\left(\sum_{\substack{n=0\\n\neq m}}^{N-1}\int_0^T\int_0^T E[c^*(t_2)c(t_3)]e^{-j2\pi\frac{m-n}{T}t_3}dt_2dt_3\right)$$

Expanding $c(t)$ and rewriting:

$$K(\left|\alpha a\right|^2, \left|IBI\right|^2)_{Fading} = \left(\sum_{\substack{n=0\\n\neq m}}^{N-1}\int_0^T\int_0^T e^{j2\pi\frac{m-n}{T}t_4}\int_{-\infty}^{\infty}LP(t_1-t_4+\tau_1)LP(\tau_1)d\tau_1dt_1dt_4\right) \tag{B.41}$$

$$\left(\sum_{\substack{n=0\\n\neq m}}^{N-1}\int_0^T\int_0^T e^{-j2\pi\frac{m-n}{T}t_3}\int_{-\infty}^{\infty}LP(t_3-t_2+\tau_2)LP(\tau_2)d\tau_2dt_2dt_3\right)$$

$$K(|\alpha a|^2, |IBI|^2)_{Fading} = \left(\sum_{\substack{n = 0 \\ n \neq m}}^{N-1} \int_0^T \int_0^T e^{j2\pi\frac{m-n}{T}t_4} R_{LP}(t_1 - t_4) dt_4 dt_1 \right)$$

$$\left(\sum_{\substack{n = 0 \\ n \neq m}}^{N-1} \int_0^T \int_0^T e^{-j2\pi\frac{m-n}{T}t_3} R_{LP}(t_3 - t_2) dt_3 dt_2 \right) \quad \textbf{(B.42)}$$

Where the correlation function equals:

$$R_{LP}(t) = \int_{-\infty}^{\infty} LP(t + \tau) LP(\tau) d\tau \quad \textbf{(B.43)}$$

$R_{LP}(t)$ is even, resulting in $\int_0^T e^{j2\pi\frac{m-n}{T}t_4} R_{LP}(t_1 - t_4) dt_4$ to be an odd function around

$t_1 = \dfrac{T}{2}$. Integrating by respect to t_1 from 0 to T give zero.

$$\frac{K(|\alpha a|^2, |IBI|^2)_{Fading}}{E[|\alpha a|^2] E[|IBI|^2]} = 0 \quad \textbf{(B.44)}$$

O-QAM with symmetrical pulseshaping filters

For O-QAM with symmetrical pulseshaping filters and Doppler generated IBI, the covariance equals (frame $k = 0$):

$$K(|\alpha a|^2, |IBI|^2)_{Fading} = E[|a_{0,m}\Lambda_{0,0}|^2 |(IBI_{0,m})_{O\text{-}QAM}|^2]$$
$$- E[|a_{0,m}\Lambda_{0,0}|^2] E[|(IBI_{0,m})_{O\text{-}QAM}|^2] \quad \textbf{(B.45)}$$

Mean signal power, avoiding phase correction of $c(t)$, equals:

$$E[|a_{0,m}\Lambda_{0,0}|^2] = \int_{-\infty}^{\infty}\int_{-\infty}^{\infty} h(t_1)^2 h(t_2)^2 E[Re\{c(t_1)\}Re\{c(t_2)\}] dt_1 dt_2 \quad \textbf{(B.46)}$$

$h(t)$: Pulse shaping filter

Mean IBI power equals:

$$E[|(IBI_{0,m})_{O\text{-}QAM}|^2] = \qquad\qquad\qquad\qquad\qquad \textbf{(B.47)}$$

$$E\left[\left|\sum_{\substack{n=0 \\ n\neq m \vee l\neq 0}}^{N-1}\sum_{l=-\infty}^{\infty} a_{l,n}\Lambda_{l,m-n} + \sum_{m=0}^{N-1}\sum_{l=-\infty}^{\infty} -Im\{a_{l,n}\}\Gamma_{l,m-n} + jRe\{a_{l,n}\}\Gamma_{l+1,m-n}\right|^2\right]$$

$$E[|(IBI_{0,m})_{O\text{-}QAM}|^2] = \sum_{\substack{n=0 \\ n\neq m \vee l\neq 0}}^{N-1}\sum_{l=-\infty}^{\infty} E[\Lambda_{l,m-n}^2] + \sum_{m=0}^{N-1}\sum_{l=-\infty}^{\infty} E[\Gamma_{l,m-n}^2] \quad \textbf{(B.48)}$$

Expanding:

$$E[\Lambda_{l,m-n}^2] = \qquad\qquad\qquad\qquad\qquad \textbf{(B.49)}$$

$$\int_{-\infty}^{\infty}\int_{-\infty}^{\infty} h(t_3 - lT)h(t_3)h(t_4 - lT)h(t_4)$$

$$\left(E[Re\{c(t_3)\}Re\{c(t_4)\}]\cos\left(\left(\frac{2\pi}{T}t_3 + \frac{\pi}{2}\right)(m-n)\right)\cos\left(\left(\frac{2\pi}{T}t_4 + \frac{\pi}{2}\right)(m-n)\right)\right.$$

$$\left.-E[Im\{c(t_3)\}Im\{c(t_4)\}]\sin\left(\left(\frac{2\pi}{T}t_3 + \frac{\pi}{2}\right)(m-n)\right)\sin\left(\left(\frac{2\pi}{T}t_4 + \frac{\pi}{2}\right)(m-n)\right)\right)$$

$$dt_3 dt_4$$

$$E[\Gamma^2_{l,\,m-n}] \;=\; \tag{B.50}$$

$$\int_{-\infty}^{\infty}\int_{-\infty}^{\infty} h\left(t_3 - lT + \frac{T}{2}\right)h(t_3)h\left(t_4 - lT + \frac{T}{2}\right)h(t_4)$$

$$\left(E[Re\{c(t_3)\}Re\{c(t_4)\}]\sin\left(\left(\frac{2\pi}{T}t_3 + \frac{\pi}{2}\right)(m-n)\right)\sin\left(\left(\frac{2\pi}{T}t_4 + \frac{\pi}{2}\right)(m-n)\right)\right.$$

$$\left.+\,E[Im\{c(t_3)\}Im\{c(t_4)\}]\cos\left(\left(\frac{2\pi}{T}t_3 + \frac{\pi}{2}\right)(m-n)\right)\cos\left(\left(\frac{2\pi}{T}t_4 + \frac{\pi}{2}\right)(m-n)\right)\right)$$

$$dt_3 dt_4$$

Cross product between signal and noise power equals (including the approximations of Equation B.16 and B.17):

$$E[|a_{0,\,m}\Lambda_{0,\,0}|^2|(IBI_{0,\,m})_{O\text{-}QAM}|^2] \;\approx\; \tag{B.51}$$

$$\sum_{\substack{n\,=\,0 \\ n\neq m\,\vee\,l\neq 0}}^{N-1}\sum_{l\,=\,-\infty}^{\infty} E[\Lambda^2_{0,\,0}\Lambda^2_{l,\,m-n}] \;+\; \sum_{m\,=\,0}^{N-1}\sum_{l\,=\,-\infty}^{\infty} E[\Lambda^2_{0,\,0}\Gamma^2_{l,\,m-n}]$$

$$E[\Lambda_{0,0}^2 \Lambda_{l,m-n}^2] = \tag{B.52}$$

$$\int_{-\infty}^{\infty} \int_{-\infty}^{\infty} \int_{-\infty}^{\infty} \int_{-\infty}^{\infty} h(t_1)^2 h(t_2)^2 h(t_3 - lT)h(t_3)h(t_4 - lT)h(t_4)$$

$$\left(E[Re\{c(t_1)\}Re\{c(t_2)\}Re\{c(t_3)\}Re\{c(t_4)\}] \right.$$

$$\cos\left(\left(\frac{2\pi}{T}t_3 + \frac{\pi}{2}\right)(m-n)\right)\cos\left(\left(\frac{2\pi}{T}t_4 + \frac{\pi}{2}\right)(m-n)\right)$$

$$-E[Re\{c(t_1)\}Re\{c(t_2)\}]E[Im\{c(t_3)\}Im\{c(t_4)\}]$$

$$\left. \sin\left(\left(\frac{2\pi}{T}t_3 + \frac{\pi}{2}\right)(m-n)\right)\sin\left(\left(\frac{2\pi}{T}t_4 + \frac{\pi}{2}\right)(m-n)\right) \right)$$

$$dt_1 dt_2 dt_3 dt_4$$

$$E[\Lambda_{0,0}^2 \Gamma_{l,m-n}^2] = \tag{B.53}$$

$$\int\limits_{-\infty}^{\infty} \int\limits_{-\infty}^{\infty} \int\limits_{-\infty}^{\infty} \int\limits_{-\infty}^{\infty} h(t_1)^2 h(t_2)^2 h\left(t_3 - lT + \frac{T}{2}\right)h(t_3)h\left(t_4 - lT + \frac{T}{2}\right)h(t_4)$$

$$\left(E[Re\{c(t_1)\}Re\{c(t_2)\}Re\{c(t_3)\}Re\{c(t_4)\}]\right.$$

$$\sin\left(\left(\frac{2\pi}{T}t_3 + \frac{\pi}{2}\right)(m-n)\right)\sin\left(\left(\frac{2\pi}{T}t_4 + \frac{\pi}{2}\right)(m-n)\right)$$

$$+ E[Re\{c(t_1)\}Re\{c(t_2)\}]E[Im\{c(t_3)\}Im\{c(t_4)\}]$$

$$\cos\left(\left(\frac{2\pi}{T}t_3 + \frac{\pi}{2}\right)(m-n)\right)\cos\left(\left(\frac{2\pi}{T}t_4 + \frac{\pi}{2}\right)(m-n)\right)\right)$$

$$dt_1 dt_2 dt_3 dt_4$$

Where, (Nikias and Petropulu 93):

$$E[Re\{c(t_1)\}Re\{c(t_2)\}Re\{c(t_3)\}Re\{c(t_4)\}] = \tag{B.54}$$
$$E[Re\{c(t_1)\}Re\{c(t_2)\}]E[Re\{c(t_3)\}Re\{c(t_4)\}]$$
$$+ E[Re\{c(t_1)\}Re\{c(t_3)\}]E[Re\{c(t_2)\}Re\{c(t_4)\}]$$
$$+ E[Re\{c(t_1)\}Re\{c(t_4)\}]E[Re\{c(t_2)\}Re\{c(t_3)\}]$$

Inserting Equation B.17, B.18, B.22 and B.23 into Equation B.15:

$$K(|\alpha a|^2, |IBI|^2)_{Fading} \approx \tag{B.55}$$

$$
A \begin{cases}
\displaystyle\sum_{\substack{n=0 \\ n \neq m \vee l \neq 0}}^{N-1} \sum_{l=-\infty}^{\infty} \left(\int_{-\infty}^{\infty}\int_{-\infty}^{\infty}\int_{-\infty}^{\infty}\int_{-\infty}^{\infty} h(t_1)^2 h(t_2)^2 h(t_3 - lT) h(t_3) h(t_4 - lT) h(t_4) \right. \\[2ex]
(E[Re\{c(t_1)\}Re\{c(t_3)\}]E[Re\{c(t_2)\}Re\{c(t_4)\}] \\[2ex]
+ E[Re\{c(t_1)\}Re\{c(t_4)\}]E[Re\{c(t_2)\}Re\{c(t_3)\}]) \\[2ex]
\displaystyle\cos\left(\left(\frac{2\pi}{T}t_3 + \frac{\pi}{2}\right)(m-n)\right)\cos\left(\left(\frac{2\pi}{T}t_4 + \frac{\pi}{2}\right)(m-n)\right)dt_1 dt_2 dt_3 dt_4 \Bigg)
\end{cases}
$$

$$
B \begin{cases}
\displaystyle+ \sum_{m=0}^{N-1} \sum_{l=-\infty}^{\infty} \left(\int_{-\infty}^{\infty}\int_{-\infty}^{\infty}\int_{-\infty}^{\infty}\int_{-\infty}^{\infty} h(t_1)^2 h(t_2)^2 h\left(t_3 - lT + \frac{T}{2}\right) h(t_3) h\left(t_4 - lT + \frac{T}{2}\right) h(t_4) \right. \\[2ex]
(E[Re\{c(t_1)\}Re\{c(t_3)\}]E[Re\{c(t_2)\}Re\{c(t_4)\}] \\[2ex]
+ E[Re\{c(t_1)\}Re\{c(t_4)\}]E[Re\{c(t_2)\}Re\{c(t_3)\}]) \\[2ex]
\displaystyle\sin\left(\left(\frac{2\pi}{T}t_3 + \frac{\pi}{2}\right)(m-n)\right)\sin\left(\left(\frac{2\pi}{T}t_4 + \frac{\pi}{2}\right)(m-n)\right)dt_1 dt_2 dt_3 dt_4 \Bigg)
\end{cases}
$$

$$A =$$

(B.56)

$$\sum_{\substack{n = 0 \\ n \neq m \vee l \neq 0}}^{N-1} \sum_{l = -\infty}^{\infty} \left(\int_{-\infty}^{\infty} h(t_1)^2 \int_{-\infty}^{\infty} h(t_3 - lT) h(t_3) R_{LP}(t_1 - t_3) \right.$$

$$\cos\left(\left(\frac{2\pi}{T} t_3 + \frac{\pi}{2}\right)(m - n)\right) dt_3 dt_1$$

$$\int_{-\infty}^{\infty} h(t_2)^2 \int_{-\infty}^{\infty} h(t_4 - lT) h(t_4) R_{LP}(t_2 - t_4) \cos\left(\left(\frac{2\pi}{T} t_4 + \frac{\pi}{2}\right)(m - n)\right) dt_4 dt_2$$

$$+ \int_{-\infty}^{\infty} h(t_1)^2 \int_{-\infty}^{\infty} h(t_4 - lT) h(t_4) R_{LP}(t_1 - t_4) \cos\left(\left(\frac{2\pi}{T} t_4 + \frac{\pi}{2}\right)(m - n)\right) dt_4 dt_1$$

$$\left. \int_{-\infty}^{\infty} h(t_2)^2 \int_{-\infty}^{\infty} h(t_3 - lT) h(t_3) R_{LP}(t_2 - t_3) \cos\left(\left(\frac{2\pi}{T} t_3 + \frac{\pi}{2}\right)(m - n)\right) dt_3 dt_2 \right)$$

$$B \; = \tag{B.57}$$

$$\sum_{\substack{n = 0 \\ n \neq m \vee l \neq 0}}^{N-1} \sum_{l = -\infty}^{\infty} \left(\int_{-\infty}^{\infty} h(t_1)^2 \int_{-\infty}^{\infty} h\left(t_3 - lT + \frac{T}{2}\right) h(t_3) R_{LP}(t_1 - t_3) \right.$$

$$\sin\left(\left(\frac{2\pi}{T} t_3 + \frac{\pi}{2}\right)(m - n)\right) dt_3 dt_1$$

$$\int_{-\infty}^{\infty} h(t_2)^2 \int_{-\infty}^{\infty} h\left(t_4 - lT + \frac{T}{2}\right) h(t_4) R_{LP}(t_2 - t_4) \sin\left(\left(\frac{2\pi}{T} t_4 + \frac{\pi}{2}\right)(m - n)\right) dt_4 dt_2$$

$$+ \int_{-\infty}^{\infty} h(t_1)^2 \int_{-\infty}^{\infty} h\left(t_4 - lT + \frac{T}{2}\right) h(t_4) R_{LP}(t_1 - t_4) \sin\left(\left(\frac{2\pi}{T} t_4 + \frac{\pi}{2}\right)(m - n)\right) dt_4 dt_1$$

$$\left. \int_{-\infty}^{\infty} h(t_2)^2 \int_{-\infty}^{\infty} h\left(t_3 - lT + \frac{T}{2}\right) h(t_3) R_{LP}(t_2 - t_3) \sin\left(\left(\frac{2\pi}{T} t_3 + \frac{\pi}{2}\right)(m - n)\right) dt_3 dt_2 \right)$$

To obtain zero IBI for zero CFO and stationary channel, the OFDM pulse shaping filters must fulfill the requirements of Equation B.28 for $n \neq m \vee l \neq 0$:

$$\int_{-\infty}^{\infty} h(t_3 - lT) h(t_3) \cos\left(\left(\frac{2\pi}{T} t_3 + \frac{\pi}{2}\right)(m - n)\right) dt_3 \; = \; 0$$

$$\tag{B.58}$$

$$\int_{-\infty}^{\infty} h\left(t_3 - lT + \frac{T}{2}\right) h(t_3) \sin\left(\left(\frac{2\pi}{T} t_3 + \frac{\pi}{2}\right)(m - n)\right) dt_3 \; = \; 0$$

The integrands are odd functions around respectively $-\dfrac{lT}{2}$ and $-\dfrac{(l-1/2)T}{2}$. With $R_{LP}(t_1 - t_3)$ even around t_1 with respect to t_3, Equation B.29 is an odd function around $t_1 = -\dfrac{lT}{2}$

$$\int_{-\infty}^{\infty} h(t_3 - lT)h(t_3)R_{LP}(t_1 - t_3)\cos\left(\left(\frac{2\pi}{T}t_3 + \frac{\pi}{2}\right)(m-n)\right)dt_3 \tag{B.59}$$

Similar is Equation B.30 odd around $t_1 = -\dfrac{(l-1/2)T}{2}$

$$\int_{-\infty}^{\infty} h\left(t_3 - lT + \frac{T}{2}\right)h(t_3)R_{LP}(t_1 - t_3)\sin\left(\left(\frac{2\pi}{T}t_3 + \frac{\pi}{2}\right)(m-n)\right)dt_3 \tag{B.60}$$

With $h(t_1)^2$ even around zero, and the results of Equation B.29 and B.30:

$$\begin{aligned} A(l) &= -A(-l) \\ B(l+1) &= -B(-l) \end{aligned} \tag{B.61}$$

$A(l), B(l)$: Term l in the sums of Equation B.26 and B.27.

Inserting Equation B.31 in B.26, all terms cancels except for $l = 0$. Inserting Equation B.31 in B.27, all terms cancels. For $l = 0$, Equation B.29 is odd around $t_1 = 0$, resulting in:

$$A(0) = 0 \tag{B.62}$$

Inserting in Equation B.25:

$$\frac{K(|\alpha a|^2, |IBI|^2)_{Fading}}{E[|\alpha a|^2]E[|IBI|^2]} \approx 0 \tag{B.63}$$

References

(Armstrong et. al 98)   Armstrong, J., Grant, P.M., Povey, G., "Polynomial Can-
                           cellation to reduce intercarrier interference due to doppler
                           spread", Proceedings IEEE GlobeCom'98, 1998

(Van de Beek et. al 97)   Van de Beek, J.J., Sandell, M., Börjesson, P.O., "ML Esti-
                           mation of Time and Frequency Offset in OFDM Systems"
                           IEEE Transactions on Signal Processing, July 1997.

(Bingham 88)   Bigham, J. A. C., "The theory and practise of modem
                           design", John Wiley & Sons, Inc., New York, USA 1988

(Bingham 90)   Bigham, J. A. C., "Multicarrier modulation for data trans-
                           mission: An Idea whose time has come", IEEE Communi-
                           cation Magazine, vol. 28, pp. 5-14, May 1990

(Cariolaro and Vagliani 95) Cariolaro, G., Vagliani, F., C., "An OFDM scheme with
                           a half complexity", IEEE Journal on Selected areas in
                           Commun., vol. 13, no. 9, December 1995.

(Chang 66)   Chang, R.W., "Synthesis of band-limmited orthogonal sig-
                           nals for multi channel data transmission", Bell Syst. Tech.
                           J., vol. 45, pp. 1775-1796, December 1966

(Chang and Gibby 68)   Chang, R. W., Gibby, R. A., "A theoretical study of per-
                           formance of an orthogonal multiplexing data transmission
                           system", IEEE Trans. Commun. TECHNOL., VOL. com-
                           16, NO. 4, pp. 529-540, August 1968

(Chow et. al. 91)   Chow, J.S., Tu, J.C., Cioffi, J.M., "Performance evaluation
                           of a multichannel tranceiver system for ADSL and

VHDSL services", IEEE J. select. Areas of Com., vol. 9, no. 6, pp.909-919, August 1991

(Clasen and Meyr 94)   F. Classen and H. Meyr, "Frequency Synchronization Algorithms for OFDM Systems suitable for Communication over Frequency Selective Fading Channels", Proceedings IEEE VTC'94, p1655-1659, 1994.

(Daffra and Chouly 93)   Daffara, F., Chouly, A.,"Maximum Likelihood Frequency Detectors for Orthogonal Multicarrier Systems", Proceedings ICC 93, pp766-771, 1993

(Dinis and Gusmao 97)   Dinis, R., Gusmao, A., "Carrier synchronization with CEPB-OFDM", Proceedings IEEE VTC'97, 1997

(Doelz et.al 57)   Doelz, M.L., Heald, E.T.,Martin,D.L.,"Binary data transmission techniques for linear systems", Proc. IRE, vol. 45, pp. 656-661, May 1957.

(El-Tanany and Wu 97)   El-Tanany, M.S., Wu, Y., "Impact of phase noise on the performance of OFDM systems over frequency selective channels", Proceedings IEEE VTC'97, 1997.

(Godard 80)   Godard, D.N., "Self-recovering equalization and carrier tracking in two-dimensional data communication systems", IEEE Trans. on Commun., COM-28, pp. 1867-1875, November 1980.

(Harmuth 60)   Harmuth, H.F.,"On the transmission of information by orthogonal time functions",AIEE Trans (Communications and Electronics), vol. 79, pp. 248-255, July 1960

(Haykin 96)   Haykin, S., "Adaptive filter theory", third edition, Prentice Hall, New Jersey, USA, 1996.

(Hirosaki 81)   Hirosaki, B., "An orthogonally multiplexed QAM system useing the discrete Fourier transform", IEEE Trans. on Commun., vol. com-29, no. 7, pp. 982-989, July 1981.

(Hirosaki 84)   Hirosaki, B., "A maximum likelihood receiver for an orthogonaly multiplexed QAM system", in Proc. Int. Conf.

Commun., pp. 373-376, Amsterdam, The Netherlands, May 1984.

(Jakes 74) Jakes, W. C.,"Microwave mobile communications",Reprint by IEEE PRESS, 445 Hoes Lane, Piscataway, New Yearsy, USA, 1994

(Jeruchim 84) Jeruchim, M.C., "Techniques for estimating the bit error rate in the simmulation of digiltal communication systems", IEEE Journal on Selected areas in Commun., vol. sac-2, no. 1, Januar 1984.

(Jesupret et. al 91) T. Jesupret, M. Moeneclaey, G. Ascheid, "Digital demodulator synchronization", Final report ESTEC contract No. 8437/89/NL/RE June, 1991

(Kang et. al 94) Kang, W.K., Ann, J., Lee, H.S., "Decision-directed maximum-likelihood estimation of OFDM frame synchronization offset", Electronics letters, vol. 30, no. 25, December 1994.

(Kay 89) S. Kay, "A fast and accurate single frequency estimator", IEEE Trans. Acoust., Speech, Signal Processing, ASSP-37(12):1987-1990, December 1989.

(Lambrette et. al 97a) Lambrette, U., Speth, M., Meyr, H., "OFDM burst frequency synchronization by single carrier training data", IEEE commun. letters, vol. 1, no. 2, March 1997

(Lambrette et. al 97b) Lambrette, U.,Hortsmannshoff, J., Meyr, H., "Techniques for frame synchronization on unknown frequency selective channels", Proceedings IEEE VTC'97, 1997

(Lee and Messerschmitt 94) Lee, E. A., Messerschmitt, D. G., "Digital Communication", Kluwer Academic Publishers, 3300 AH Dordrecht, The Netherlands, 2. edn.

(Lervik 96) Lervik, J.M., "Subband image communications over digital transparent and analog waveform channels" PhD thesis, Norwegian University of Science and Technology, 1995.

(Li and Stette 95)   Li, R., Stette, G., "Time limmited orthogonal multicarrier modulation schemes", IEEE Trans. Commun., vol. 43, no. 2/3/4, pp. 1269-1272, February/March/April 1995.

(Mallory 92)   Mallory, M. P., "Modulation method and apparatus for multicarrier data transmission", U.S. Patent No. 5,128,964, July 1992

(Mengali and D'Andrea 97) Mengali, U., D'Andrea, A. N., "Synchronization techniques for digital receivers", Plenum Press, New York, USA, 1997

(Meyr and Ascheid 90)   Meyr, H., Ascheid, G., "Synchronization in digital communications", vol. 1, John Wiley & Sons, Inc., New York, USA 1990

(Meyr et. al 98)   Meyr, H., Moeneclaey, M., Fechtel, S.A., "Digital communication receivers", John Wiley & Sons, Inc., New York, USA 1998

(Mochizuki et. al 98)   Mochizuki, N., Matsumoto, Y., Mizoguchi, M., Onizawa, T., Umehira, M., "A high performance frequency and timing synchronization technique for OFDM", Proceedings IEEE GlobeCom'98, 1998

(Moose 94)   Moose, P.H.,"A technique for orthogonal frequency division multiplexing frequency offset correction", IEEE Trans. Commun., vol. 42, no. 10, pp. 2908-2914, October 1994.

(Mueller and Müller 74) Mueller, K.H., Müller, M., "Timing recovery in digital synchronous data receivers", IEEE Trans. on Commun., vol. com-24, no. 5, May 1976

(Negi and Cioffi 98)   Negi, R., Cioffi, J., "Blind OFDM symbol synchronization in ISI channels", Proceedings IEEE GlobeCom'98, 1998

(Nikias and Petropulu 93) Nikias, C.L., Petropulu, A.P., "Higher-order spectra analysis, a nonlinear signal processing framework", Prentice Hall, New Jersey, USA, 1993.

(Oh et. al 96)   Oh, J. S., Chung, Y. M., Lee, S. U.,"A carrier synchroniza-
                         tion technique for OFDM on the frequency-selective fad-
                         ing environment", Proceedings IEEE VTC'96, p 1574-
                         1578, 1996.

(Palin and Rinne 98)   Palin, A., Rinne, J., "Enhanced symbol synchronization
                         method for OFDM system in SFN channels", Proceedings
                         IEEE GlobeCom'98, 1998

(Pollet and Moencleclaey 95) Pollet, T., Moeneclaey, M., "Synchronizability of
                         OFDM signals", Proceedings IEEE GlobeCom'95, p
                         2054-2058, 1996.

(Pollet et. al 95)   Pollet, T., VanBladel, M., Moeneclaey, M., "BER Sensitiv-
                         ity of OFDM Systems to Carrier Frequency Offset and
                         Wiener Phase Noise", IEEE Trans. on Com., vol.43, no 2/
                         3/4 Febr./Mar./Apr. 1995.

(Proakis 95)   Proakis, J. G., "Digital Communications", 3rd
                         ed.McGraw-Hill, 1995

(Reimers 97)   Reimers, U., "DVB-T: the COFDM-based system for ter-
                         restrial television", Electronics & Communications Enge-
                         neering Journal, vol. 9, no. 1, pp. 28-32, February 1997

(Remvik and Holte 96)   Remvik, P.K., Holte, N.,"Decision directed carrier fre-
                         quency synchronization for OFDM", Proceedings NOR-
                         SIG 96, pp. 143-146, 1996

(Remvik and Holte 97a)   Remvik, P.K., Holte, N., "Carrier acquisition in OFDM,
                         using fourth order cumulants", Proceedings NORSIG 97,
                         pp. 93-97, 1997

(Remvik and Holte 97b)   Remvik, P.K., Holte, N., "Carrier frequency offset robust-
                         ness for OFDM Systems with different pulse shaping fil-
                         ters", Proceedings IEEE GlobeCom'97, pp. 11-15, 1997.

(Remvik et. al 98)   Remvik, P.K., Holte, N., Vahlin, A., "Fading and carrier
                         frequency offset robustness for different pulseshaping, fil-
                         ters in OFDM" Proceedings IEEE VTC '98, pp. 777-781,
                         May 1998

(Rummler et al. 86)   Rummler, W.D., Coutts, R.P., Liniger, M., "Multipath fading channel models for microwave digital radio", IEEE Communications Magazine, vol. 24, no. 11, pp. 30-42, November 1986

(Saltzberg 67)   Saltzberg, M.R., "Performance of an efficient paralell data transmission system", IEEE Trans. Commun. Technol., vol. COM-15, no. 6, pp. 805-811, December 1967

(Sari et. al. 95)   Sari, H., Karam, G., Jeanclaude, I., "Transmission techniques for digital terrestrial TV broadcasting", IEEE Commun. magazine, vol. 33, no. 2, pp 100-109, February 1995

(Schmidl and Cox 97)   Schmidl, T.M., Cox, D.C., "Robust frequency and timing synchronization for OFDM", Trans. on Commun., vol. 45, no. 12, December 1997

(Shannon 48a)   Shannon, C.E., "A mathematical theory of communication I", Bell System Technical Journal, vol. 27, no. 3, pp. 379-423, July 1948

(Shannon 48b)   Shannon, C.E., "A mathematical theory of communication II", Bell System Technical Journal, vol. 27, no. 4, pp. 623-656, October 1948

(Speth et. al 97)   Speth, M., Classen, F., Meyr, H., "Frame synchronization of OFDM systems in frequency selective fading channels", Proceedings IEEE VTC'97, 1997

(Speth et. al 98)   Speth, M., Daecke, D., Meyr, H.,"Minimum overhead burst synchronization for OFDM based broadband transmission", Proceedings IEEE GlobeCom'98, 1998

(Steele 92)   Steele, R.,"Mobile radio communications", Pentech Press 1992

(Tufvesson 97)   Tufvesson, F., Maseng, T., "Pilot assisted channel estimation for OFDM in mobile cellular systems", Proceedings IEEE VTC'97, 1997

(Vahlin and Holte 96)   Vahlin, A., Holte, N.,"Optimal Finite Duration Pulses for OFDM", IEEE Transactions on communications, Vol. 44, No. 1, Jan. 1996

(Vahlin 96)   Vahlin, A., "Optimisation and Analysis of OFDM Communication System" PhD thesis, The Norwegian Institute of Technology, 1995.

(Viterbi and Omura 79)   Viterbi, A.J., Omura, J.K., "Principles of digital communications and coding", McGraw-Hill, New York, 1979

(Warner and Leung 93)   Warner, W.D., Leung, C., "OFDM/FM frame synchronization for mobile radio data communications", IEEE Trans. on Vehic. Tech., vol. 42, no. 3, August 1993

(Weinstein and Ebert 71) Weinstein, S. B., Ebert, P. M., "Data transmission by frequency-division multiplexing using the discrete Fourier transform", IEEE Trans. Commun., vol. COM-19, no. 5, pp. 628-634, October 1971.

(Ytrehus 97)   Ytrehus, Ø.,"On Codes for Error Correction and Block Synchronization", Proc.35th Annual Allerton Conf. on Commun., Control and Computing, Allerton, Illinois, USA October 1997.

(Zimmermann 96)   Zimmermann, G., Rosenberger, M., Dostert, S., "Theoretical bit error rate for uncoded and coded data transmission in digital audio broadcasting", Proc. IEEE International Conference on Communications, pp. 297-301, Dallas, USA, June 1996